Analytical solutions for thermo-mechanical soil structure interaction in energy piles

by

Aaron Cossel

B.S., Kansas State University, 2014

A THESIS

submitted in partial fulfillment of the requirements for the degree

MASTER OF SCIENCE

Department of Civil Engineering
College of Engineering

KANSAS STATE UNIVERSITY
Manhattan, Kansas

2019

Approved by:

Major Professor
Dr. Dunja Perić

Copyright

Abstract

While traditional pile foundations have been used for many years to transfer loads from superstructures to the subsurface, energy piles became especially popular in the last 15 years. Energy piles are thermo-active foundations that enable transfer of thermal energy between the subsurface and the superstructure. They rely on the use of ground source heat, which is economically efficient, environmentally friendly, and sustainable way to heat and cool large structures. Unlike air, the temperature of the soil remains relatively constant throughout the year below the certain depth that depends on the climatic zone. To extract the thermal energy from the ground geothermal loops are embedded into energy piles. The main purpose of such thermo-active foundation systems is to transfer deep ground heat into a building during the winter and out of the building during the summer through fluid circulating within the geothermal loop. These thermo-active foundations may need to be supplemented with air based heating/cooling systems.

This study investigates thermo-mechanical response of end bearing and semi floating energy piles through use of mathematical modeling. To this end, it is assumed that the energy pile behaves as thermo-elastic material while the soil-pile interface remains in the elastic state. These assumptions have been used and verified in several other studies. The analytical solutions for axial displacement, strain, and stress have been found for a single layered and multi layered soils underlain by the bedrock. Furthermore, the analytical solutions for mechanical and thermal loads have been validated against the full scale in situ tests. It is found that in case of net heating the end bearing pile model gives better predictions than the semi floating pile model and in the case of a combined thermal and mechanical semi floating pile model is better.

The analytical solutions developed herein provide in depth qualitative understanding of the load transfer mechanism in energy piles as well as quick, simple, and elegant computation of displacement, stress, and strain.

Table of Contents

List of Figures

List of Tables

Acknowledgements

I would like to thank my major professor, Prof. Dunja Perić, for all her teaching, guidance, and advice throughout my tenure at Kansas State University. I would also like to thank my other committee members, Prof. Hani Melhem and Dr. Krishna Ghimire, for their teaching and guidance.

I am also grateful for all the assistance provided by the Department of Civil Engineering, who have supported me through my work and studies.

Finally, I want to thank my friends and family who have provided love, support, encouragement, and most of all stress relief in times of need.

Chapter 1 - Introduction and Literature Review

Heat Exchanger Piles (HEP) are a form of geothermally active foundation. As implied by the name, they are a Pile Foundation that in addition to supporting the superstructure they exchanges geothermal energy between the structure and the earth around them. It has been found that below 3 to 5 m deep the soil maintains at a constant temperature about equal to the yearly average air temperature (Burger et al. 1985), this has been used as a stable thermal energy source to exchange energy between the soil and superstructure (Brandl 2006). A loop of tubing embedded in the pile allows for fluid to be circulated between the superstructure and foundation where in the summer the fluid is heated in the superstructure and cooled in the foundation, and the inverse in the winter. This energy exchange reduces the need to use other means of heating or cooling reducing the energy demand of the building and consequently reducing the carbon dioxide emotions in the atmosphere.

When the temperature of the HEP changes, it tries to change length; however, due to the HEP being embedded in soil or rock, it is restrained against this movement inducing additional forces in both the surrounding material and the HEP. In order to properly design a HEP the additional stresses, strains, and displacements caused by this interaction need to be known. In the past, both numerical and physical modeling have been used. Numerical modeling uses finite element and finite difference methods, while physical modeling uses small scale centrifuge laboratory tests and full scale field tests.

Finite difference approach needs a characteristic equation that describes the soil pile interface known as the load transfer function. Load transfer analyses for mechanical loads were first proposed by Seed and Reese (1957) and Coyle and Reese (1966). Numerous load transfer

functions have been proposed since (Randolph and Wroth 1978; Frank and Zhao 1982; Armaleh and Desai 1987; Frank et al. 1991). Knellwolf et al. (2011) appear to be the first to propose the use of load transfer function for the use in understanding energy pile stresses. Using piecewise linear T-z curves proposed by Frank and Zhao (1982) for mechanical loads Knellwolf et al. (2011) added an unloading branch describing the irreversible behavior. Chen and McCartney (2017) calibrated Plaseied's (2012) smooth non-linear T-z curve with a large initial linear portion model with the results of full scale and centrifuge tests to better understand the range and effects of the parameters of the model.

Bourne-Webb et al. (2009 and 2013) developed schematic of load transfer in HEP based on the full scale in situ tests. Rotta Loria and Laloui (2019) called for the explanation of a number of conditions of validity of Bourne- Webb et al. (2009 and 2013) and proposed new schematics based on global equilibrium of HEP.

Chapter 2 - Analytical Solutions for Soil Structure Interaction in Heat Exchanger Piles

Preliminaries

To capture the main features of energy pile response to thermal and mechanical loads it is assumed that both, pile and pile-soil interface remain in the elastic regime under working stresses. The assumption was justified by findings of Laloui et al. (2003) and Bourne-Webb et al. (2009) based on the full scale in situ tests, and Laloui et al. (2006), Knellwolf et al. (2011), Ozudogru et al. (2015) and Perić et al. (2017) based on the numerical models. Furthermore, Laloui et al. (2003) stated that horizontal displacements of energy piles are negligible compared to vertical displacements. Consequently, one dimensional model is used herein whereby axial or vertical displacement, strain and stress are often referred to simply as displacement, strain or stress.

A tensile strain and stress are positive while a positive displacement is directed upwards. Thus, a compressive axial force is negative. A temperature change (ΔT) is difference between the temperature of the pile and the temperature of the surrounding soil. Thus, heating of the pile relative to the soil causes positive temperature change and vice versa. It is noted that it is assumed that the entire pile is experiencing the same temperature change.

The kinematic relationship between displacement ($u(x)$) and strain ($\varepsilon(x)$) is given by:

$$\varepsilon = \frac{du}{dx} \tag{1}$$

The thermo-elastic stress ($\sigma(x)$) strain ($\varepsilon(x)$) relationship of the pile is given by:

$$\sigma = E(\varepsilon - \alpha \Delta T) \tag{2}$$

where E is the Young's modulus of the pile and α is the coefficient of thermal expansion of the pile. Finally, the constitutive model of the soil pile interface is given by:

$$|\tau| = k_s|u| \tag{3}$$

where $\tau(x)$ is the shear stress at the soil-pile interface while k_s is the stiffness of a continuous linear elastic shear spring that is attached to the pile. The spring substitutes the surrounding soil.

End Bearing Pile

The solutions are first presented for an end bearing pile whereby the pile tip is supported by a very stiff bedrock. Ideally, it can be assumed that the pile tip displacement is zero. This assumption is used herein.

Homogeneous Soil Profile

The first soil profile considered consists of a single soil layer that is underlain by the bedrock. The bedrock is flush with the pile tip. This profile is also referred to as a homogenous profile.

Self-Weight

First, a self-weight load is considered. The free body diagrams (FBDs) of the entire end bearing energy pile and its infinitesimal segment are depicted in Figure 2.1.

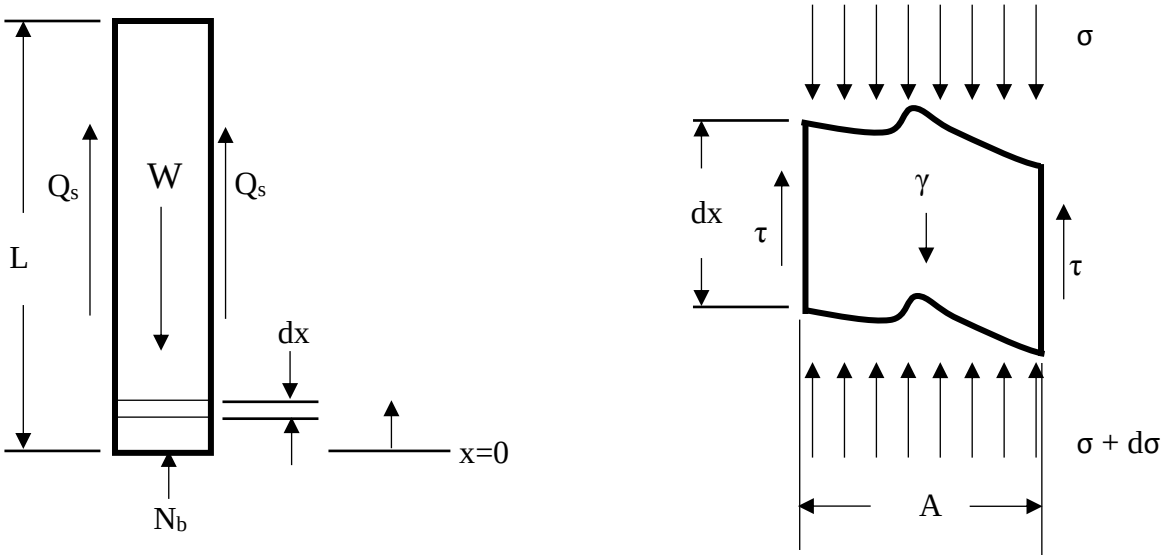

Figure 2.1 Self-Weight Loading for End Bearing Pile Embedded into Homogeneous Soil Profile

As the only load comes from the self-weight (W) of the pile it must be in equilibrium with the resultant (Q_s) of the shear stress that is acting at the pile-soil interface, and the normal reaction (N_b) at the pile tip. As indicated in Figure 2.1 the positive x-axis is directed upward.

As stated by Knellwolf et al. (2011) k_s can be obtained from in situ static pile tests. Enforcing the equilibrium in the vertical direction of the pile segment of infinitesimal length (Figure 2.1) and combining it with Eqs. (1), (2), and (3) results in the following non-homogeneous second order ordinary differential equation (ODE).

$$\frac{d^2u}{dx^2} - \psi^2 u = \frac{\gamma_c}{E} \tag{4}$$

and $\gamma_c$is a unit weight of the pile while ψ is a constant given by:

$$\psi^2 = \left(\frac{p}{A}\right)\left(\frac{k_s}{E}\right) = \xi_g \xi_s \tag{5}$$

where *A*, and *p* are cross sectional area and perimeter of a pile respectively. Solving for the unknown function $u(x)$ from Eq.(4) results in:

$$u(x) = C_1 e^{\psi x} + C_2 e^{-\psi x} - \frac{\gamma_c}{E\psi^2} \tag{6}$$

Imposing the following boundary conditions:

$$u(0) = 0 \qquad \text{and} \qquad \sigma(L) = 0 \tag{7}$$

where *L* is the length of the pile, leads to the following solution of Eq. (6)

$$u(x) = \frac{\gamma_c}{E\psi^2}\left(\frac{\cosh\big(\psi(L-x)\big)}{cosh(\psi L)} - 1\right) \tag{8}$$

which gives

$$u_{min} = u(L) = \frac{\gamma_c}{E\psi^2}\left(\frac{1}{cosh(\psi L)} - 1\right) < 0 \tag{9}$$

The axial strain in the pile is obtained by combining Eqs. (1) and (8) as

$$\varepsilon(x) = -\frac{\gamma_c}{E\psi}\left(\frac{sinh\big(\psi(L-x)\big)}{cosh(\psi L)}\right) \tag{10}$$

which gives

$$\varepsilon(0) = \frac{-\gamma_c}{E\psi} tanh(\psi L) < 0 \tag{11}$$

$$\varepsilon(L) = 0 \tag{12}$$

The axial stress in the pile is obtained by combining Eq. (2) in the absence of temperature change and Eq. (10) as

$$\sigma(x) = E\varepsilon(x) = \frac{-\gamma_c}{\psi}\left[\frac{\sinh(\psi(L-x))}{\cosh(\psi L)}\right] \tag{13}$$

which gives

$$\sigma(0) = \frac{-\gamma_c}{\psi}\tanh(\psi L) < 0 \tag{14}$$

The axial force at the pile tip is then given by

$$N_b = A\sigma(L) = -\left(W + pk_s\int_0^L u(x)dx\right) \tag{15}$$

Thermal Load

Next, a thermal load is considered whereby the only load is coming from the temperature change. The FBD of the end bearing HEP is shown in Fig. 2.2 for $\Delta T > 0$.

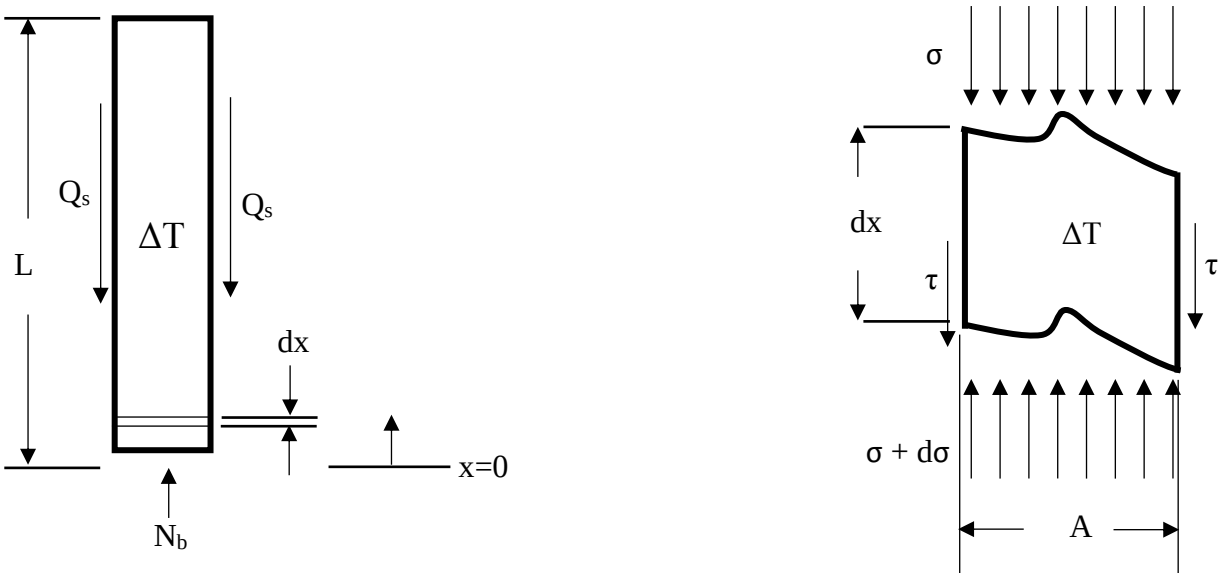

Figure 2.2 Thermal Load (*ΔT* > 0) for End Bearing Pile Embedded into Homogeneous Soil Profile

Imposing equilibrium in the vertical direction of the infinitesimal pile segment and combining it with Eqs. (1), (2), and (3) results in the following homogeneous second order ODE.

$$\frac{d^2u}{dx^2} - \psi^2 u = 0 \tag{16}$$

Solving for unknown function *u(x)* from Eq. (16) results in

$$u(x) = C_1 e^{\psi x} + C_2 e^{-\psi x} \tag{17}$$

After imposing boundary conditions Eq. (7) the following is obtained

$$u(x) = \frac{\alpha \Delta T}{\psi} \frac{sinh(\psi x)}{\cosh(\psi L)} \tag{18}$$

which gives

$$u(L) = \frac{\alpha \Delta T}{\psi} \tanh(\psi L) \tag{19}$$

The axial strain in the pile is obtained by combining the kinematic relationship with Eq. (18). It is given by

$$\varepsilon(x) = \alpha \Delta T \frac{cosh(\psi x)}{\cosh(\psi L)} \tag{20}$$

which gives

$$\varepsilon(0) = \frac{\alpha \Delta T}{\cosh(\psi L)} \tag{21}$$

$$\varepsilon(L) = \alpha \Delta T \tag{22}$$

The axial stress in the pile is obtained by combining the constitutive relationship with Eq. (20). It is given by

$$\sigma(x) = E\alpha \Delta T \left[\frac{cosh(\psi x)}{\cosh(\psi L)} - 1\right] \tag{23}$$

which gives the maximum magnitude of axial stress as

$$|\sigma_{max}| = |\sigma(0)| = E\alpha |\Delta T| \left[\frac{1}{\cosh(\psi L)} - 1\right] \tag{24}$$

Mechanical Load

The third load case considered is axial loading. The only load in this case comes from the superstructure in the form of an axial compressive force applied at the pile head, thus inducing compressive stress in the pile. The FBD of the end bearing HEP is shown in Figure 2.3 for a compressive load.

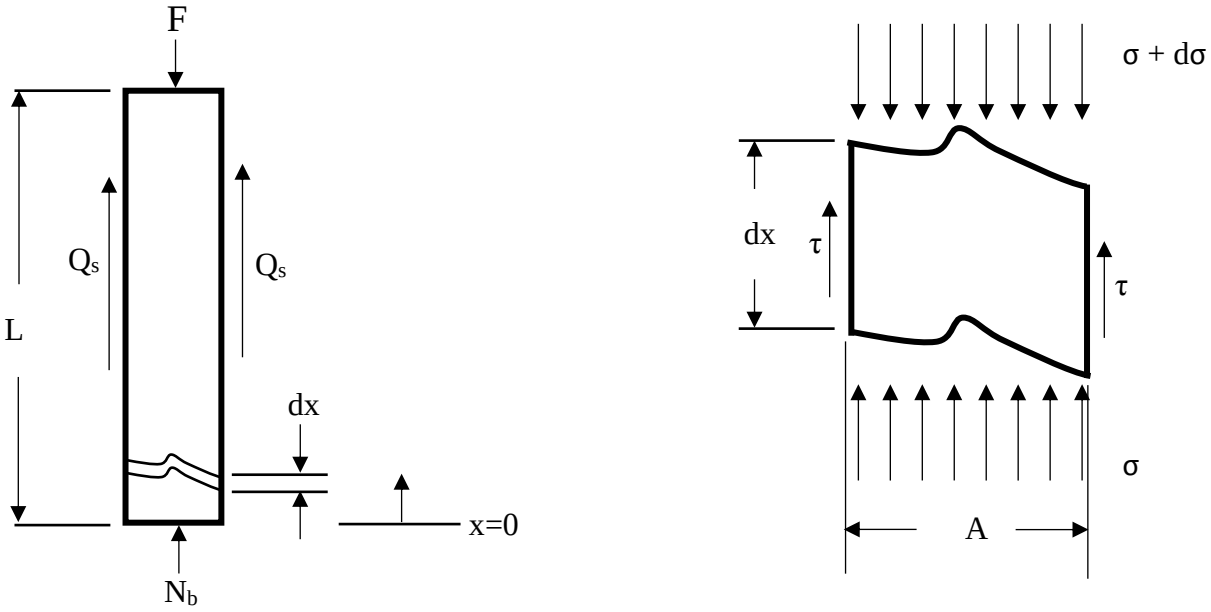

Figure 2.3 Compressive Force at the Pile Head for End Bearing Pile Embedded into Homogeneous Soil Profile

Imposing equilibrium of the infinitesimal pile segment in the vertical direction and combining it with Eqs. (1), (2), and (3) results in

$$\frac{d^2u}{dx^2} - \psi^2 u = 0 \tag{25}$$

Solving for the unknown function *u(x)* form Eq. (25) results in

$$u(x) = C_1 e^{\psi x} + C_2 e^{-\psi x} \tag{26}$$

Imposing the boundary conditions

$$u(0) = 0 \qquad \text{and} \qquad \sigma(L) = \frac{F}{A} \tag{27}$$

results in

$$u(x) = \frac{F}{AE\psi}\frac{sinh(\psi x)}{\cosh(\psi L)} \tag{28}$$

which gives

$$u(L) = \frac{F}{AE\psi}\tanh(\psi L) \tag{29}$$

The axial strain in the pile is obtained by combining the kinematic relationship with Eq. (28). It is given by

$$\varepsilon(x) = \frac{F}{AE}\frac{cosh(\psi x)}{\cosh(\psi L)} \tag{30}$$

which for an applied compressive force *F* gives

$$\varepsilon_{max} = \varepsilon(0) = \frac{F}{\mathrm{AE}\cosh(\psi L)} < 0 \tag{31}$$

$$\varepsilon(L) = \frac{F}{\mathrm{AE}} < 0 \tag{32}$$

The axial stress in the pile is obtained by combining the constitutive relationship in the absence of thermal load and Eq. (30). It is given by

$$\sigma(x) = \frac{F\ cosh(\psi x)}{A\ \cosh(\psi L)} \tag{33}$$

which for an applied compressive load gives the minimum stress as

$$\sigma_{min} = \sigma(0) = \frac{F}{\text{Acosh}(\psi L)} < 0 \tag{34}$$

Thermal Load with Head Restraint

This load combination is the same as the thermal load except for the changed boundary condition at the pile head. This change is to represent a restraint imposed on the pile by the superstructure. Figure 2.4 Shows the FDB

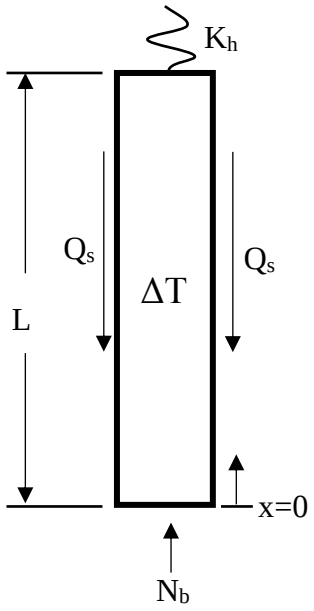

Figure 2.4 Thermal Load with Head Restraint for End Bearing Pile Embedded into Homogeneous Soil Profile

For this loading condition. The head restraint is represented by the equivalent linear spring having stiffness K_h. The boundary conditions for this loading case are given by

$$u(0) = 0 \qquad \text{and} \qquad K_h u(L) = -\sigma(L) \tag{35}$$

Eq. (35) implies that the superstructure induces a compressive force on the pile head in the case that the pile head moves upwards. After solving the governing ODE (16) with the boundary conditions given in Eq. (35) the displacement of the HEP is obtained as

$$u(x) = \alpha \Delta T \frac{sinh(\psi x)}{\psi \cosh(\psi L) + \frac{K_h}{E} sinh(\psi L)} \tag{36}$$

which gives

$$u(L) = \alpha \Delta T \frac{1}{\psi \coth(\psi L) + \frac{K_h}{E}} \tag{37}$$

After differentiating Eq. (36) the strain is found to be

$$\varepsilon(x) = \alpha \Delta T \frac{\psi cosh(\psi x)}{\psi \cosh(\psi L) + \frac{K_h}{E} sinh(\psi L)} \tag{38}$$

which gives

$$\varepsilon(0) = \alpha \Delta T \frac{\psi}{\psi \cosh(\psi L) + \frac{K_h}{E} sinh(\psi L)} \tag{39}$$

$$\varepsilon(L) = \alpha \Delta T \frac{\psi}{\psi + \frac{K_h}{E} tanh(\psi L)} \tag{40}$$

The axial stress is obtained by combining the constitutive equation with Eq. (38) as

$$\sigma(x) = E\alpha\Delta T\left(\frac{\psi cosh(\psi x)}{\psi\cosh(\psi L) + \frac{K_h}{E}sinh(\psi L)} - 1\right) \tag{41}$$

which gives

$$\sigma(0) = E\alpha\Delta T\left(\frac{\psi}{\psi\cosh(\psi L) + \frac{K_h}{E}sinh(\psi L)} - 1\right) \tag{42}$$

$$\sigma(L) = E\alpha\Delta T\left(\frac{\psi}{\psi + \frac{K_h}{E}tanh(\psi L)} - 1\right) \tag{43}$$

It is noted that for $K_h = 0$ the superstructure does not resist the expansion of the energy pile and this solution fully corresponds to the previously obtained solution for thermal loading in the absence of the head restraint.

Combined Load

The final load condition considered for the end bearing pile embedded in a homogenous soil profile is a combination of self-weight, thermal loading, and loading due to axial compressive force applied at the pile head. Using superposition of the individual responses discussed previously results in the displacement

$$u(x) = \frac{\sinh(\psi x)}{E\psi \cosh(\psi L)} \left[\frac{\gamma_c}{\psi} \frac{cosh\big(\psi(L-x)\big) - \cosh(\psi L)}{\sinh(\psi x)} + \frac{F}{A} + \frac{E\alpha\Delta T}{1 + \frac{K_h}{E\psi} tanh(\psi L)} \right] \quad (44)$$

which gives

$$u(L) = \frac{\tanh(\psi L)}{E\psi} \left[\frac{\gamma_c}{\psi} \frac{1 - \cosh(\psi L)}{\sinh(\psi L)} + \frac{F}{A} + \frac{E\alpha\Delta T}{1 + \frac{K_h}{E\psi} tanh(\psi L)} \right] \quad (45)$$

The axial strain in the pile is given by

$$\varepsilon(x) = \frac{\cosh(\psi x)}{E \cosh(\psi L)} \left[-\frac{\gamma_c}{\psi} \frac{\sinh\big(\psi(L-x)\big)}{\cosh(\psi x)} + \frac{F}{A} + \frac{E\alpha\Delta T}{1 + \frac{K_h}{E\psi} tanh(\psi L)} \right] \quad (46)$$

which gives

$$\varepsilon(0) = \frac{1}{Ecosh(\psi L)} \left[-\frac{\gamma_c}{\psi} \sinh(\psi L) + \frac{F}{A} + \frac{E\alpha\Delta T}{1 + \frac{K_h}{E\psi} tanh(\psi L)} \right] \quad (47)$$

and

$$\varepsilon(L) = \frac{F}{AE} + \frac{\alpha\Delta T}{1 + \frac{K_h}{E\psi} tanh(\psi L)} \quad (48)$$

Axial stress in the pile is given by

$$\sigma(x) = \frac{\cosh(\psi x)}{\cosh(\psi L)}\left[-\frac{\gamma_c}{\psi}\,\frac{\sinh\big(\psi(L-x)\big)}{\cosh(\psi x)} + \frac{F}{A} + E\alpha\Delta T\left(\frac{1}{1+\frac{K_h}{E\psi}\,tanh(\psi L)} - \frac{\cosh(\psi L)}{\cosh(\psi x)}\right)\right] \tag{49}$$

which gives

$$\sigma(0) = \frac{1}{\cosh(\psi L)}\left[-\frac{\gamma_c}{\psi}\,\sinh(\psi L) + \frac{F}{A} + E\alpha\Delta T\left(\frac{1}{1+\frac{K_h}{E\psi}\,tanh(\psi L)} - \cosh(\psi L)\right)\right] \tag{50}$$

and

$$\sigma(L) = \frac{F}{A} + E\alpha\Delta T\left(\frac{1}{1+\frac{K_h}{E\psi}\,tanh(\psi L)} - 1\right) \tag{51}$$

Layered Soil Profile

Next, the energy pile is embedded into a layered soil profile that consists of four different soil layers underlain by the bedrock as shown in Fig. 2.5

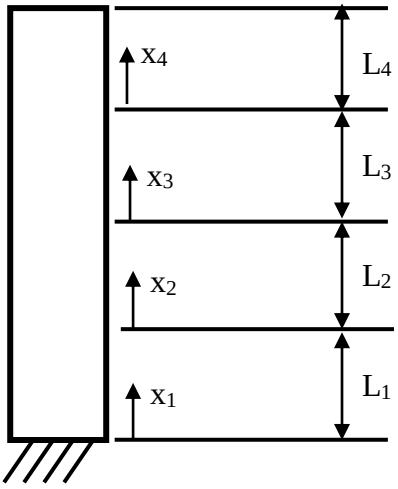

Figure 2.5 Layered Soil Profile

Here in L_i is the length of the i-th layer (i = 1 to 4) while x_i is measured from the bottom of each interface of the layers and it increases from bottom to top.

Thermal Load

The first loading condition considered for this scenario is thermal whereby the only load comes from the temperature change. Each of the four layers has its own governing equation which is equivalent to Eq. (17). Thus, the solution for displacement is given by

$$u_i(x_i) = C_{1i}e^{\psi_i x_i} + C_{2i}e^{-\psi_i x_i} \tag{52}$$

The stress is obtained by using kinematic and constitutive relationship. It is given by

$$\sigma_i(x_i) = E\left(\psi_i\left(C_{1i}e^{\psi_i x_i} - C_{2i}e^{-\psi_i x_i}\right) - \alpha\Delta T\right) \tag{53}$$

Where (i=1 to 4) denotes individual soil layers shown in Fig. 2.5. Boundary conditions are given by

$$u_1(0) = 0 \qquad \text{and} \qquad \sigma_4(L_4) = 0 \tag{54}$$

In addition, the compatibility between displacements and stresses at the interface of any two different layers is enforced in Eq. (55)

$$u_n(L_n) = u_{n+1}(0) \quad \text{and} \quad \sigma_n(L_n) = \sigma_{n+1}(0) \quad \text{where n = 1, 2, 3} \tag{55}$$

By combining Eqs. (52) through (55) with kinematic and constitutive relationships the constants $C_{1(i+1)}$ and $C_{2\,(i+1)}$, where n = 1 to 3 are determined as

$$C_{1(i+1)} = \frac{1}{2}\left[C_{1i}e^{\psi_i L_i}\left(1 + \frac{\psi_i}{\psi_{(i+1)}}\right) + C_{2i}e^{-\psi_i L_i}\left(1 - \frac{\psi_i}{\psi_{(i+1)}}\right)\right] \tag{56}$$

$$C_{2(i+1)} = \frac{1}{2}\left[C_{1i}e^{\psi_i L_i}\left(1 - \frac{\psi_i}{\psi_{(i+1)}}\right) + C_{2i}e^{-\psi_i L_i}\left(1 + \frac{\psi_i}{\psi_{(i+1)}}\right)\right] \tag{57}$$

Denoting $CH_i = \cosh(\psi_i L_i)$ and $SH_i = \sinh(\psi_i L_i)$ and

$$\mathrm{B} = \psi_1 CH_1\left(\frac{CH_2SH_3}{\psi_3} + \frac{SH_2CH_3}{\psi_2}\right) + SH_1\left(CH_2CH_3 + \frac{\psi_2}{\psi_3}SH_2SH_3\right) \tag{58}$$

$$\mathrm{C} = \frac{\psi_1}{\psi_4}CH_1\left(CH_2CH_3 + \frac{\psi_3}{\psi_2}SH_2SH_3\right) + \frac{SH_1}{\psi_4}(\psi_3 CH_2SH_3 + \psi_2 SH_2CH_3) \tag{59}$$

The bottom boundary condition (54) provides the relationship between the constants C_{11} and C_{21}. By using the compatibility equations (55) the constants for remaining layers can be expressed in terms of C_{11}, which is finally determined from the top boundary condition from Eq. (54). Subsequently, all other constants can be determined as they were previously expressed as functions of C_{11}. After substituting the constants for each section into Eqs. (53) and (55) the final solutions are obtained. Strain is obtained by applying the kinematic relationship to Eq. (52). Consequently; displacement, strain, and stress for the first segment are given by

$$u_1(x_1) = \frac{\alpha \Delta T sinh(\psi_1 x_1)}{\psi_4 (SH_4 B + CH_4 C)} \tag{60}$$

$$\varepsilon_1(x_1) = \frac{\alpha \Delta T\, \psi_1 cosh(\psi_1 x_1)}{\psi_4 (SH_4 B + CH_4 C)} \tag{61}$$

$$\sigma_1(x_1) = E\alpha \Delta T \left(\frac{\psi_1 cosh(\psi_1 x_1)}{\psi_4 (SH_4 B + CH_4 C)} - 1 \right) \tag{62}$$

Displacement, strain, and stress for the second layer are given by

$$u_2(x_2) = \frac{\alpha \Delta T \left(SH_1 \cosh(\psi_2 x_2) + \frac{\psi_1}{\psi_2} CH_1 \sinh(\psi_2 x_2) \right)}{\psi_4 (SH_4 B + CH_4 C)} \tag{63}$$

$$\varepsilon_2(x_2) = \frac{\alpha \Delta T\, \psi_2 \left(SH_1 \sinh(\psi_2 x_2) + \frac{\psi_1}{\psi_2} CH_1 \cosh(\psi_2 x_2) \right)}{\psi_4 (SH_4 B + CH_4 C)} \tag{64}$$

$$\sigma_2(x_2) = E\alpha \Delta T \left(\frac{\psi_2 \left(SH_1 \sinh(\psi_2 x_2) + \frac{\psi_1}{\psi_2} CH_1 \cosh(\psi_2 x_2) \right)}{\psi_4 (SH_4 B + CH_4 C)} - 1 \right) \tag{65}$$

where

$$D = \frac{\psi_1}{\psi_2} CH_1 SH_2 + SH_1 CH_2 \tag{66}$$

$$G = \frac{\psi_1}{\psi_3} CH_1 CH_2 + \frac{\psi_2}{\psi_3} SH_1 SH_2 \tag{67}$$

Displacement, strain, and stress for the third layer are given by

$$u_3(x_3) = \frac{\alpha \Delta T (D \cosh(\psi_3 x_3) + G \sinh(\psi_3 x_3))}{\psi_4 (SH_4 B + CH_4 C)} \tag{68}$$

$$\varepsilon_3(x_3) = \frac{\alpha \Delta T \, \psi_3 (D \sinh(\psi_3 x_3) + G \cosh(\psi_3 x_3))}{\psi_4 (SH_4 B + CH_4 C)} \tag{69}$$

$$\sigma_3(x_3) = E \alpha \Delta T \left(\frac{\psi_3 (D \sinh(\psi_3 x_3) + G \cosh(\psi_3 x_3))}{\psi_4 (SH_4 B + CH_4 C)} - 1 \right) \tag{70}$$

Displacement, strain and stress for the fourth or top layer are given by

$$u_4(x_4) = \frac{\alpha \Delta T (B \cosh(\psi_4 x_4) + C \sinh(\psi_4 x_4))}{\psi_4 (SH_4 B + CH_4 C)} \tag{71}$$

$$\varepsilon_4(x_4) = \frac{\alpha \Delta T (B \sinh(\psi_4 x_4) + C \cosh(\psi_4 x_4))}{SH_4 B + CH_4 C} \tag{72}$$

$$\sigma_4(x_4) = E \alpha \Delta T \left(\frac{B \sinh(\psi_4 x_4) + C \cosh(\psi_4 x_4)}{SH_4 B + CH_4 C} - 1 \right) \tag{73}$$

Mechanical Load

The second loading condition for this soil profile is axial loading whereby a compressive force is applied at the pile head. Equilibrium of the infinitesimal segment combined with the kinematic relationship, and constitutive laws for the pile and the soil pile interface within each layer results in Eq. (16), the solution of which is given by

$$u_i(x_i) = C_{1i}e^{\psi_i x_i} + C_{2i}e^{-\psi_i x_i} \tag{74}$$

By applying kinematic relationship and the constitutive relationship in the absence of a temperature change Eq. (74) results in

$$\sigma_i(x_i) = E\psi_i\left(C_{1i}e^{\psi_i x_i} - C_{2i}e^{-\psi_i x_i}\right) \tag{75}$$

Using a similar procedure to the one followed while solving for the response to thermal load constants C_{1i} and C_{2i} (i = 1 to 4) are determined. Specifically, the bottom boundary condition from Eq. (54), displacement and stress compatibility conditions from Eq. (55), and modified top boundary condition provide six equations that are used to solve for eight unknown constants. The boundary condition at the pile head is given by

$$u_1(0) = 0 \qquad \text{and} \qquad \sigma_4(L_4) = \frac{F}{A} \tag{76}$$

After solving for the constants and substituting them back into Eq. (74) the following solutions for displacement, stress and strain within the first segment are obtained

$$u_1(x_1) = \frac{F\sinh(\psi_1 x_1)}{AE\psi_4(SH_4B + CH_4C)} \tag{77}$$

$$\varepsilon_1(x_1) = \frac{F\,\psi_1\,\cosh(\psi_1 x_1)}{AE\psi_4(SH_4B + CH_4C)} \tag{78}$$

$$\sigma_1(x_1) = \frac{F\,\psi_1\,\cosh(\psi_1 x_1)}{A\psi_4(SH_4B + CH_4C)} \tag{79}$$

Displacement, strain, and stress for the second layer are given by

$$u_2(x_2) = \frac{F\left[\mathrm{SH}_1\cosh(\psi_2 x_2) + \frac{\psi_1}{\psi_2}\,CH_1\sinh(\psi_2 x_2)\right]}{AE\psi_4(SH_4B + CH_4C)} \tag{80}$$

$$\varepsilon_2(x_2) = \frac{F\,\psi_2\left[\mathrm{SH}_1\sinh(\psi_2 x_2) + \frac{\psi_1}{\psi_2}\,CH_1\cosh(\psi_2 x_2)\right]}{AE\psi_4(SH_4B + CH_4C)} \tag{81}$$

$$\sigma_2(x_2) = \frac{F\,\psi_2\left[\mathrm{SH}_1\sinh(\psi_2 x_2) + \frac{\psi_1}{\psi_2}\,CH_1\cosh(\psi_2 x_2)\right]}{A\psi_4(SH_4B + CH_4C)} \tag{82}$$

Displacement, strain, and stress for the third pile segment are given by

$$u_3(x_3) = \frac{F\,[D\cosh(\psi_3 x_3) + G\,\sinh(\psi_3 x_3)]}{\mathrm{AE}\psi_4(SH_4B + CH_4C)} \tag{83}$$

$$\varepsilon_3(x_3) = \frac{F\,\psi_3\,[D\sinh(\psi_3 x_3) + G\,cosh(\psi_3 x_3)]}{\mathrm{AE}\,\psi_4(SH_4B + CH_4C)} \tag{84}$$

$$\sigma_3(x_3) = \frac{F\,\psi_3\,[D\sinh(\psi_3 x_3) + G\,cosh(\psi_3 x_3)]}{\mathrm{A}\,\psi_4(SH_4B + CH_4C)} \tag{85}$$

Displacement, strain, and stress for the fourth or top pile segment are given by

$$u_4(x_4) = \frac{F\,[B\cosh(\psi_4 x_4) + C\,\sinh(\psi_4 x_4)]}{\mathrm{AE}\,\psi_4(SH_4B + CH_4C)} \tag{86}$$

$$\varepsilon_4(x_4) = \frac{F\,[B\sinh(\psi_4 x_4) + C\,\cosh(\psi_4 x_4)]}{\mathrm{AE}\,(SH_4B + CH_4C)} \tag{87}$$

$$\sigma_4(x_4) = \frac{F\,[B\sinh(\psi_4 x_4) + C\,\cosh(\psi_4 x_4)]}{\mathrm{A}\,(SH_4B + CH_4C)} \tag{88}$$

Thermal Load with Head Restraint

This case represents the loading scenario whereby the pile head is restrained against a thermally induced movement by a superstructure. Compared to the case without the head restraint only the boundary condition at the pile head changes. It is given by

$$\sigma_4(L_4) = -K_h u_4(L_4) \tag{89}$$

The same procedure as the one employed previously for the case of thermal loading is followed except for the top boundary condition given in Eq. (89). It results in the following solution for displacement, strain and stress within the first pile segment

$$u_1(x_1) = \frac{\alpha\Delta T sinh(\psi_1 x_1)}{\psi_4(SH_4B + CH_4C) + \frac{K_h}{E}(CH_4B + SH_4C)} \tag{90}$$

$$\varepsilon_1(x_1) = \frac{\alpha\Delta T \psi_1 cosh(\psi_1 x_1)}{\psi_4(SH_4B + CH_4C) + \frac{K_h}{E}(CH_4B + SH_4C)} \tag{91}$$

$$\sigma_1(x_1) = E\alpha\Delta T\left(\frac{\psi_1 cosh(\psi_1 x_1)}{\psi_4(SH_4B + CH_4C) + \frac{K_h}{E}(CH_4B + SH_4C)} - 1\right) \tag{92}$$

Displacement, strain, and stress for the second layer are given by

$$u_2(x_2) = \frac{\alpha\Delta T\left(SH_1\cosh(\psi_2 x_2) + \frac{\psi_1}{\psi_2}CH_1\sinh(\psi_2 x_2)\right)}{\psi_4(SH_4B + CH_4C) + \frac{K_h}{E}(CH_4B + SH_4C)} \tag{93}$$

$$\varepsilon_2(x_2) = \frac{\alpha\Delta T\ (\psi_2 SH_1\sinh(\psi_2 x_2) + \psi_1 CH_1\cosh(\psi_2 x_2))}{\psi_4(SH_4B + CH_4C) + \frac{K_h}{E}(CH_4B + SH_4C)} \tag{94}$$

$$\sigma_2(x_2) = E\alpha\Delta T\left(\frac{(\psi_2 SH_1\sinh(\psi_2 x_2) + \psi_1 CH_1\cosh(\psi_2 x_2))}{\psi_4(SH_4B + CH_4C) + \frac{K_h}{E}(CH_4B + SH_4C)} - 1\right) \tag{95}$$

Displacement, strain, and stress for the third layer are given by

$$u_3(x_3) = \frac{\alpha\Delta T(D\cosh(\psi_3 x_3) + G\sinh(\psi_3 x_3))}{\psi_4(SH_4B + CH_4C) + \frac{K_h}{E}(CH_4B + SH_4C)} \tag{96}$$

$$\varepsilon_3(x_3) = \frac{\alpha\Delta T\ \psi_3(D\sinh(\psi_3 x_3) + G\cosh(\psi_3 x_3))}{\psi_4(SH_4B + CH_4C) + \frac{K_h}{E}(CH_4B + SH_4C)} \tag{97}$$

$$\sigma_3(x_3) = E\alpha\Delta T\left(\frac{\psi_3(D\sinh(\psi_3 x_3) + G\cosh(\psi_3 x_3))}{\psi_4(SH_4B + CH_4C) + \frac{K_h}{E}(CH_4B + SH_4C)} - 1\right) \tag{98}$$

Displacement, strain and stress for the fourth or the top layer are given by

$$u_4(x_4) = \frac{\alpha\Delta T(B\cosh(\psi_4 x_4) + C\sinh(\psi_4 x_4))}{\psi_4(SH_4B + CH_4C) + \frac{K_h}{E}(CH_4B + SH_4C)} \tag{99}$$

$$\varepsilon_4(x_4) = \frac{\alpha\Delta T\ \psi_4(B\sinh(\psi_4 x_4) + C\cosh(\psi_4 x_4))}{\psi_4(SH_4B + CH_4C) + \frac{K_h}{E}(CH_4B + SH_4C)} \tag{100}$$

$$\sigma_4(x_4) = E\alpha\Delta T\left(\frac{\psi_4(B\sinh(\psi_4 x_4) + C\cosh(\psi_4 x_4))}{\psi_4(SH_4B + CH_4C) + \frac{K_h}{E}(CH_4B + SH_4C)} - 1\right) \tag{101}$$

Combined Load

Finally, the solution for a combined thermal loading with head restraint and mechanical loading is obtained by the superposition. Displacement, strain and stress for the first segment are given by

$$u_1(x_1) = \frac{\sinh(\psi_1 x_1)}{\psi_4(SH_4B + CH_4C)}\left(\frac{F}{AE} + \frac{\alpha\Delta T}{1 + \frac{K_h}{E\psi_4}\frac{CH_4B + SH_4C}{SH_4B + CH_4C}}\right) \tag{102}$$

$$\varepsilon_1(x_1) = \frac{\psi_1 cosh(\psi_1 x_1)}{\psi_4(SH_4B + CH_4C)}\left(\frac{F}{AE} + \frac{\alpha\Delta T}{1 + \frac{K_h}{E\psi_4}\frac{CH_4B + SH_4C}{SH_4B + CH_4C}}\right) \tag{103}$$

$$\sigma_1(x_1) = \frac{\psi_1 cosh(\psi_1 x_1)}{\psi_4(SH_4B + CH_4C)}\left(\frac{F}{A} + \frac{E\alpha\Delta T}{1 + \frac{K_h}{E\psi_4}\frac{CH_4B + SH_4C}{SH_4B + CH_4C}}\right) - E\alpha\Delta T \tag{104}$$

Displacement, strain, and stress for the second layer are given by

$$u_2(x_2) = \frac{SH_1 \cosh(\psi_2 x_2) + \frac{\psi_1}{\psi_2} CH_1 \sinh(\psi_2 x_2)}{\psi_4(SH_4B + CH_4C)} \left(\frac{F}{AE} + \frac{\alpha \Delta T}{1 + \frac{K_h}{E\psi_4} \frac{CH_4B + SH_4C}{SH_4B + CH_4C}} \right) \tag{105}$$

$$\varepsilon_2(x_2) = \frac{\psi_2 SH_1 \sinh(\psi_2 x_2) + \psi_1 CH_1 \cosh(\psi_2 x_2)}{\psi_4(SH_4B + CH_4C)} \left(\frac{F}{AE} + \frac{\alpha \Delta T}{1 + \frac{K_h}{E\psi_4} \frac{CH_4B + SH_4C}{SH_4B + CH_4C}} \right) \tag{106}$$

$$\sigma_2(x_2) = \frac{\psi_2 SH_1 \sinh(\psi_2 x_2) + \psi_1 CH_1 \cosh(\psi_2 x_2)}{\psi_4(SH_4B + CH_4C)} \left(\frac{F}{A} + \frac{E\alpha \Delta T}{1 + \frac{K_h}{E\psi_4} \frac{CH_4B + SH_4C}{SH_4B + CH_4C}} \right) - E\alpha \Delta T \tag{107}$$

Displacement, strain, and stress for the third layer are given by

$$u_3(x_3) = \frac{D \cosh(\psi_3 x_3) + G \sinh(\psi_3 x_3)}{\psi_4(SH_4B + CH_4C)} \left(\frac{F}{AE} + \frac{\alpha \Delta T}{1 + \frac{K_h}{E\psi_4} \frac{CH_4B + SH_4C}{SH_4B + CH_4C}} \right) \tag{108}$$

$$\varepsilon_3(x_3) = \frac{\psi_3(D \sinh(\psi_3 x_3) + G \cosh(\psi_3 x_3))}{\psi_4(SH_4B + CH_4C)} \left(\frac{F}{AE} + \frac{\alpha \Delta T}{1 + \frac{K_h}{E\psi_4} \frac{CH_4B + SH_4C}{SH_4B + CH_4C}} \right) \tag{109}$$

$$\sigma_3(x_3) = \frac{\psi_3(D \sinh(\psi_3 x_3) + G \cosh(\psi_3 x_3))}{\psi_4(SH_4B + CH_4C)} \left(\frac{F}{A} + \frac{E\alpha \Delta T}{1 + \frac{K_h}{E\psi_4} \frac{CH_4B + SH_4C}{SH_4B + CH_4C}} \right) - E\alpha \Delta T \tag{110}$$

Displacement, strain and stress for the fourth layer are given by

$$u_4(x_4) = \frac{B\cosh(\psi_4 x_4) + C\sinh(\psi_4 x_4)}{\psi_4(SH_4B + CH_4C)}\left(\frac{F}{AE} + \frac{\alpha\Delta T}{1 + \frac{K_h}{E\psi_4}\frac{CH_4B + SH_4C}{SH_4B + CH_4C}}\right) \quad (111)$$

$$\varepsilon_4(x_4) = \frac{B\sinh(\psi_4 x_4) + C\cosh(\psi_4 x_4)}{SH_4B + CH_4C}\left(\frac{F}{AE} + \frac{\alpha\Delta T}{1 + \frac{K_h}{E\psi_4}\frac{CH_4B + SH_4C}{SH_4B + CH_4C}}\right) \quad (112)$$

$$\sigma_4(x_4) = \frac{B\sinh(\psi_4 x_4) + C\cosh(\psi_4 x_4)}{SH_4B + CH_4C}\left(\frac{F}{A} + \frac{E\alpha\Delta T}{1 + \frac{K_h}{E\psi_4}\frac{CH_4B + SH_4C}{SH_4B + CH_4C}}\right) - E\alpha\Delta T \quad (113)$$

Semi Floating Pile

In this section the assumption of strictly fixed pile tip, which is an idealized view of the end bearing pile, is relaxed. Specifically, the pile tip is now allowed to move as well as to transfer some load onto the soil as shown in Fig. 2.6. Thus, the pile is referred to as semi floating. The corresponding boundary condition at the pile tip for any loading condition is given by

$$\sigma_b = K_b u_b \quad (114)$$

Where subscript "*b*" refers to the bottom boundary condition or the condition at the pile tip.

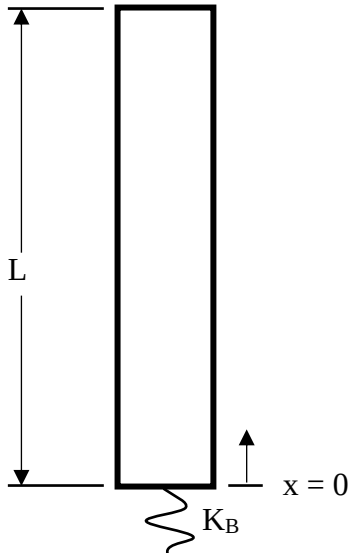

Figure 2.6 Schematic of Semi Floating Pile

Homogeneous Soil Profile

A homogeneous soil profile consists of a single soil layer above the bedrock whereby the pile tip is flush with the bedrock as shown in Fig. 2.6.

Thermal Load

In the case of thermal load the only load comes from the temperature change of the pile relative to the surrounding soil. The FBD of the pile is shown in Fig. 2.7

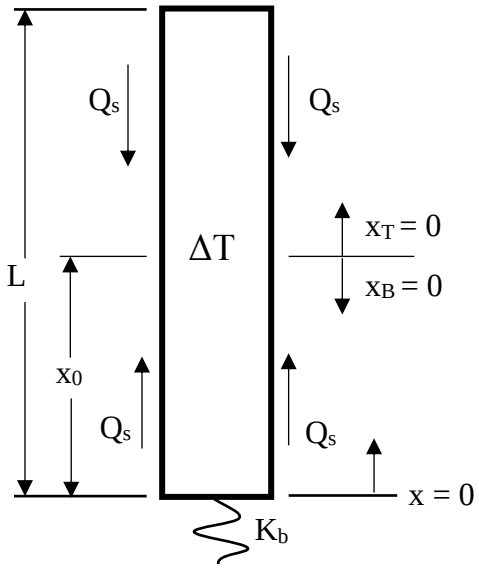

Figure 2.7 Thermal Loading of Semi Floating Pile Embedded into Homogeneous Soil

The location of zero vertical displacement, which is denoted as x_0, is also known as a null point. In case that the pile is exposed to heating the region of the pile located above the null point will move upward while the region of the pile located below the null point will move downward. The pile moves in opposite directions when exposed to cooling. To solve this problem the energy pile is divided into two parts. The portion above the null point has its local coordinate x_T, whose positive direction points upward. The portion below the null point has its local coordinate x_B, whose negative direction is pointed downward. The global coordinate system is the same as used previously. Thus, the relationship between the global and local coordinates is given by

$$x_T = x - x_0 \geq 0 \qquad \text{and} \qquad x_B = x - x_0 \leq 0 \tag{115}$$

Based on the FBD of the infinitesimal part of the pile (Fig. 2.2) the solutions for displacements of the bottom and top parts are given by

$$u_i = C_{1i}e^{\psi x_i} + C_{2i}e^{-\psi x_i} \qquad \text{where } i=B,T \tag{116}$$

Thus, there are total of five unknowns, out of which four are constants C_{1i} and C_{2i}, and the remaining unknown is the location of the null point (x_0). They are determined from the boundary conditions at the pile tip and pile head, compatibility of displacements and stresses at the null point, and by enforcing the zero displacement at the null point. The boundary conditions in the local coordinate systems are given by

$$\sigma_B(x_0) = K_B u_B(x_0) \quad \text{and} \qquad \sigma_T(L - x_0) = 0 \tag{117}$$

The compatibility conditions in local coordinate systems are given by

$$u_B(0) = u_T(0) = 0 \quad \text{and} \qquad \sigma_B(0) = \sigma_T(0) \tag{118}$$

The boundary condition at the pile tip implies that in the case of heating the tip of the energy pile moves downwards while the bedrock imposes a compressive force on the pile.

By combining Eqs. (116), (117), and (118) with the kinematic relationship, and constitutive relationships for the pile and the soil pile interface the solutions are obtained. They are expressed in global coordinates as

$$u(x) = \frac{\alpha \Delta T \, sinh\big(\psi(x - x_0)\big)}{\psi \, cosh\big(\psi(L - x_0)\big)} \quad 0 \le x \le L \tag{119}$$

Strain in global coordinates is given by

$$\varepsilon(x) = \frac{\alpha \Delta T \, cosh\big(\psi(x - x_0)\big)}{cosh\big(\psi(L - x_0)\big)} \quad 0 \le x \le L \tag{120}$$

Stress in global coordinates is given by

$$\sigma(x) = \mathrm{E}\alpha \Delta T \left(\frac{cosh\big(\psi(x - x_0)\big)}{cosh\big(\psi(L - x_0)\big)} - 1 \right) \quad 0 \le x \le L \tag{121}$$

where x_0 is given by

$$x_0 = \frac{1}{\psi} \tanh^{-1} \left(\frac{\psi \, cosh(\psi L) - \psi}{\psi \, sinh(\psi L) + \frac{K_B}{E}} \right) \tag{122}$$

Mechanical Load

Solution of the governing equation for mechanical load was given by Eq. (116). The boundary conditions in the case of semi floating pile are given by

$$K_B u(0) = \sigma_B(0) \qquad \text{and} \qquad \sigma_T(L) = \frac{F}{A} \tag{123}$$

By combining Eq. (116), kinematic relationship and constitutive relationship for the pile and the soil pile interface the following solution is obtained

$$u(x) = \frac{F}{AE\psi} \, \frac{E\psi \cosh(\psi x) + K_b \sinh(\psi x)}{E\psi \sinh(\psi L) + K_b \cosh(\psi L)} \tag{124}$$

$$\varepsilon(x) = \frac{F}{AE} \, \frac{E\psi \sinh(\psi x) + K_b \cosh(\psi x)}{E\psi \sinh(\psi L) + K_b \cosh(\psi L)} \tag{125}$$

$$\sigma(x) = \frac{F}{A}\,\frac{E\psi\sinh(\psi x) + K_b\cosh(\psi x)}{E\psi\sinh(\psi L) + K_b\cosh(\psi L)} \tag{126}$$

Thermal Load with Head Restraint

This load combination is the same as the thermal except for the change of the boundary conditions at the pile head. To this end, a restraint imposed by the superstructure is represented by the normal spring that has stiffness K_h. Thus, the boundary conditions for this loading scenario are expressed in local coordinates as follows

$$K_b u_B(x_0) = \sigma_B(x_0) \quad \text{and} \quad K_h u_T(L - x_0) = -\sigma_T(L - x_0) \tag{127}$$

After applying Eqs. (127) and (118) to Eq. (52) displacement of the energy pile is obtained. In global coordinates it is given by

$$u(x) = \alpha\Delta T\,\frac{sinh\big(\psi(x - x_0)\big)}{\psi\,cosh\big(\psi(L - x_0)\big) + \frac{K_h}{E}\sinh\big(\psi(L - x_0)\big)} \quad 0 \le x \le L \tag{128}$$

Strain is obtained by differentiating the displacement. It is given by

$$\varepsilon(\mathrm{x}) = \alpha\Delta T\,\frac{\psi\,cosh\big(\psi(x - x_0)\big)}{\psi\,cosh\big(\psi(L - x_0)\big) + \frac{K_h}{E}\sinh\big(\psi(L - x_0)\big)} \quad 0 \le x \le L \tag{129}$$

and for thermo-elastic constitutive relationship the stress becomes

$$\sigma(\mathrm{x}) = E\alpha\Delta T\left(\frac{\psi\, cosh\big(\psi(x-x_0)\big)}{\psi\, cosh\big(\psi(L-x_0)\big)+\frac{K_h}{E}\sinh\big(\psi(L-x_0)\big)}-1\right) \quad 0\le x\le L \tag{130}$$

where x_0 is

$$x_0 = \frac{1}{\psi}tanh^{-1}\left(\frac{\psi\cosh(\psi L)+\frac{K_h}{E}\sinh(\psi L)-\psi}{\psi\sinh(\psi L)+\frac{K_h}{E}\cosh(\psi L)+\frac{K_b}{E}}\right) \tag{131}$$

Again, the solutions for the thermal loading in the presence of head restraint reduce to the solutions for thermal loading in the absence of head restraint by setting $K_h = 0$.

Layered Soil Profile

This section covers a soil profile comprising four layers underlain by the bedrock that is not infinitely stiff. Resting on bed rock that is not infinitely stiff. The bottom boundary condition is given by

$$K_b u_1(0) = \sigma_1(0) \tag{132}$$

The displacement and stress compatibility conditions, which were given in Eq. (55) hold for the present case as well.

Thermal Load

This loading condition takes into account only the loading due to the temperature change of the pile relative to the soil. Since the bedrock is not infinitely stiff the null point is located above the pile tip, and its location is not known a priori. To solve for the null point it is first assumed that it is located in each of the four layers. Once the solutions are obtained they are checked against the actual parameters, which subsequently indicates the correct location of the null point. The boundary condition at the pile head was given by Eq. (54). In addition, for i-th layer (i = 1 through 4) the displacement and stress compatibility conditions are enforced at the null point in local coordinates x_{iT} and x_{iB} that are shown in Figure 2.8 as follows

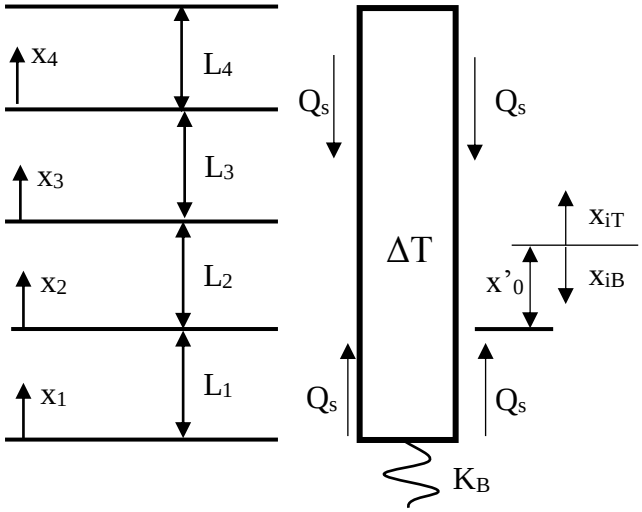

Figure 2.8 FBD of Semi Floating Pile Embedded into the Layered Soil Profile Subjected to Thermal Loading (ΔT > 0)

$$u_{iB}(0) = u_{iT}(0) = 0, \sigma_{iB}(0) = \sigma_{iT}(0) \tag{133}$$

Applying Eq. (133) to Eq. (52) results in

$$C_{2iT} = C_{2iB} = -C_{1iT} \tag{134}$$

$$C_{1iB} = C_{1iT} \tag{135}$$

The constants are finally determined from the compatibility of displacements and stresses at the interface of different layers (Eq. (55)). For the first layer above the null point

$$C_{1(i+1)} = C_{1iT}\left(sinh\left(\Psi_i(L_i - x'_0)\right) + \frac{\Psi_i}{\Psi_{(i+1)}} cosh\left(\Psi_i(L_i - x'_0)\right)\right) \tag{136}$$

$$C_{2(i+1)} = C_{1iT}\left(sinh\left(\Psi_i(L_i - x'_0)\right) - \frac{\Psi_i}{\Psi_{(i+1)}} cosh\left(\Psi_i(L_i - x'_0)\right)\right) \tag{137}$$

where x'_0 is given by

$$x'_0 = x_0 - \sum_{i=1}^{n-1} L_i \tag{138}$$

for null point located in the n-th layer. Let

$$sinh\left(\Psi_i(L_i - x'_0)\right) = SH_{iT} \tag{139}$$

$$cosh\left(\Psi_i(L_i - x'_0)\right) = CH_{iT} \tag{140}$$

The constants for the second layer two above the null point are

$$C_{1(i+2)} = C_{1iT}\left(SH_{iT}\left(CH_{(i+1)} + \frac{\Psi_{(i+1)}}{\Psi_{(i+2)}} SH_{(i+1)}\right) + CH_{iT}\left(\frac{\Psi_i}{\Psi_{(i+1)}} SH_{(i+1)} + \frac{\Psi_i}{\Psi_{(i+2)}} CH_{(i+1)}\right)\right) \tag{141}$$

$$C_{2(i+2)} = C_{1iT}\left(SH_{iT}\left(CH_{(i+1)} - \frac{\Psi_{(i+1)}}{\Psi_{(i+2)}}SH_{(i+1)}\right) + CH_{iT}\left(\frac{\Psi_i}{\Psi_{(i+1)}}SH_{(i+1)} - \frac{\Psi_i}{\Psi_{(i+2)}}CH_{(i+1)}\right)\right) \tag{142}$$

The constants for the third layer above the null point are

$$C_{1(i+3)} = C_{1iT}\left(\left(\Psi_{(i+1)}SH_{iT}SH_{(i+1)} + \Psi_i CH_{iT}CH_{(i+1)}\right)\left(\frac{SH_{(i+2)}}{\Psi_{(i+2)}} + \frac{CH_{(i+2)}}{\Psi_{(i+3)}}\right) + \left(SH_{iT}CH_{(i+1)} + \frac{\Psi_i}{\Psi_{(i+1)}}CH_{iT}SH_{(i+1)}\right)\left(CH_{(i+2)} + \frac{\Psi_{(i+2)}}{\Psi_{(i+3)}}SH_{(i+2)}\right)\right) \tag{143}$$

$$C_{2(i+3)} = C_{1iT}\left(\left(\Psi_{(i+1)}SH_{iT}SH_{(i+1)} + \Psi_i CH_{iT}CH_{(i+1)}\right)\left(\frac{SH_{(i+2)}}{\Psi_{(i+2)}} - \frac{CH_{(i+2)}}{\Psi_{(i+3)}}\right) + \left(SH_{iT}CH_{(i+1)} + \frac{\Psi_i}{\Psi_{(i+1)}}CH_{iT}SH_{(i+1)}\right)\left(CH_{(i+2)} - \frac{\Psi_{(i+2)}}{\Psi_{(i+3)}}SH_{(i+2)}\right)\right) \tag{144}$$

In general the constants of a subsequent layer in terms of the previous layer were given by Eq. (56) and Eq. (57) provided that both layers are above the null point. The constants for the first layer below the null point are

$$C_{1(i-1)} = C_{1iT}\left(\sinh(\Psi_i x'_0) + \frac{\Psi_i}{\Psi_{(i-1)}}cosh(\Psi_i x'_0)\right) \tag{145}$$

$$C_{2(i-1)} = C_{1iT}\left(\sinh(\Psi_i x'_0) - \frac{\Psi_i}{\Psi_{(i-1)}}cosh(\Psi_i x'_0)\right) \tag{146}$$

Let

$$sinh(\Psi_i x'_0) = SH_{iB} \tag{147}$$

$$cosh(\Psi_i x'_0) = CH_{iB} \tag{148}$$

The constants for the second layer below the null point are

$$C_{1(i-2)} = C_{1iT}\left(SH_{iB}\left(CH_{(i-1)} + \frac{\Psi_{(i-1)}}{\Psi_{(i-2)}}SH_{(i-1)}\right) + CH_{iB}\left(\frac{\Psi_i}{\Psi_{(i-1)}}SH_{(i-1)} + \frac{\Psi_i}{\Psi_{(i-2)}}CH_{(i-1)}\right)\right) \tag{149}$$

$$C_{2(i-2)} = C_{1iT}\left(SH_{iB}\left(CH_{(i-1)} - \frac{\Psi_{(i-1)}}{\Psi_{(i-2)}}SH_{(i-1)}\right) + CH_{iB}\left(\frac{\Psi_i}{\Psi_{(i-1)}}SH_{(i-1)} - \frac{\Psi_i}{\Psi_{(i-2)}}CH_{(i-1)}\right)\right) \tag{150}$$

The constants for the third layer below the null point are

$$C_{1(i-3)} = C_{1iT}\left(\left(\Psi_{(i-1)}SH_{iB}SH_{(i-1)} + \Psi_i CH_{iB}CH_{(i-1)}\right)\left(\frac{SH_{(i-2)}}{\Psi_{(i-2)}} + \frac{CH_{(i-2)}}{\Psi_{(i-3)}}\right) + \left(SH_{iB}CH_{(i-1)} + \frac{\Psi_i}{\Psi_{(i-1)}}CH_{iB}SH_{(i-1)}\right)\left(CH_{(i-2)} + \frac{\Psi_{(i-2)}}{\Psi_{(i-3)}}SH_{(i-2)}\right)\right) \tag{151}$$

$$C_{2(i-3)} = C_{1iT}\left(\left(\Psi_{(i-1)}SH_{iB}SH_{(i-1)} + \Psi_i CH_{iB}CH_{(i-1)}\right)\left(\frac{SH_{(i-2)}}{\Psi_{(i-2)}} - \frac{CH_{(i-2)}}{\Psi_{(i-3)}}\right) + \left(SH_{iB}CH_{(i-1)} + \frac{\Psi_i}{\Psi_{(i-1)}}CH_{iB}SH_{(i-1)}\right)\left(CH_{(i-2)} - \frac{\Psi_{(i-2)}}{\Psi_{(i-3)}}SH_{(i-2)}\right)\right) \tag{152}$$

In general the constants of the previous layer in terms of the subsequent layer are

$$C_{1(i-1)} = \frac{1}{2}\left(C_{1i}e^{\Psi_i L_i}\left(1 + \frac{\Psi_i}{\Psi_{(i-1)}}\right) + C_{2i}e^{-\Psi_i L_i}\left(1 - \frac{\Psi_i}{\Psi_{(i-1)}}\right)\right) \tag{153}$$

$$C_{2(i-1)} = \frac{1}{2}\left(C_{1i}e^{\Psi_i L_i}\left(1-\frac{\Psi_i}{\Psi_{(i-1)}}\right)+C_{2i}e^{-\Psi_i L_i}\left(1+\frac{\Psi_i}{\Psi_{(i-1)}}\right)\right) \tag{154}$$

provided that both layers are blow the null point.

Using the top boundary condition from Eq. (54) and the above constants it was obtained that C_{1iT} for the null point in each layer is

$$C_{11T} = \frac{\alpha\Delta T}{2}\left(\left(SH_{1T}CH_2+\frac{\Psi_1}{\Psi_2}CH_{1T}SH_2\right)(\Psi_4 CH_3 SH_4+\Psi_3 SH_3 CH_4)+(\Psi_2 SH_{1T}SH_2+\Psi_1 CH_{1T}CH_2)\left(\frac{\Psi_4}{\Psi_3}SH_3SH_4+CH_3CH_4\right)\right)^{-1} \tag{155}$$

$$C_{12T} = \frac{\alpha\Delta T}{2}\left(SH_{2T}(\Psi_4 CH_3 SH_4+\Psi_3 SH_3 CH_4)+\Psi_2 CH_{2T}\left(\frac{\Psi_4}{\Psi_3}SH_3SH_4+CH_3CH_4\right)\right)^{-1} \tag{156}$$

$$C_{13T} = \frac{\alpha\Delta T}{2}(\Psi_4 SH_{3T}SH_4+\Psi_3 CH_{3T}CH_4)^{-1} \tag{157}$$

$$C_{14T} = \frac{\alpha\Delta T}{2\,\Psi_4 CH_{4T}} \tag{158}$$

If a general forms for C_{11}, C_{21}, and C_{1iT} are taken as

$$C_{11} = C_{1iT}\left(SH_{iT}(a+b)+CH_{iT}(c+d)\right) \tag{159}$$

$$C_{21} = C_{1iT}\left(SH_{iT}(a-b)+CH_{iT}(c-d)\right) \tag{160}$$

$$C_{1iT} = \frac{\alpha\Delta T}{2}(SH_{iT}*f+CH_{iT}*g)^{-1} \tag{161}$$

Using the bottom boundary condition from Eq. (136) a general form for x'_0 is found to be

$$x'_0 = \frac{1}{\Psi_i}\tanh^{-1}\left(\frac{fSH_i+gCH_i-\left(c\left(\Psi_1SH_1+\frac{K_b}{E}CH_1\right)+d\left(\Psi_1CH_1+\frac{K_b}{E}SH_1\right)\right)}{fCH_i+gSH_i+a\left(\Psi_1SH_1+\frac{K_b}{E}CH_1\right)+b\left(\Psi_1CH_1+\frac{K_b}{E}SH_1\right)}\right) \tag{162}$$

Using *i*=1 and combining it with Eqs. (136), (137), and (155) and letting

$$Z_1 = CH_3CH_4 + \frac{\Psi_4}{\Psi_3}SH_3SH_4 \tag{163}$$

$$Z_2 = \Psi_3SH_3CH_4 + \Psi_4CH_3SH_4 \tag{164}$$

x'_0 is found to be

$$x'_0 = \frac{1}{\Psi_1}\tanh^{-1}\left(\frac{Z_1(\Psi_2SH_1SH_2+\Psi_1CH_1CH_2)+Z_2\left(SH_1CH_2+\frac{\Psi_1}{\Psi_2}CH_1SH_2\right)-\frac{K_b}{E}}{Z_1(\Psi_2CH_1SH_2+\Psi_1SH_1CH_2)+Z_2\left(CH_1CH_2+\frac{\Psi_1}{\Psi_2}SH_1SH_2\right)+\Psi_1}\right) \tag{165}$$

if in layer one. Using *i*=2 along with $C_{1(i-1)}$, $C_{2(i-1)}$, and C_{12T} x'_0 is found to be

$$x'_0 = \frac{1}{\Psi_2}\tanh^{-1}\left(\frac{Z_1SH_2+Z_2\Psi_2CH_2-\left(\Psi_2CH_1+\frac{K_b\Psi_2}{E\ \Psi_1}SH_1\right)}{Z_1CH_2+Z_2\Psi_2SH_2+\Psi_1SH_1+\frac{K_b}{E}CH_1}\right) \tag{166}$$

When *i*=3 with $C_{1(i-2)}$, $C_{2(i-2)}$, and C_{13T} x'_0 is found to be

$$x'_0 = \frac{1}{\Psi_3}\tanh^{-1}\left(\frac{\Psi_4SH_4SH_3+\Psi_3CH_4CH_3-\left(\frac{\Psi_3}{\Psi_2}SH_2\left(\Psi_1SH_1+\frac{K_b}{E}CH_1\right)+\frac{\Psi_3}{\Psi_1}CH_2\left(\Psi_1CH_1+\frac{K_b}{E}SH_1\right)\right)}{Z_2+CH_2\left(\Psi_1SH_1+\frac{K_b}{E}CH_1\right)+\frac{\Psi_2}{\Psi_3}SH_2\left(\Psi_1CH_1+\frac{K_b}{E}SH_1\right)}\right) \tag{167}$$

For *i*=4 with $C_{1(i-3)}$, $C_{2(i-3)}$, and C_{14T} x'_0 is found to be

$$x'_0 = \frac{1}{\Psi_4}\tanh^{-1}\left(\frac{CH_4-\Psi_4\left(\left(\frac{CH_2SH_3}{\Psi_3}+\frac{SH_2CH_3}{\Psi_2}\right)\left(\Psi_1SH_1+\frac{K_b}{E}CH_1\right)+\left(CH_2CH_3+\frac{\Psi_2}{\Psi_3}SH_2SH_3\right)\left(CH_1+\frac{K_bSH_1}{E\ \Psi_1}\right)\right)}{SH_4+\left(CH_2CH_3+\frac{\Psi_3}{\Psi_2}SH_2SH_3\right)\left(\Psi_1SH_1+\frac{K_b}{E}CH_1\right)+(\Psi_3CH_2SH_3+\Psi_2SH_2CH_3)\left(CH_1+\frac{K_bSH_1}{E\ \Psi_1}\right)}\right) \quad (168)$$

Mechanical Load

This loading condition only takes into account an axial compressive force applied to the head of the energy pile. The pile tip is resting on the bedrock that is not infinitely stiff. The entire pile moves downward, thus resulting in the absence of null point for this loading condition. The bottom boundary condition was given by Eq. (132) while the top boundary condition is described by Eq. (169)

$$\sigma_4(L_4) = \frac{F}{A} \quad (169)$$

The solutions are obtained after applying the boundary conditions to Eqs. (74) and (75) and letting

$$\lambda = \frac{E\Psi_1 - K_b}{E\Psi_1 + K_b} \quad (170)$$

$$e^{\Psi_i L_i}\left(1+\frac{\Psi_i}{\Psi_{(i+1)}}\right) = ep_i \quad (171)$$

$$e^{\Psi_i L_i}\left(1-\frac{\Psi_i}{\Psi_{(i+1)}}\right) = em_i \quad (172)$$

$$e^{-\Psi_i L_i}\left(1+\frac{\Psi_i}{\Psi_{(i+1)}}\right) = e^{-}p_i \quad (173)$$

$$e^{-\Psi_i L_i}\left(1-\frac{\Psi_i}{\Psi_{(i+1)}}\right)=e^{-}m_i \tag{174}$$

$$\begin{aligned}C_{11}=\frac{8F}{AE\Psi_4}\Big((ep_1+\lambda e^{-}m_1)\big((ep_2ep_3+em_2e^{-}m_3)e^{\Psi_4L_4}-(ep_2em_3+\\ em_2e^{-}p_3)e^{-\Psi_4L_4}\big)+(em_1+\lambda e^{-}p_1)\big((e^{-}m_2ep_3+e^{-}p_2e^{-}m_3)e^{\Psi_4L_4}-\\ (e^{-}m_2em_3+e^{-}p_2e^{-}p_3)e^{-\Psi_4L_4}\big)\Big)^{-1}\end{aligned} \tag{175}$$

The displacement, strain, and stress in the bottom or first layer are given by

$$u_1(x_1)=C_{11}(e^{\Psi_1x_1}+\lambda e^{-\Psi_1x_1}) \tag{176}$$

$$\varepsilon_1(x_1)=C_{11}\Psi_1(e^{\Psi_1x_1}-\lambda e^{-\Psi_1x_1}) \tag{177}$$

$$\sigma_1(x_1)=EC_{11}\Psi_1(e^{\Psi_1x_1}-\lambda e^{-\Psi_1x_1}) \tag{178}$$

The displacement, strain and stress in the second layer are given by

$$u_2(x_2)=\frac{C_{11}}{2}\big((ep_1+\lambda e^{-}m_1)e^{\Psi_2x_2}+(em_1+\lambda e^{-}p_1)e^{-\Psi_2x_2}\big) \tag{179}$$

$$\varepsilon_2(x_2)=C_{11}\frac{\Psi_2}{2}\big((ep_1+\lambda e^{-}m_1)e^{\Psi_2x_2}-(em_1+\lambda e^{-}p_1)e^{-\Psi_2x_2}\big) \tag{180}$$

$$\sigma_2(x_2)=EC_{11}\frac{\Psi_2}{2}\big((ep_1+\lambda e^{-}m_1)e^{\Psi_2x_2}-(em_1+\lambda e^{-}p_1)e^{-\Psi_2x_2}\big) \tag{181}$$

The displacement, strain, and stress in the third layer are

$$\begin{aligned}u_3(x_3)=\frac{C_{11}}{4}\Big((ep_1+\lambda e^{-}m_1)(ep_2e^{\Psi_3x_3}+em_2e^{-\Psi_3x_3})\\ +(em_1+\lambda e^{-}p_1)(e^{-}m_2e^{\Psi_3x_3}+e^{-}p_2e^{-\Psi_3x_3})\Big)\end{aligned} \tag{182}$$

$$\varepsilon_3(x_3) = C_{11}\frac{\Psi_3}{4}\big((ep_1 + \lambda e^{-}m_1)(ep_2 e^{\Psi_3 x_3} - em_2 e^{-\Psi_3 x_3}) + (em_1 + \lambda e^{-}p_1)(e^{-}m_2 e^{\Psi_3 x_3} - e^{-}p_2 e^{-\Psi_3 x_3})\big) \tag{183}$$

$$\sigma_3(x_3) = EC_{11}\frac{\Psi_3}{4}\big((ep_1 + \lambda e^{-}m_1)(ep_2 e^{\Psi_3 x_3} - em_2 e^{-\Psi_3 x_3}) + (em_1 + \lambda e^{-}p_1)(e^{-}m_2 e^{\Psi_3 x_3} - e^{-}p_2 e^{-\Psi_3 x_3})\big) \tag{184}$$

The displacement, strain, and stress in the top of the fourth layer are

$$u_4(x_4) = \frac{C_{11}}{8}\Big(\big((ep_1 + \lambda e^{-}m_1)ep_2 + (em_1 + \lambda e^{-}p_1)e^{-}m_2\big)(ep_3 e^{\Psi_4 x_4} + em_3 e^{-\Psi_4 x_4}) + \big((ep_1 + \lambda e^{-}m_1)em_2 + (em_1 + \lambda e^{-}p_1)e^{-}p_2\big)(e^{-}m_3 e^{\Psi_4 x_4} + e^{-}p_3 e^{-\Psi_4 x_4})\Big) \tag{185}$$

$$\varepsilon_4(x_4) = C_{11}\frac{\Psi_4}{8}\Big(\big((ep_1 + \lambda e^{-}m_1)ep_2 + (em_1 + \lambda e^{-}p_1)e^{-}m_2\big)(ep_3 e^{\Psi_4 x_4} - em_3 e^{-\Psi_4 x_4}) + \big((ep_1 + \lambda e^{-}m_1)em_2 + (em_1 + \lambda e^{-}p_1)e^{-}p_2\big)(e^{-}m_3 e^{\Psi_4 x_4} - e^{-}p_3 e^{-\Psi_4 x_4})\Big) \tag{186}$$

$$\sigma_4(x_4) = EC_{11}\frac{\Psi_4}{8}\Big(\big((ep_1 + \lambda e^{-}m_1)ep_2 + (em_1 + \lambda e^{-}p_1)e^{-}m_2\big)(ep_3 e^{\Psi_4 x_4} - em_3 e^{-\Psi_4 x_4}) + \big((ep_1 + \lambda e^{-}m_1)em_2 + (em_1 + \lambda e^{-}p_1)e^{-}p_2\big)(e^{-}m_3 e^{\Psi_4 x_4} - e^{-}p_3 e^{-\Psi_4 x_4})\Big) \tag{187}$$

Thermal Load with Head Restraint

This load combination is the same as the thermal load except for the boundary condition at the pile head. To this end, a normal spring having stiffness K_h is attached to the pile head to

represent the restraint to its free movement that may be imposed by the superstructure. The boundary condition at the pile head is given by

$$K_h u_4(L_4) = -\sigma_4(L_4) \tag{188}$$

Using the top boundary condition given by Eq. (188) and Eqs. (134) through (144) where C_{14} and C_{24} are given by

$$C_{14} = C_{1iT}\big(SH_{iT}(a+b) + CH_{iT}(c+d)\big) \tag{189}$$

$$C_{24} = C_{1iT}\big(SH_{iT}(a-b) + CH_{iT}(c-d)\big) \tag{190}$$

along with *a*, *b*, *c*, and *d* being given in Table 2-1 the general from for C_{1iT} was found to be

$$C_{1iT} = \frac{\alpha\Delta T}{2}\big(SH_{iT}(f+g) + CH_{iT}(h+j)\big)^{-1} \tag{191}$$

where

$$f = \Psi_4(aSH_4 + bCH_4) \tag{192}$$

$$g = \frac{K_h}{E}(aCH_4 + bSH_4) \tag{193}$$

$$h = \Psi_4(cSH_4 + dCH_4) \tag{194}$$

$$j = \frac{K_h}{E}(cCH_4 + dSH_4) \tag{195}$$

The exact form C_{1iT} in each layer is

$$C_{11T} = \frac{\alpha\Delta T}{2}\Bigg(SH_{1T}\Bigg(\Big(\frac{\Psi_2}{\Psi_3}SH_2SH_3 + CH_2CH_3\Big)\Big(\Psi_4SH_4 + \frac{K_h}{E}CH_4\Big) + (\Psi_2SH_2CH_3 + \Psi_3CH_2SH_3)\Big(CH_4 + \frac{K_h}{E}\frac{SH_4}{\Psi_4}\Big)\Bigg) + CH_{1T}\Psi_1\Bigg(\Big(\frac{SH_2CH_3}{\Psi_2} + \frac{CH_2SH_3}{\Psi_3}\Big)\Big(\Psi_4SH_4 + \frac{K_h}{E}CH_4\Big) + \Big(\frac{\Psi_3}{\Psi_2}SH_2SH_3 + CH_2CH_3\Big)\Big(CH_4 + \frac{K_h}{E}\frac{SH_4}{\Psi_4}\Big)\Bigg)\Bigg)^{-1} \tag{196}$$

$$C_{12T} = \frac{\alpha\Delta T}{2}\Bigg(SH_{2T}\Bigg(\Psi_4CH_3SH_4 + \Psi_3SH_3CH_4 + \frac{K_h}{E}\Big(CH_3CH_4 + \frac{\Psi_3}{\Psi_4}SH_3SH_4\Big)\Bigg) + CH_{2T}\Psi_2\Bigg(\frac{\Psi_4}{\Psi_3}SH_3SH_4 + CH_3CH_4 + \frac{K_h}{E}\Big(\frac{SH_3CH_4}{\Psi_3} + \frac{CH_3SH_4}{\Psi_4}\Big)\Bigg)\Bigg)^{-1} \tag{197}$$

$$C_{13T} = \frac{\alpha\Delta T}{2}\Bigg(SH_{3T}\Big(\Psi_4SH_4 + \frac{K_h}{E}CH_4\Big) + CH_{3T}\Psi_3\Big(CH_4 + \frac{K_h}{E}\frac{SH_4}{\Psi_4}\Big)\Bigg)^{-1} \tag{198}$$

$$C_{14T} = \frac{\alpha\Delta T}{2}\Big(\Psi_4CH_{4T} + \frac{K_h}{E}SH_{4T}\Big)^{-1} \tag{199}$$

As general forms of C_{11} and C_{21} are given by

$$C_{11} = C_{1iT}\big(SH_{iB}(l+m) + CH_{iB}(n+o)\big) \tag{200}$$

$$C_{21} = C_{1iT}\big(SH_{iB}(l-m) + CH_{iB}(n-o)\big) \tag{201}$$

where *l*, *m*, *n*, and *o* are given in Table 2-1. By using the bottom boundary condition given by Eq. (132) a general form for x'_0 is found to be:

$$x'_0 = \frac{1}{\Psi_i}\,tanh\left(\frac{SH_i(f+g)+CH_i(h+j)-\Big(n\Big(\Psi_1SH_1+\frac{K_b}{E}CH_1\Big)+o\Big(\Psi_1CH_1+\frac{K_b}{E}SH_1\Big)\Big)}{CH_i(f+g)+SH_i(h+j)+l\Big(\Psi_1SH_1+\frac{K_b}{E}CH_1\Big)+m\Big(\Psi_1CH_1+\frac{K_b}{E}SH_1\Big)}\right) \tag{202}$$

Table 2-1 gives the values of *a* through *d* and *l* through *o* with x'_0 being in layer 1-4 of a four layer system.

Table 2-1 Coefficient for C_{1iT} and x'_0

Variable	Layer of x'_0			
	1	2	3	4
a	$\frac{\Psi_2}{\Psi_3}SH_2SH_3 + CH_2CH_3$	CH_3	1	CH_4
b	$\frac{\Psi_2}{\Psi_4}SH_2CH_3 + \frac{\Psi_3}{\Psi_4}CH_2SH_3$	$\frac{\Psi_3}{\Psi_4}SH_3$	0	$-SH_4$
c	$\frac{\Psi_1}{\Psi_2}SH_2CH_3 + \frac{\Psi_1}{\Psi_3}CH_2SH_3$	$\frac{\Psi_2}{\Psi_3}SH_3$	0	$-SH_4$
d	$\frac{\Psi_1}{\Psi_4}\left(\frac{\Psi_3}{\Psi_2}SH_2SH_3 + CH_2CH_3\right)$	$\frac{\Psi_2}{\Psi_4}CH_3$	$\frac{\Psi_3}{\Psi_4}$	CH_4
l	CH_1	1	CH_2	$\frac{\Psi_3}{\Psi_2}SH_2SH_3 + CH_2CH_3$
m	$-SH_1$	0	$\frac{\Psi_2}{\Psi_1}SH_2$	$\frac{\Psi_2}{\Psi_1}SH_2CH_3 + \frac{\Psi_3}{\Psi_1}CH_2SH_3$
n	$-SH_1$	0	$\frac{\Psi_3}{\Psi_2}SH_2$	$\frac{\Psi_4}{\Psi_2}SH_2CH_3 + \frac{\Psi_4}{\Psi_3}CH_2SH_3$
o	CH_1	$\frac{\Psi_2}{\Psi_1}$	$\frac{\Psi_3}{\Psi_1}CH_2$	$\frac{\Psi_4}{\Psi_1}\left(\frac{\Psi_2}{\Psi_3}SH_2SH_3 + CH_2CH_3\right)$

Chapter 3 - Validation of the Analytical Solutions

In this chapter the analytical solutions developed in Chapter 2 are validated against full scale in situ pile tests (Laloui et al. 1999…site investigation report in French). A total of nine tests were performed at the Swiss Federal Institute of Technology in Lausanne, Switzerland. Only one out of a total 97 piles was constructed as energy pile (Laloui et al. 2006). The piles serve as a foundation to 30 m x 100 m four story building. These experiments were chosen for the validation due to the availability of a detailed site investigation report (Laloui et al. 1999) that contains results of laboratory tests and full scale field tests. The soil profile at the site is depicted in Fig. 3.1. The four soil layers shown in Fig. 3.1 were determined by Perić et al. (2017) to be low plasticity clays (CL) based on the site investigation report. The bedrock was described as claystone/sandstone by Laloui et al. (2003). Consequently, this soil profile is suitable for validation of the analytical solutions for end bearing and semi floating energy piles.

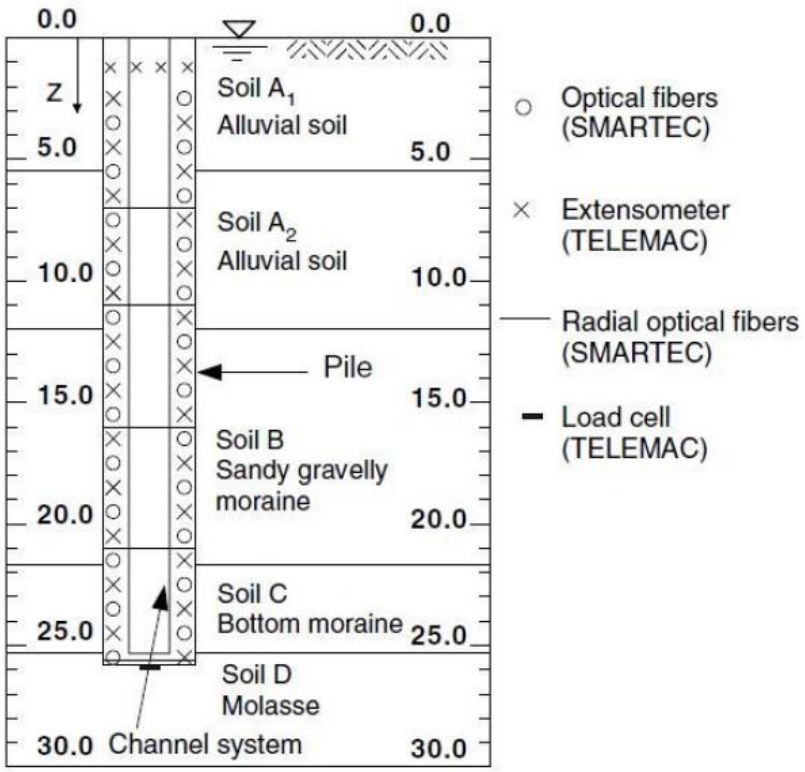

Figure 3.1 Soil Profile and Energy Pile Instrumentation (Laloui el al. 2006)

The stiffness of shear spring (K_s) representing the load transfer along the pile shaft and of normal spring (K_b) representing the load transfer at the pile tip are listed in Table 3-1. They were obtained from Knellwolf et al. (2011) based on the full scale field tests.

Table 3-1 Stiffness of Soil Substituting Springs

Property	Soil				
	A1	A2	B	C	D
Poisson's Ration, ν	0.22	0.22	0.49	0.49	0.157
Shear Spring Stiffness, K_s (MPa/m)	16.7	10.8	18.2	121.4	-
Normal Spring Stiffness, K_b (MPa/m)	-	-	-	-	125

Table 3-2 list the properties of the energy pile required by the analytical solutions. There were obtained from Laloui et al. (2006).

Table 3-2 Properties of Concrete

Property	Value
Young's Modulus, E (MPa)	29,200
Coefficient of Thermal Expansion, α (°C^{-1})	$1x10^{-5}$
Mass Density, γ_c (kg/m^3)	2500

As shown in Fig. 3.1 the bottom 0.5 m of the pile is embedded into the bedrock. In our model the bottom soil layer is simply extended by 0.5 m while two different boundary conditions at the pile tip are investigated. The first one is complete fixity and the other one is partial fixity of the pile tip.

Multiple heating and cooling cycles where applied to the energy pile as the building was being built. Nevertheless, only test T1 conducted before any of the building structure was completed and Test T7 conducted after the completion of the building are considered in this study. It is noted that test T1 involves only thermal loading while test T7 involves simultaneous thermal and mechanical loading. Histories of temperature difference (ΔT) for tests T1 and T7 are provided in Table 3-3. Validation of analytical solutions will be conducted at temperature differences of 3°C and 13.4°C during test T1 and 2°C and 14°C during test T7. As the building was not constructed during Test T1 both K_h and the mechanical load are taken to be zero. From structural analysis it is believed the building applies a 1.00 MN force to the pile during Test T7 (Knellwolf et al. 2011). Several values of K_h were used during validation based on the fit between the experimental data and analytical predictions.

Table 3-3 Experimental Head Displacement vs Time (Knellwolf et al. 2011)

Test T1			Test T7	
Time (days)	Temperature Difference (°C)	Head Displacement (mm)	Time (days)	Temperature Difference (°C)
0	0	-0.01	0	0
5	2	0.379	5	9
12	21	2.72	22	14
15	9	1.46	27	6
28	3	0.78	62	2

End Bearing Pile

In this section the bedrock present at the site, which is claystone/sandstone, is assumed to completely prevent the tip displacement. Perić et al. (2017) found from the computational model that the maximum tip displacement was under 0.2 mm during the test T1. Thus, the assumption of the complete fixity is not entirely correct. Nevertheless, the effects of this assumption can be evaluated by comparing the corresponding predictions with those resulting from the assumption of the partially fixed pile tip.

Homogeneous Soil Profile

As the experimental site was a layered system not a single homogeneous soil it is not expected that this analytical model will be representative; however, if the softest (A2) soil and

stiffest (C) soil are used over the entire length of the HEP it should be close to if not completely bound of the experimental results.

Test T1

Figures 3.2 and 3.3 show model predictions for vertical displacement of the pile versus depth for temperature changes of 3 °C and 13.4°C respectively during test T1. As expected the smallest displacement is consistently obtained for the stiffest soil (C) while the largest displacement is obtained for the softest soil (A2). Displacements or soils A1 and B are very close and they fall between displacements obtained for soils A2 and C. Furthermore, the larger the thermal load the less significant the effect of the self-weight is.

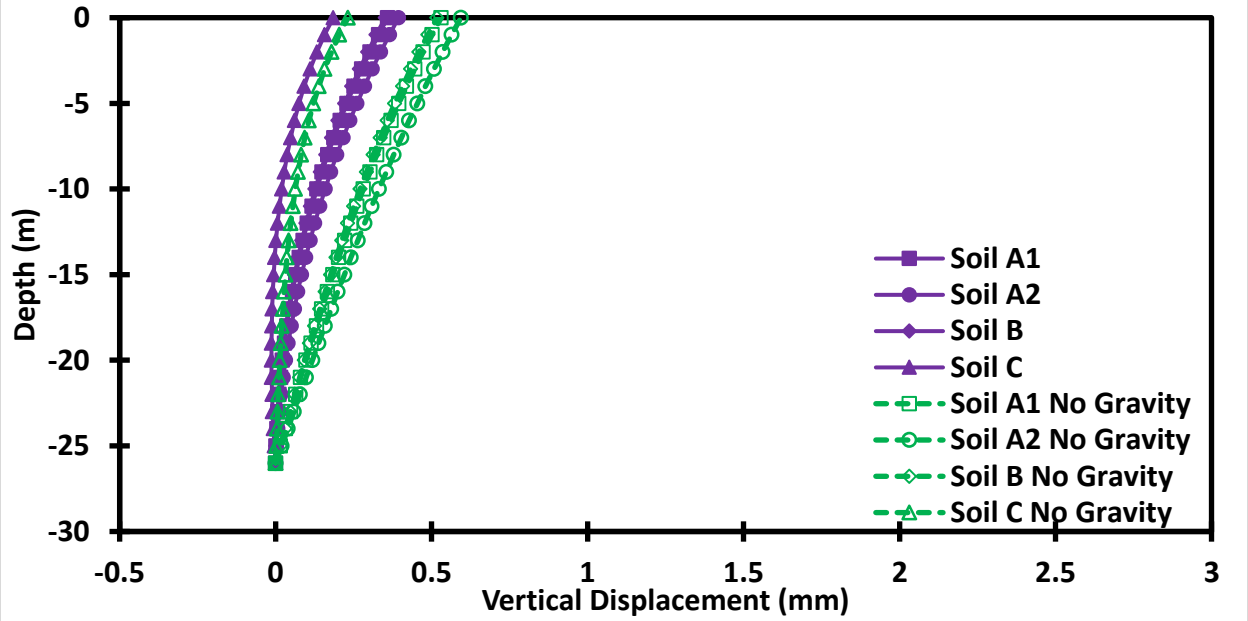

Figure 3.2 Displacement in End Bearing Pile Embedded in Homogeneous Soil (ΔT = 3°C, test T1)

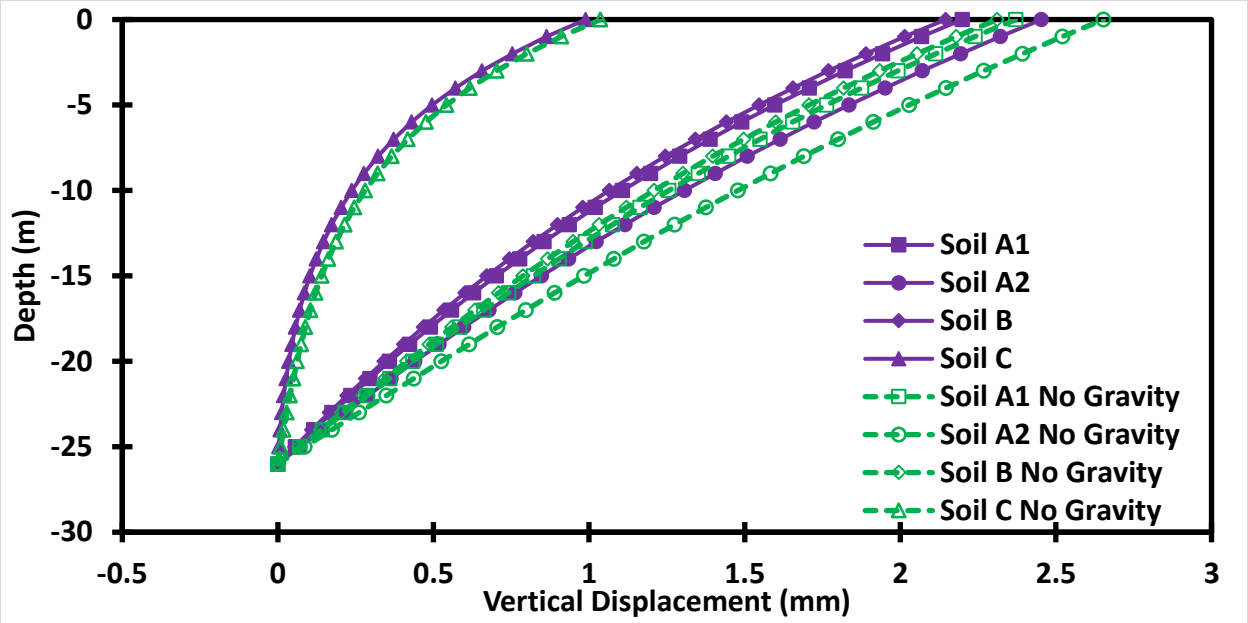

Figure 3.3 Displacement in End Bearing Pile Embedded in Homogeneous Soil (ΔT = 13.4°C, test T1)

Figures 3.4 and 3.5 show model predictions for vertical strain at temperature differences of 3°C and 13.4°C respectively during test T1. Again, the self-weight effect decreases with increasing magnitude of thermal load. Furthermore, it is noted that the head displacement is unaffected by the soil stiffness as it is always equal to so called free strain, which is in turn equal to $\alpha\Delta T$ (Eq.(22)). On the contrary the strain at the pile tip is smaller for a stiffer soil pile interface. For cases without the self-weight the absolute minimum value of strain occurs at the pile tip.

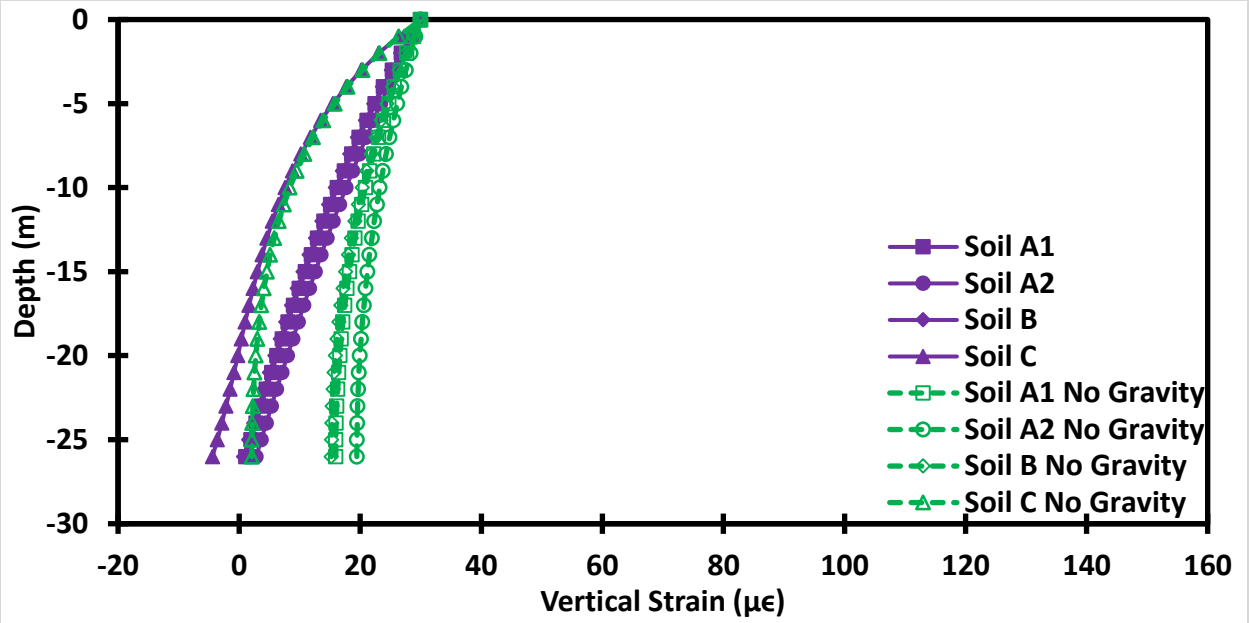

Figure 3.4 Strain in End Bearing Pile Embedded in Homogeneous Soil (ΔT = 3°C. test T1)

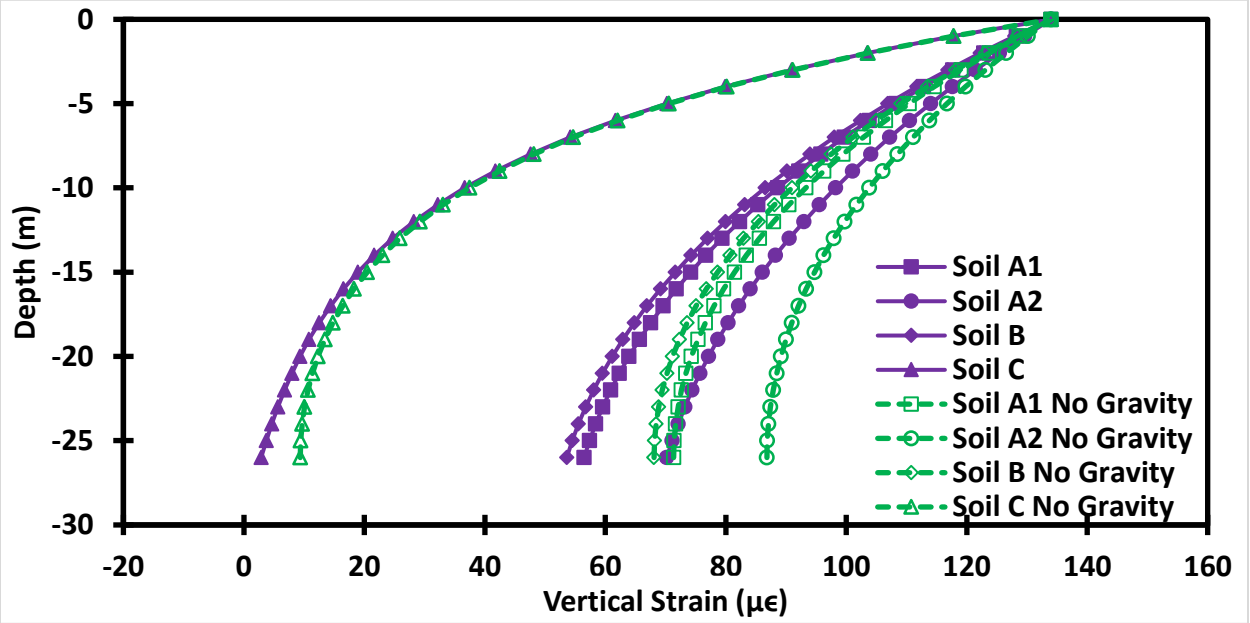

Figure 3.5 Strain in End Bearing Pile Embedded in Homogeneous Soil (ΔT = 13.4°C. test T1)

Figures 3.6 and 3.7 depict the model prediction for the vertical stress versus depth at temperature differences of 3°C and 13.4°C respectively during test T1. The effect of self-weight of the pile becomes less significant at thermal load increases. The stress at the pile head must be zero for all soils because there is no external load applied at the pile head. Nevertheless, the stiffer the soil the more rapidly the compressive stress increases with depth as shown in Figures 3.6 and 3.7. Furthermore, in the absence of gravity the absolute minimum value of vertical stress occurs at the pile tip.

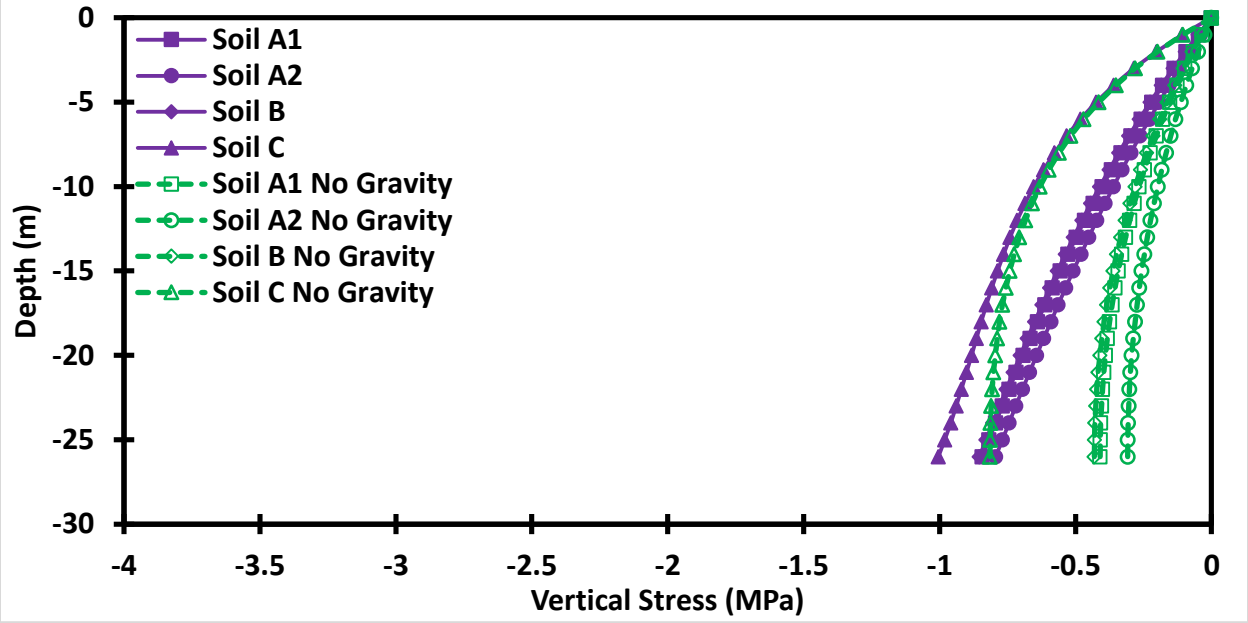

Figure 3.6 Stress in End Bearing Pile Embedded in Homogeneous Soil (ΔT = 3°C, test T1)

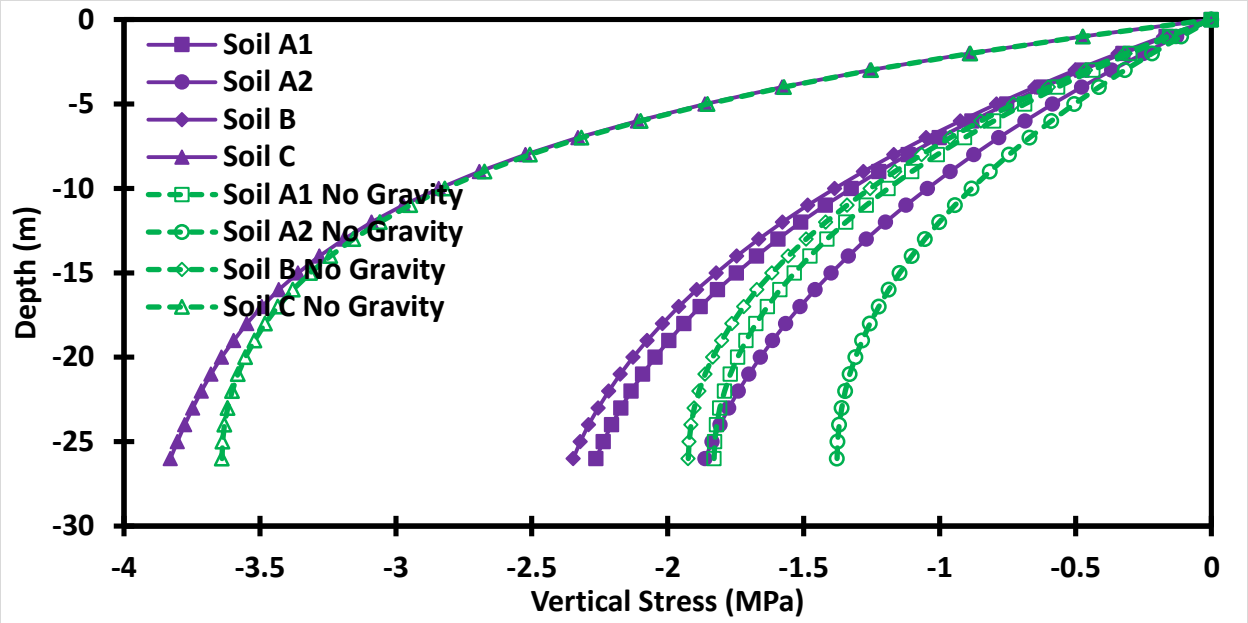

Figure 3.7 Stress in End Bearing Pile Embedded in Homogeneous Soil (ΔT = 13.4°C, test T1)

Figure 3.8 shows model prediction for the head displacement versus time during test T1. The stiffer the soil the less the pile head moves for a given temperature. It can also be observed that the larger the thermal load (Table 3-3) the larger the head displacement. Finally, the stiffer the soil or soil pile interface the smaller is the effect of gravity.

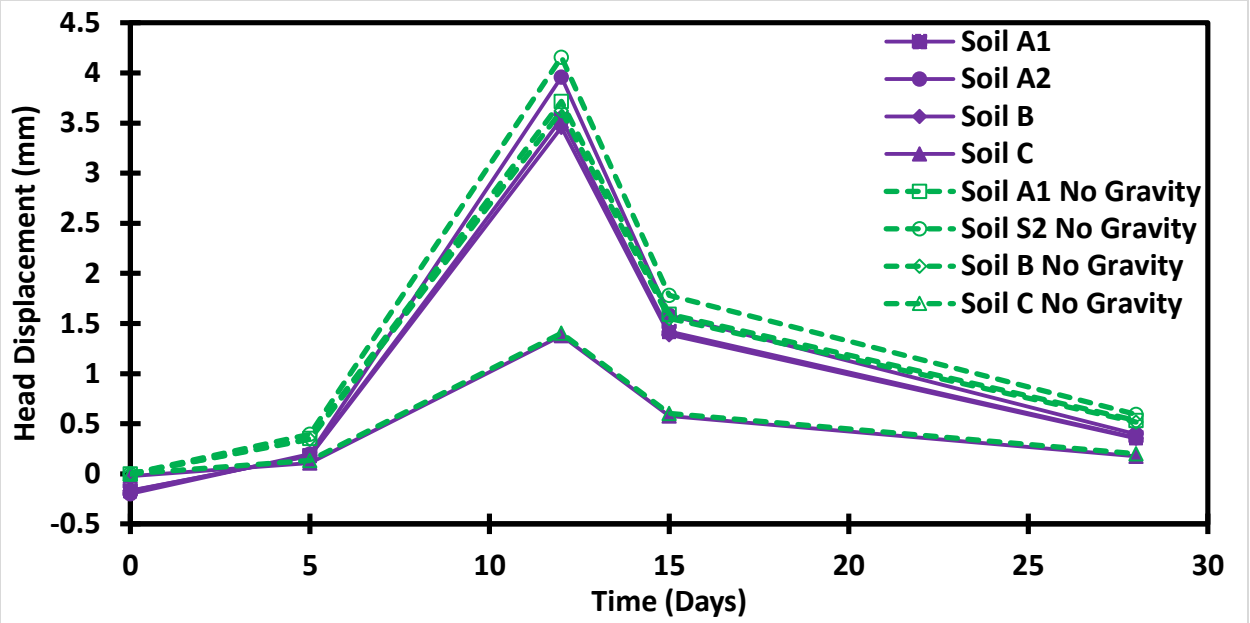

Figure 3.8 Head Displacement of End Bearing Pile Embedded in Homogenous Soil Profile (test T1)

Test T7

Since test T7 was conducted after the building was constructed the model predictions will do both, include and exclude the effects of head spring (K_h). The first set of graphs does not include the effects of K_h.

Figure 3.9 depicts the model predictions for vertical displacement versus depth at temperature difference of 2°C during test T7. It should be noted that T7 includes both thermal and mechanical loading. The later comprises compressive axial force of 1 MN applied at the

pile head. Nevertheless, all displacements are in a downward direction because mechanical load is dominant as compared to thermal load at the temperature difference of 2°C.

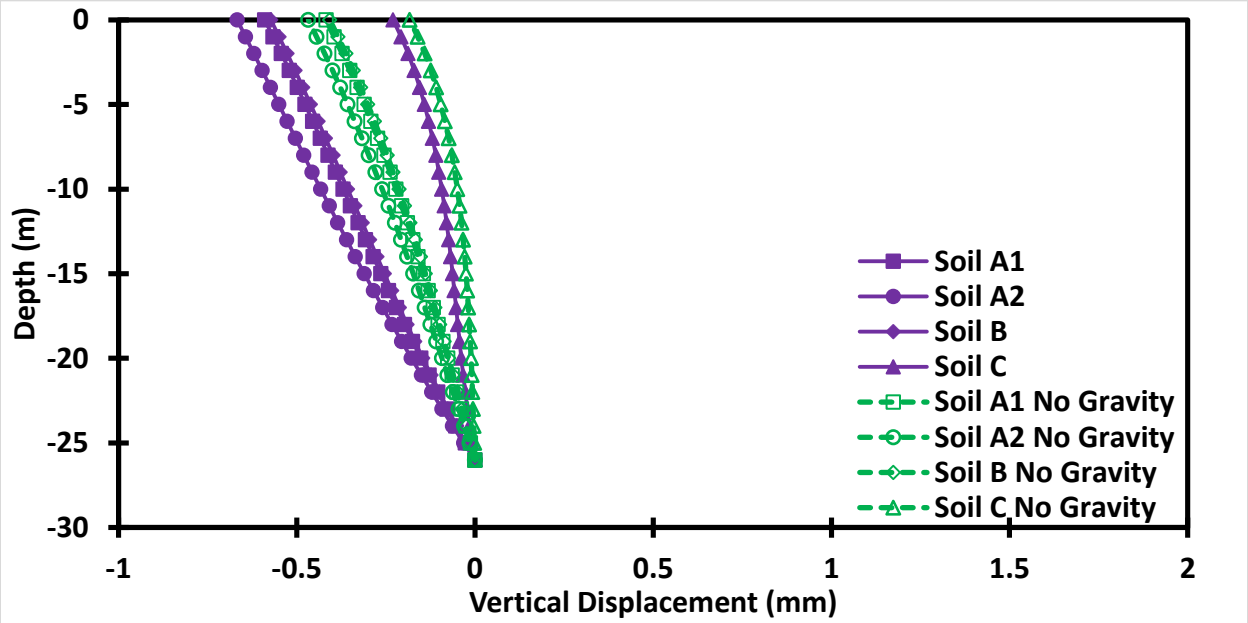

Figure 3.9 Displacement in End Bearing Pile Embedded in Homogenous Soil (ΔT = 2°C, test T7, K_h=0)

Figure 3.10 shows displacement versus depth at the temperature difference of 14°C during test T7. In this case all displacements point upward because thermal load is dominant at this larger temperature difference. Again, the effect of self-weight decreases with increasing thermal load.

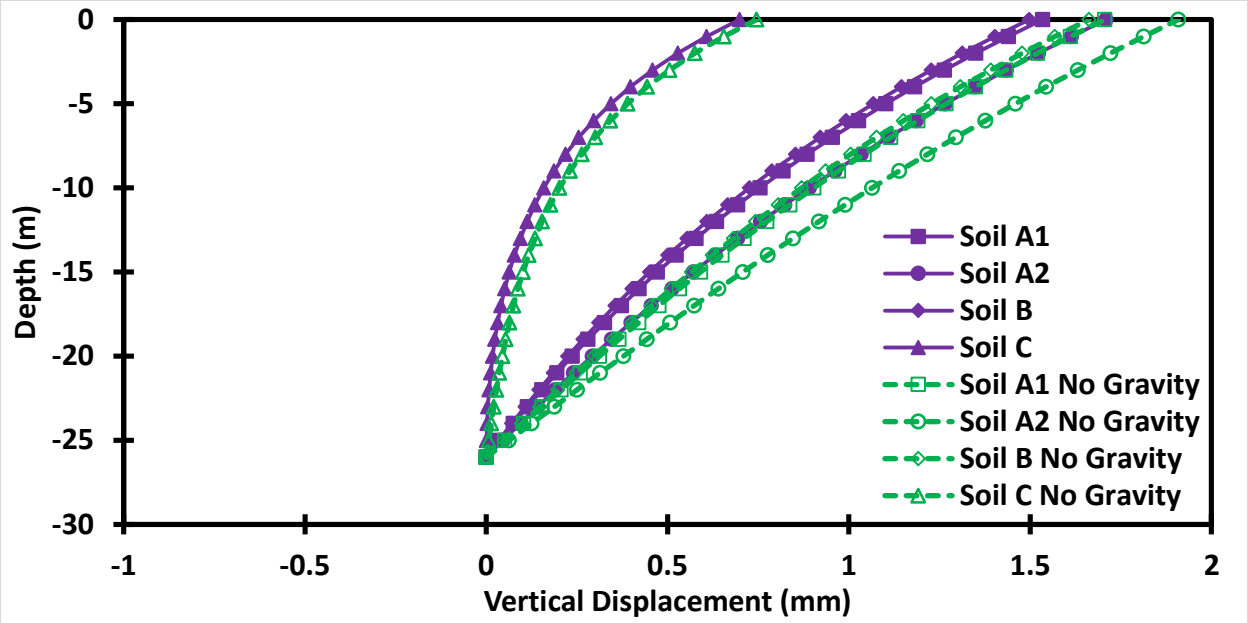

Figure 3.10 Displacement in End Bearing Pile Embedded in Homogeneous Soil (ΔT = 14°C, test T7, K_h=0)

Figure 3.11 shows strain at the temperature difference of 2°C during test T7. As expected effect of gravity is more pronounced in the bottom region of the pile. Furthermore, it is significant at ΔT = 2°C as it causes a qualitative change in the response curve.

Figure 3.12 depicts strain at the temperature difference of 14°C during test T7. It can be seen that the qualitative and quantitative difference between the case when self-weight is included and excluded is much smaller than at ΔT = 2°C. As expected the strains in Fig. 3.11 are compressive while strains in Fig. 3.12 are tensile.

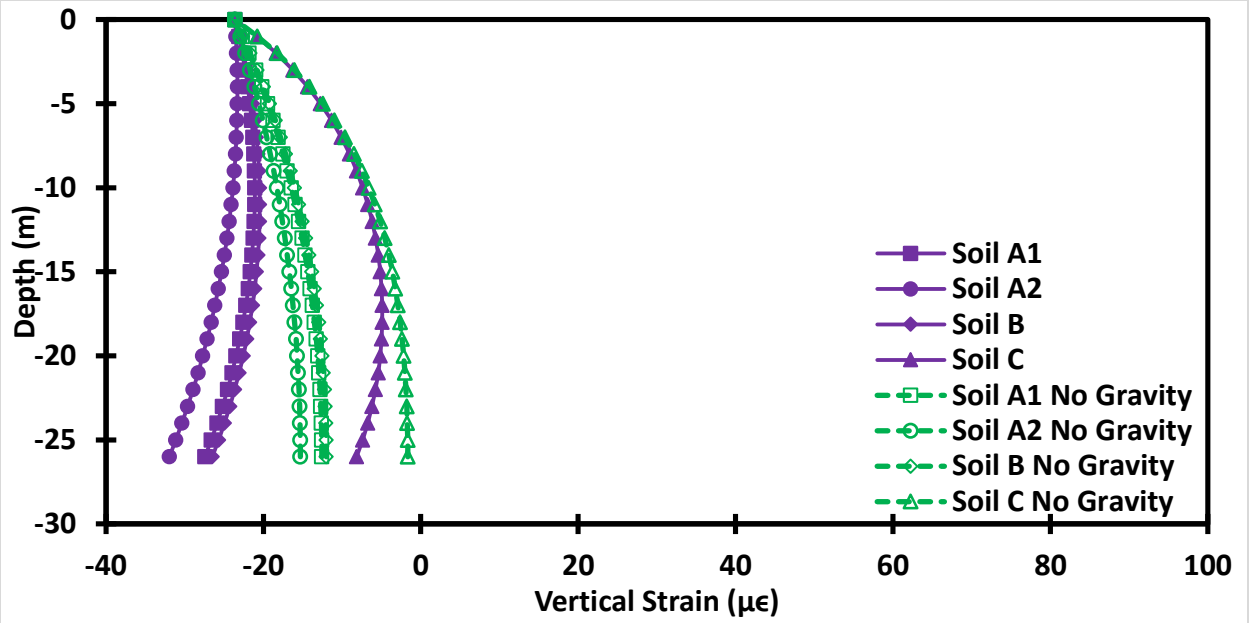

Figure 3.11 Strain in End Bearing Pile Embedded in Homogenous Soil (ΔT=2°C, test T7, K_h =0)

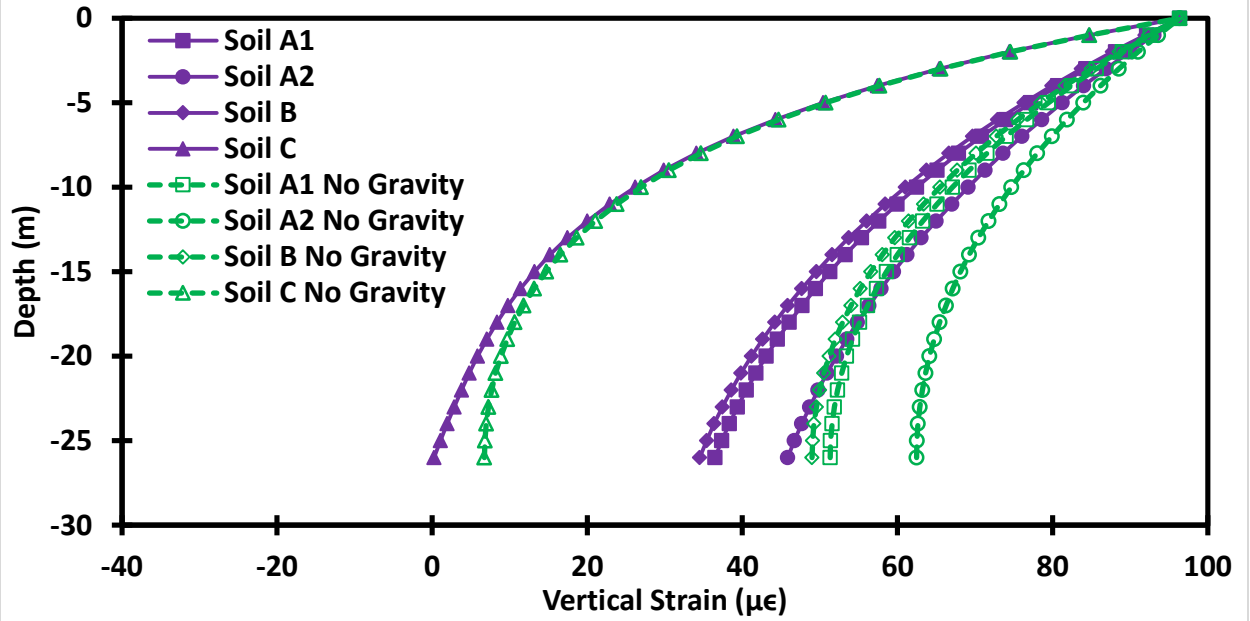

Figure 3.12 Strain in End Bearing Pile Embedded in Homogenous Soil (ΔT=14°C, test T7, K_h =0)

Figures 3.13 and 3.14 show how the stress at the pile head is only affected by the axial load on the pile and that the stiffer the soil the greater the difference between the stress at the head and tip of the pile. Whether the head or tip has the governing load is dependent on the magnitude of the axial load and maximum temperature difference but it will always be at one of these two points.

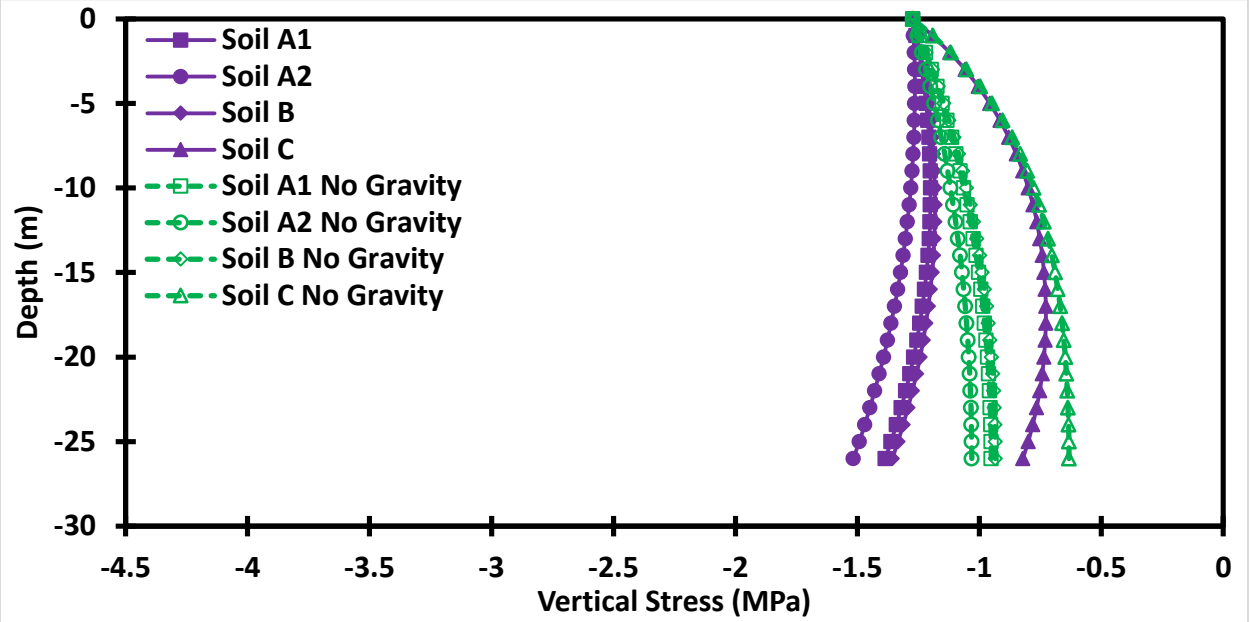

Figure 3.13 Stress in End Bearing Pile Embedded in Homogenous Soil (ΔT = 2°C, test T7, K_h=0)

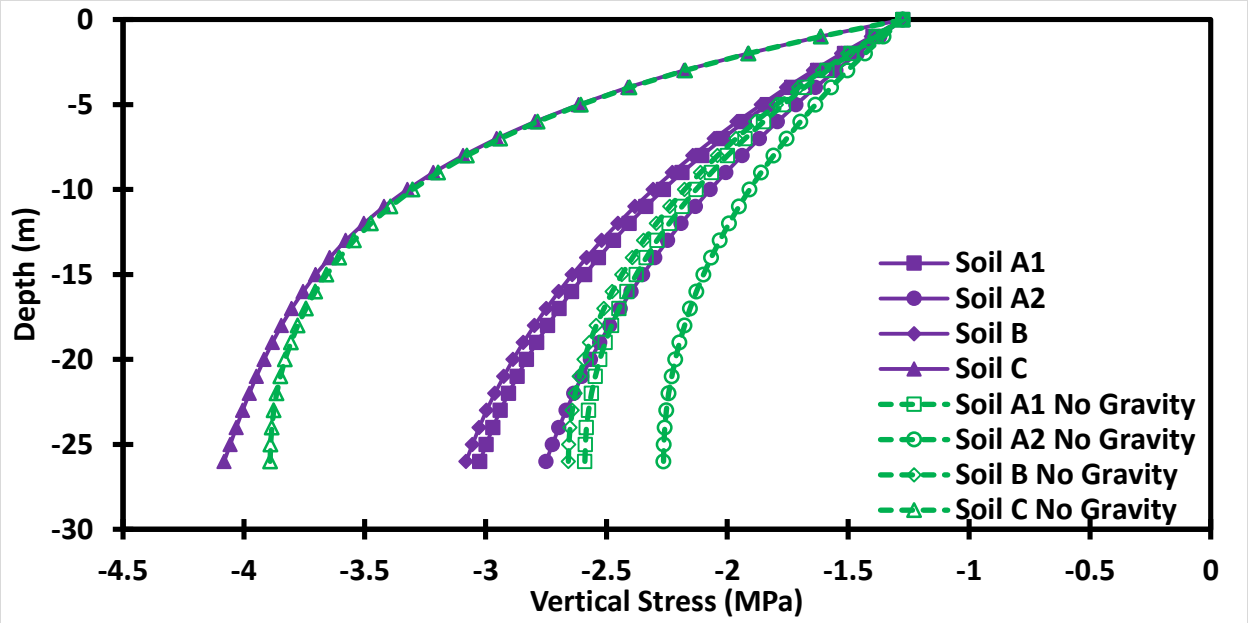

Figure 3.14 Stress in End Bearing Pile Embedded in Homogenous Soil (ΔT = 14°C, test T7, K_h=0)

Figure 3.15 shows that is the temperature difference between the pile and soil is low enough the pile will be in compressed by the axial load and vice versa if the temperature difference is high enough the pile will expand.

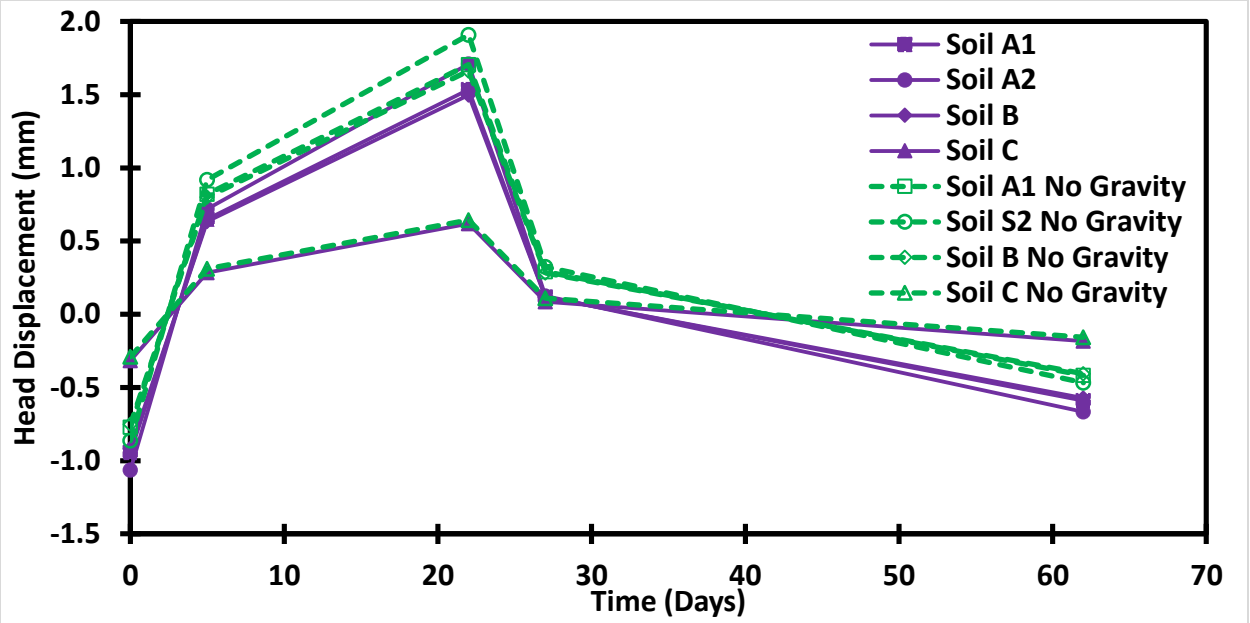

Figure 3.15 Head Displacement versus Time in End Bearing Pile Embedded in Homogenous Soil (test T7)

Figure 3.16 depicts vertical displacement versus depth for ΔT = 2°C during test T7 and K_h value of 125 MPa/m. As expected in this case displacement is slightly larger than the one corresponding to K_h=0

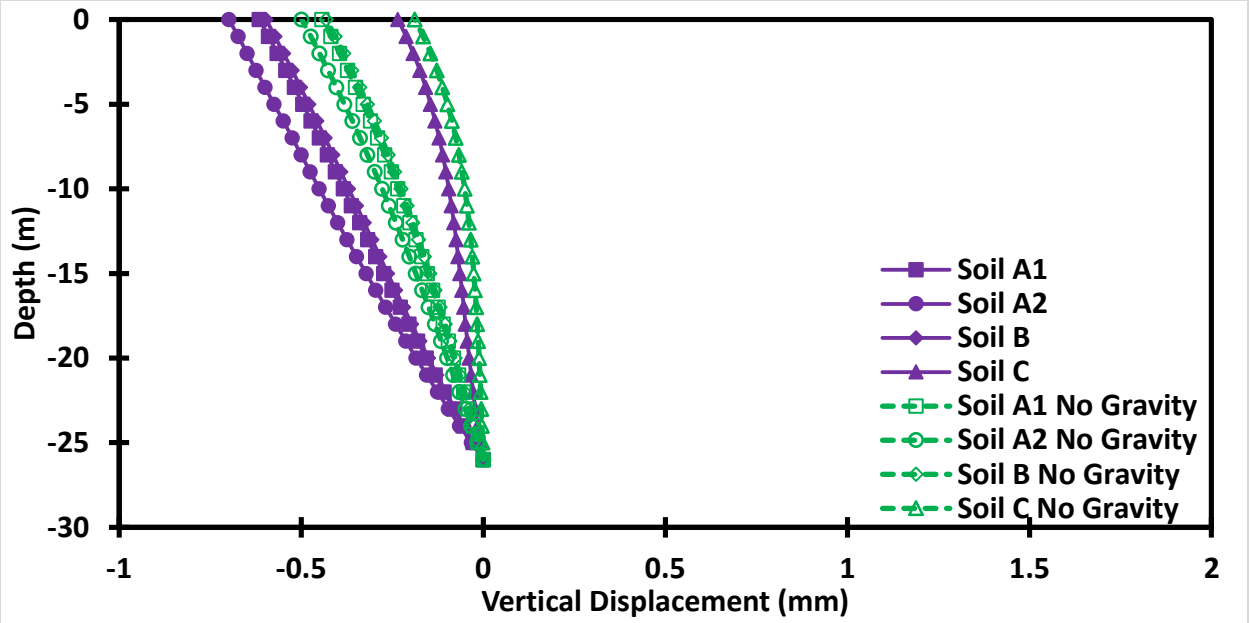

Figure 3.16 Displacement in End Bearing Pile Embedded in Homogeneous Soil (ΔT = 2°C, test T7, K_h=125 MPa/m)

Figure 3.17 depicts vertical displacement versus depth for ΔT = 14°C during test T7 and K_h value of 125 MPa/m. In this case displacement is slightly smaller than the one corresponding to K_h=0 shown in Fig. 3.10 because the displacement is controlled by thermal load (heating) at this temperature difference. Consequently, the building resists the uplift.

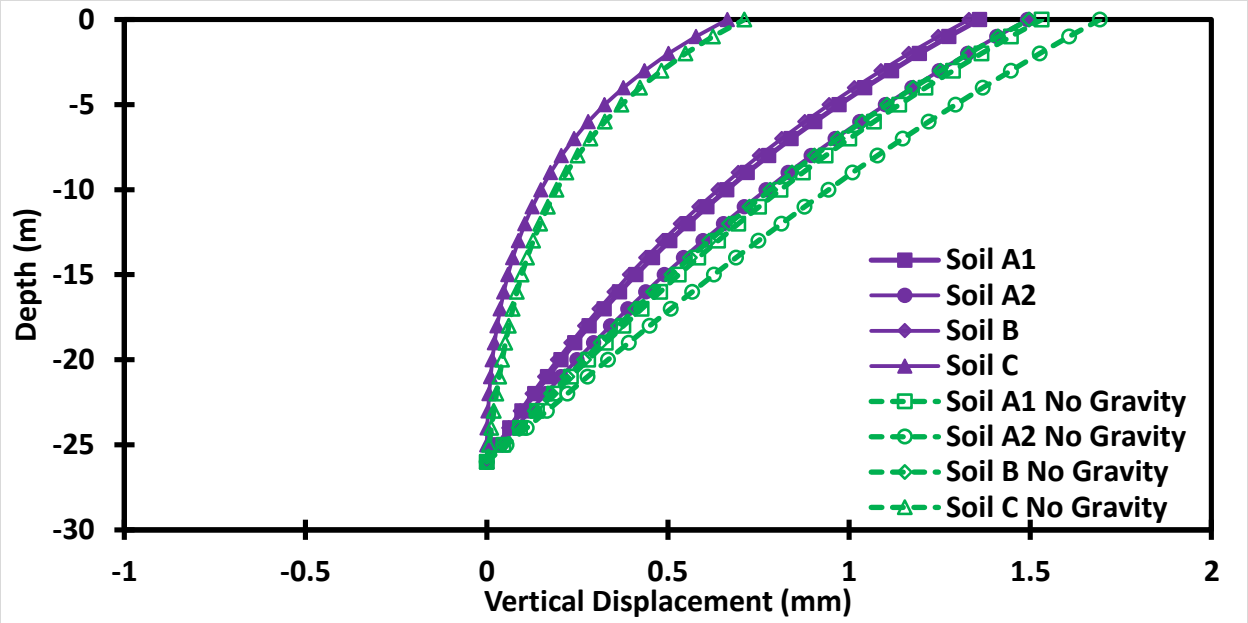

Figure 3.17 Displacement in End Bearing Pile Embedded in Homogeneous Soil (ΔT = 14°C, test T7, K_h=125 MPa/m)

Figures 3.18 and 3.19 show strain versus depth for temperature differences of 2°C and 14°C respectively during test T7 with K_h = 125 MPa/m. These figures show how strain at the pile head is affected when the pile head is restrained by the building. It is important to note that the strain at the pile head is now affected by the soil stiffness whereas in the case without the head restraint it was not. It should also be noted that gravity has less of an effect on strain at higher temperature differences and soil stiffness.

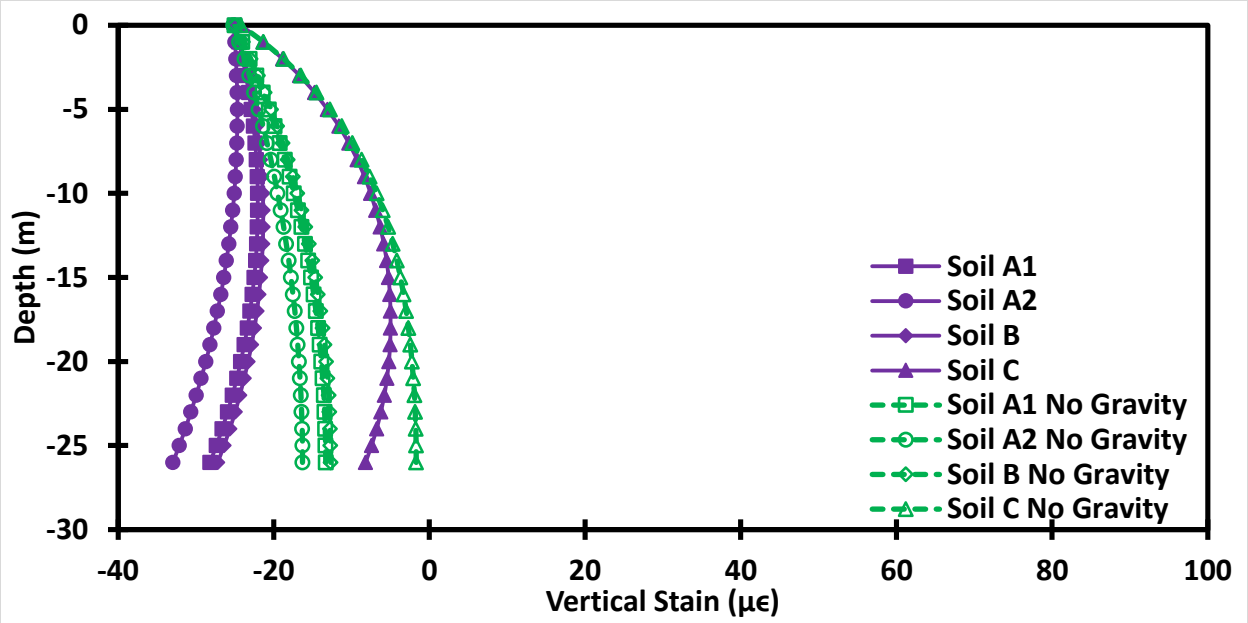

Figure 3.18 Strain in the End Bearing Pile Embedded in Homogeneous Soil (ΔT = 2°C, test T7, K_h =125 MPa/m)

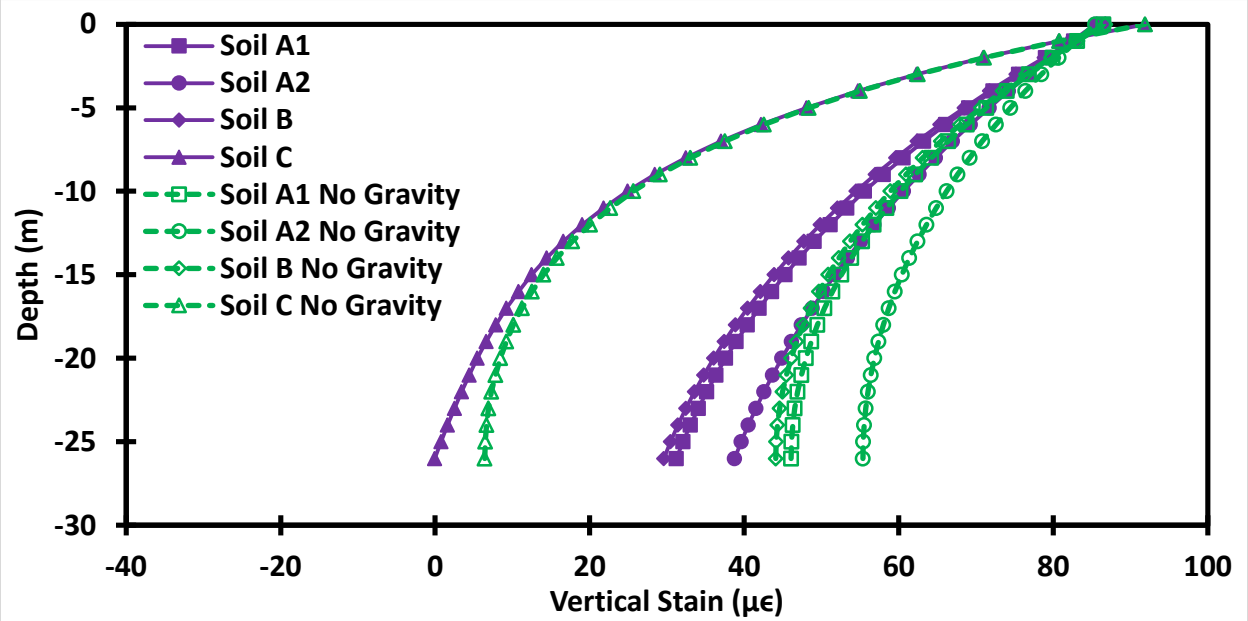

Figure 3.19 Strain in the End Bearing Pile Embedded in Homogeneous Soil (ΔT = 14°C, test T7, K_h =125 MPa/m)

Figures 3.20 and 3.21 show model predictions for change in stress versus depth at ΔT = 2°C and 14°C respectively during test T7 for K_h = 125 MPa/m. As expected the stress at the pile head is now affected by the presence of the head spring and it is larger than one depicted in figures 3.13 and 3.14. Furthermore, the magnitude of the stress at the pile head is now affected by the magnitude of the displacement at the pile head. This feature can be observed well in Fig. 3.22.

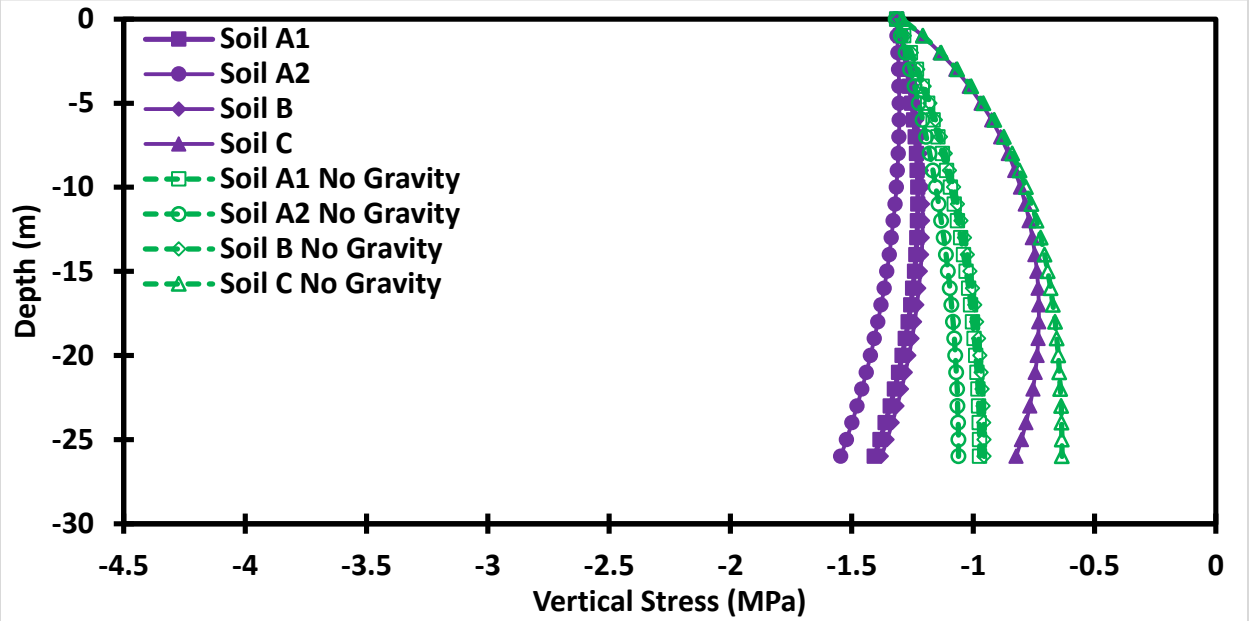

Figure 3.20 Stress in End Bearing Pile Embedded in Homogeneous Soil (ΔT = 2°C, test T7, K_h = 125 MPa/m)

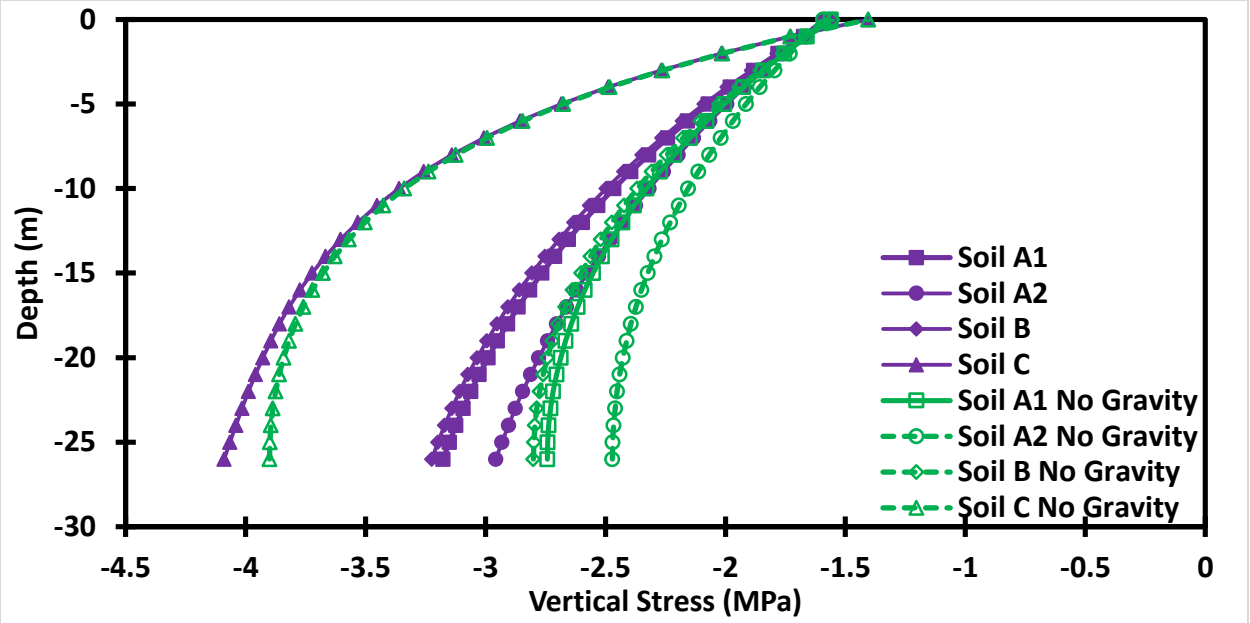

Figure 3.21 Stress in End Bearing Pile Embedded in Homogeneous Soil (ΔT = 14°C, test T7, K_h = 125 MPa/m)

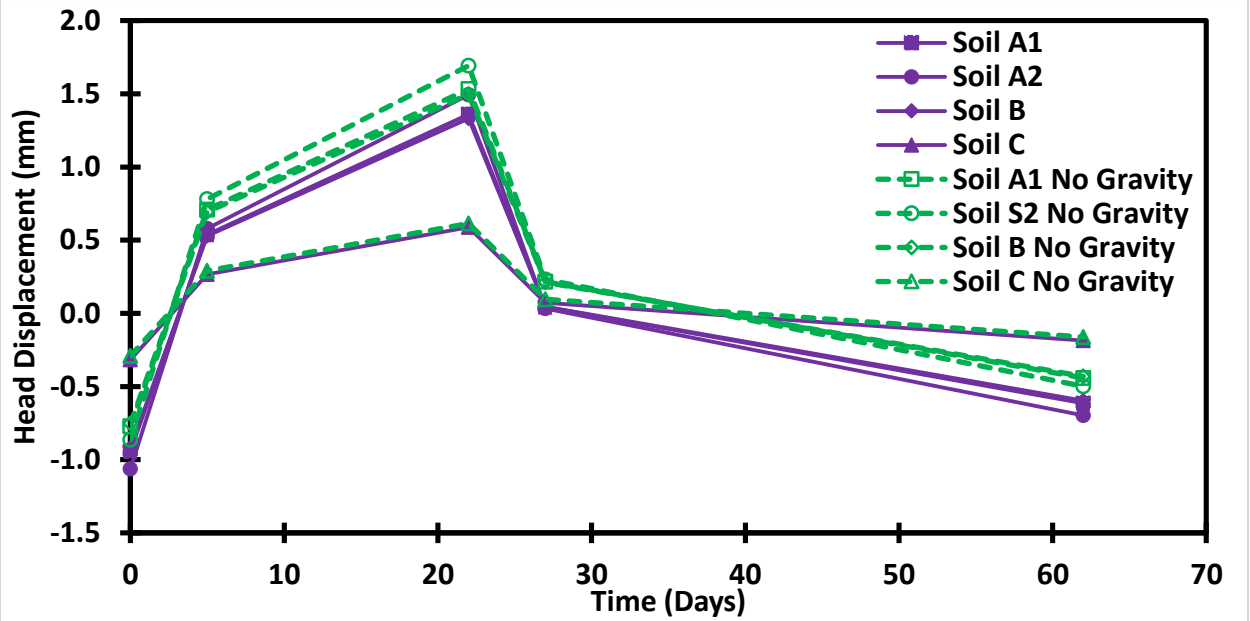

Figure 3.22 Head Displacement versus Time for End Bearing Pile Embedded in Homogenous Soil (test T7, K_h = 125 MPa/m)

Layered Soil Profile

This section presents predictions of the analytical model for the actual layered soil profile. For the purpose of validation the experimental data are also presented. Nevertheless, it is noted that the actual temperature of the energy pile varies with depth in the amount of ±2°C from the temperature history shown in Table 3-3 (Knellwolf et al. 2011). As stated previously the analytical model assumes that the temperature of the pile is constant with depth and width. Thus, it is not expected that the model predictions should provide a perfect agreement with the experimental data. Self-weight is neglected in this section.

Test T1

Figures 3.23 and 3.24 show the model prediction for displacement versus depth at ΔT = 3°C and ΔT= 13.4°C respectively during test T1. The corresponding experimental data are not available. A comparison with figures 3.2 and 3.3 indicates the predicted values are bounded by the stiffest soil (C) and the softest soil (A2).

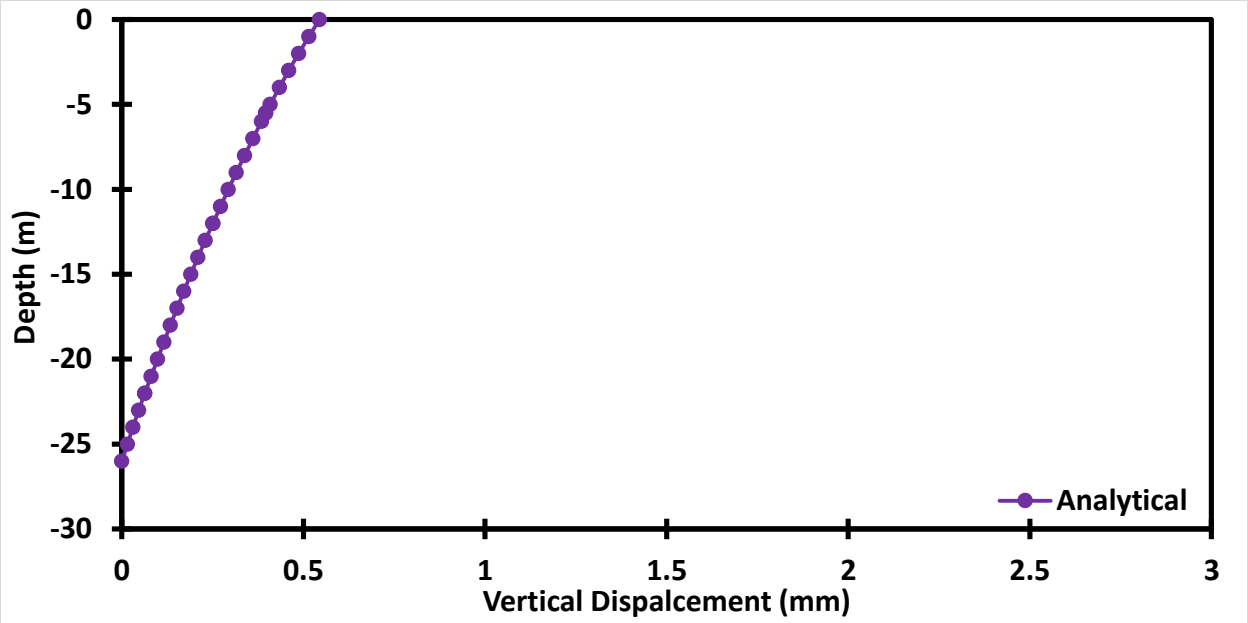

Figure 3.23 Displacement of End Bearing Pile Embedded in Layered Soil Profile (ΔT = 3°C, test T1)

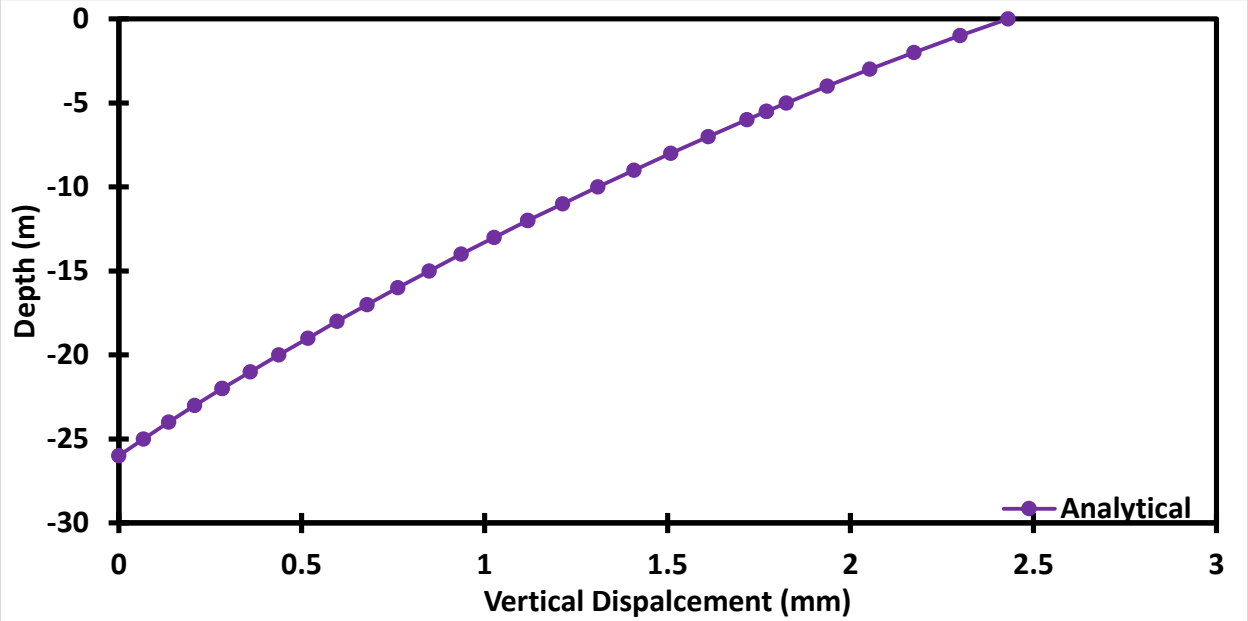

Figure 3.24 Displacement of End Bearing Pile Embedded in Layered Soil Profile (ΔT = 13.4°C, test T1)

Figures 3.25 and 3.26 show the model prediction and experimental data for strain versus depth at ΔT = 3° and ΔT = 13.4°C respectively during test T1. These two figures show good agreement between the analytical solution and experimental reading of the vibrating wire strain gage (VWSG) for all but the bottom layer of soil. While the optical fiber (OF) readings for 3°C seem to vary from the other two results while at 13.4°C the OF readings seem to fit the other data well. The deviation of the predicted strains from the measured strains in the vicinity of the pile tip is due to the assumption of a complete fixity of the pile tip.

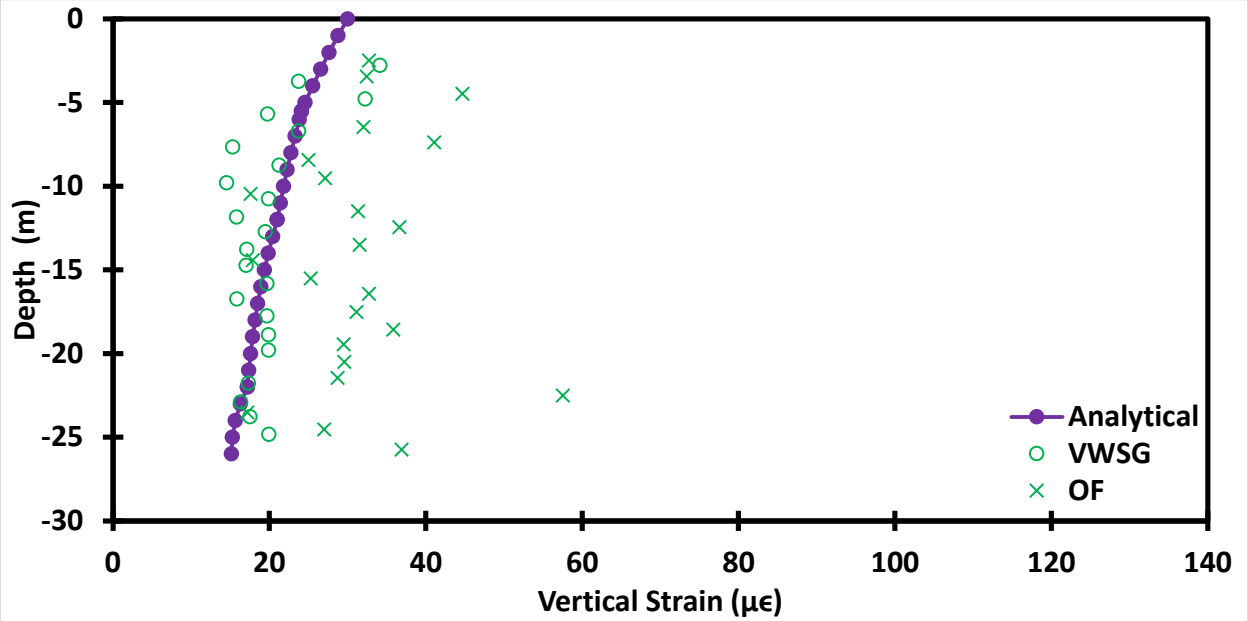

Figure 3.25 Strain of End Bearing Pile Embedded in Layered Soil Profile Fixed Strain (ΔT = 3°C. test T1)

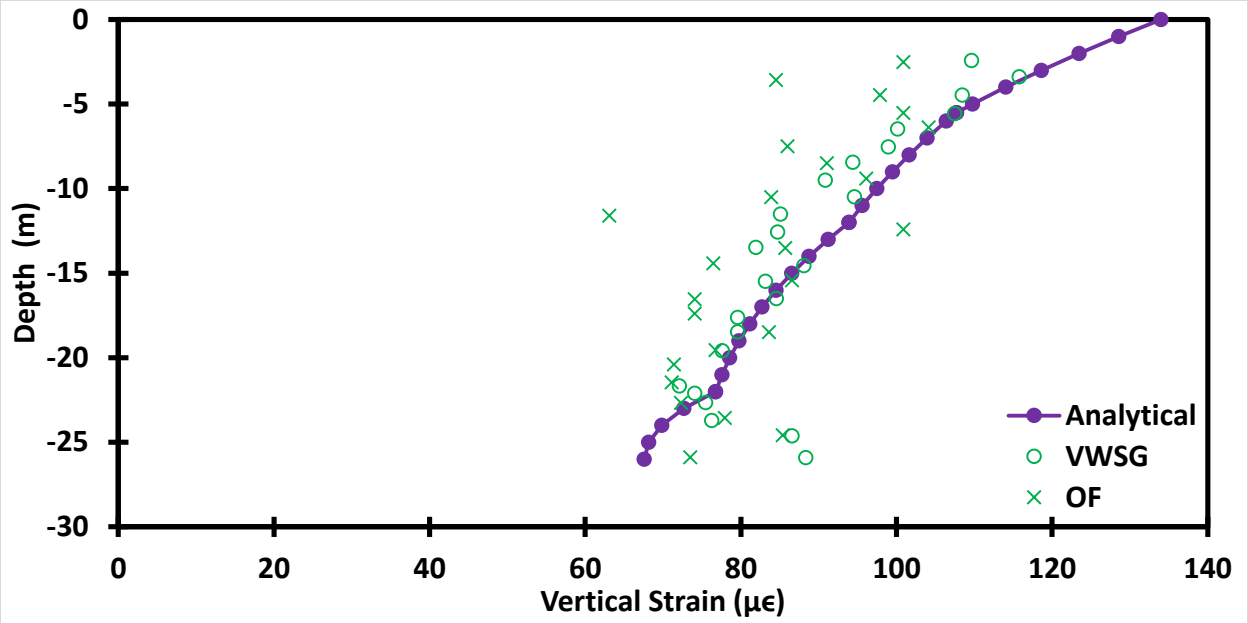

Figure 3.26 Strain of End Bearing Pile Embedded in Layered Soil Profile Fixed Strain (ΔT = 13.4°C. test T1)

Figures 3.27 and 3.28 show good correlation between the experimental data obtained from VWSG in the middle of the pile for 3°C, and in all but the bottom soil layer for 13.4°C. However in the top and bottom soil layers at 3°C measured stress was greater than what the analytical model predicted. The OF again did not fit well at 3°C but did at 13.4°C for all but the bottom layer.

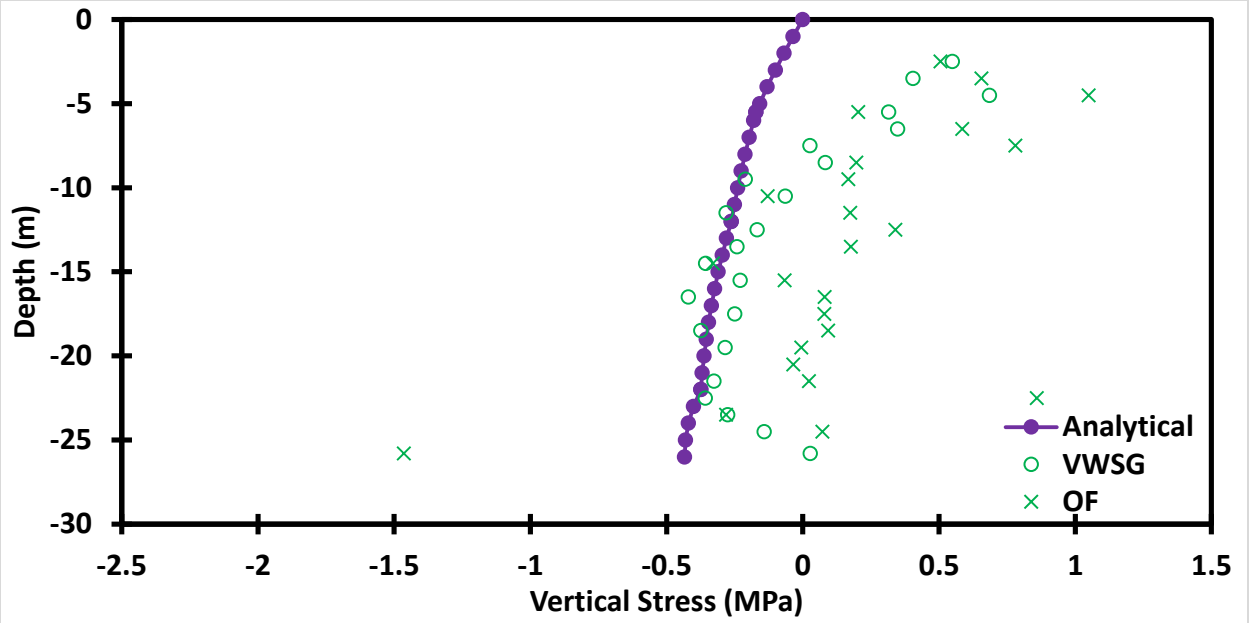

Figure 3.27 Stress in End Bearing Pile Embedded in Layered Soil Profile (ΔT =3°C, test T1)

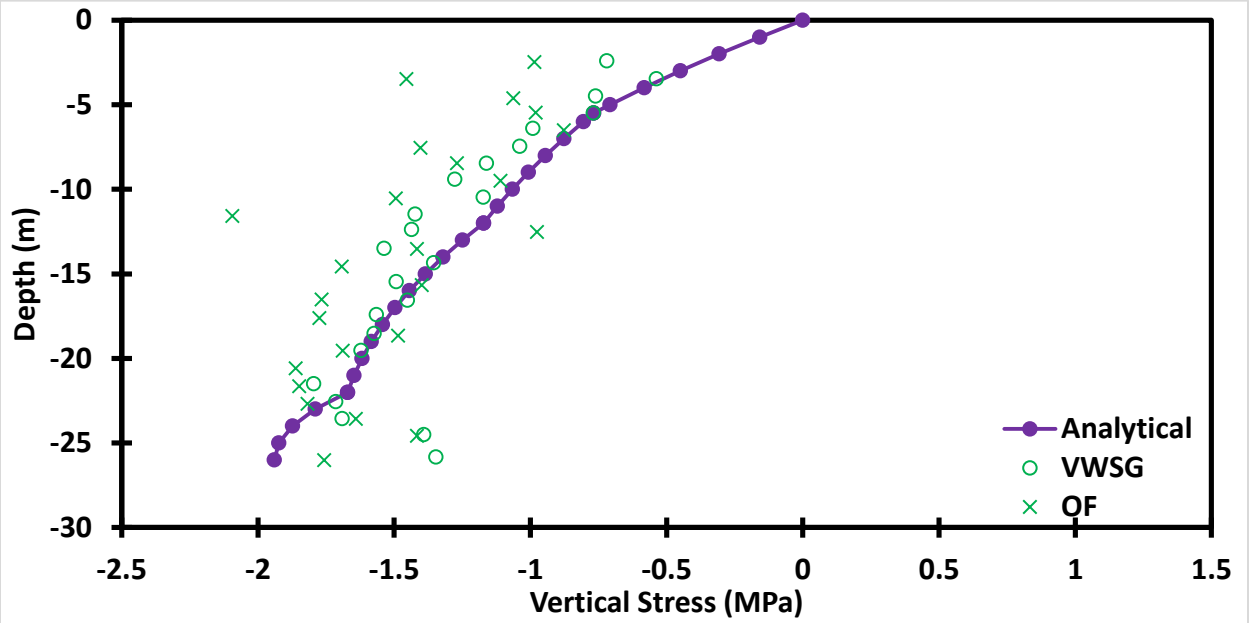

Figure 3.28 Stress in End Bearing Pile Embedded in Layered Soil Profile (ΔT =13.4°C, test T1)

Figure 3.29 shows head displacement versus time for test T1. It can be seen that the head displacement predicted by the analytical model is between the maximum and minimum experimentally measured displacements at each known temperature.

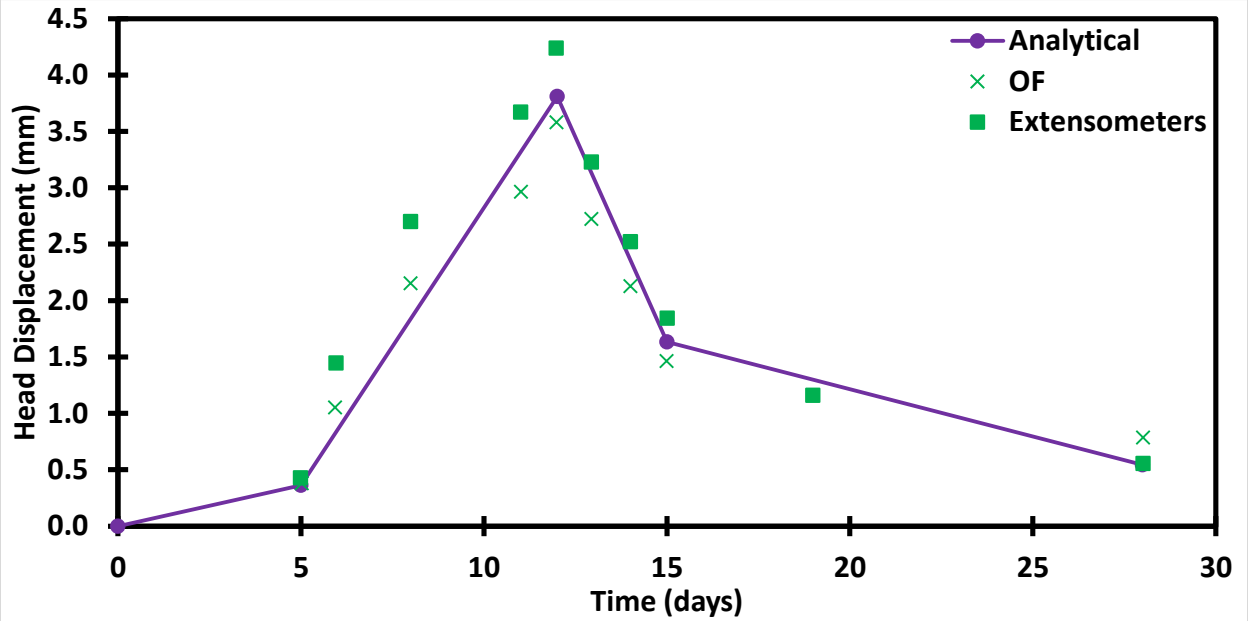

Figure 3.29 Head Displacement versus Time in End Bearing Pile Embedded in Layered Soil Profile (test T1)

Test T7

In addition to the prediction for a combined thermal and mechanical load for test T7 the predictions for the thermal only and axial force only are included as well to better understand the behavior of energy pile. Furthermore, the first set of predictions were made for K_h=0.

Figure 3.30 shows that if the axial load is large enough and the temperature difference small enough the HEP will still shrink when placed on a non-deforming bedrock. Figure 3.31 shows that if the temperature difference during heating is large enough compared to the axial

load the pile will expand. It is noted that the word "Combined" in the legend indicates the response for a combined thermal and mechanical load.

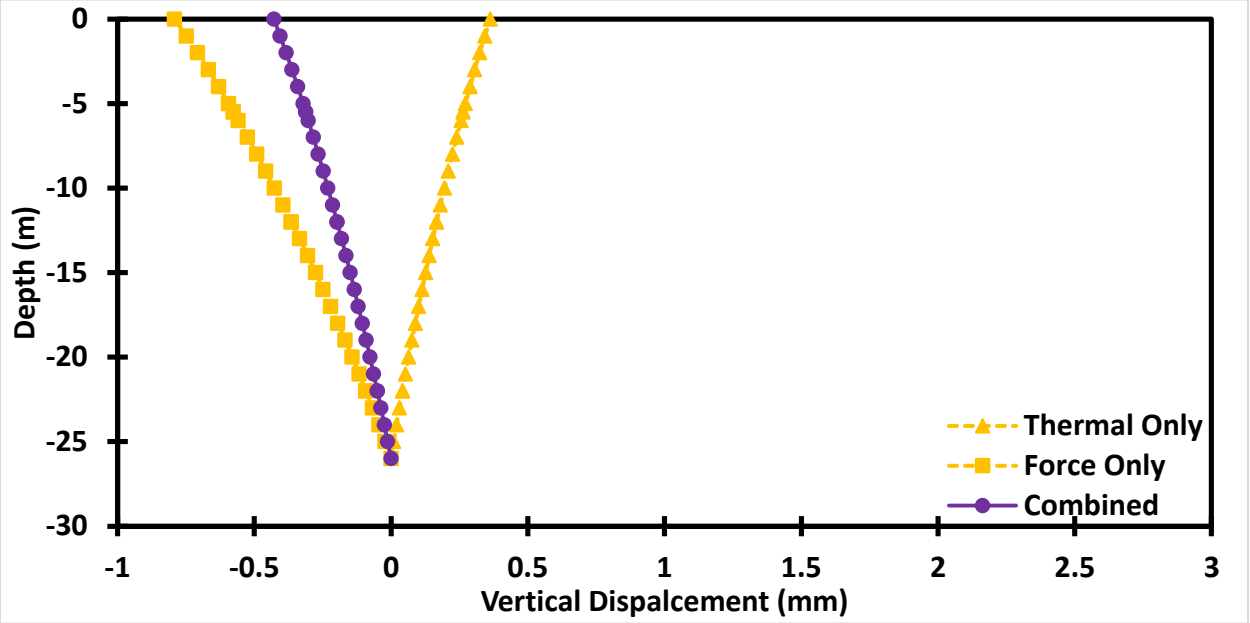

Figure 3.30 Displacement of End Bearing Pile Embedded in Layered Soil Profile (ΔT = 2°C, test T7, K_h=0)

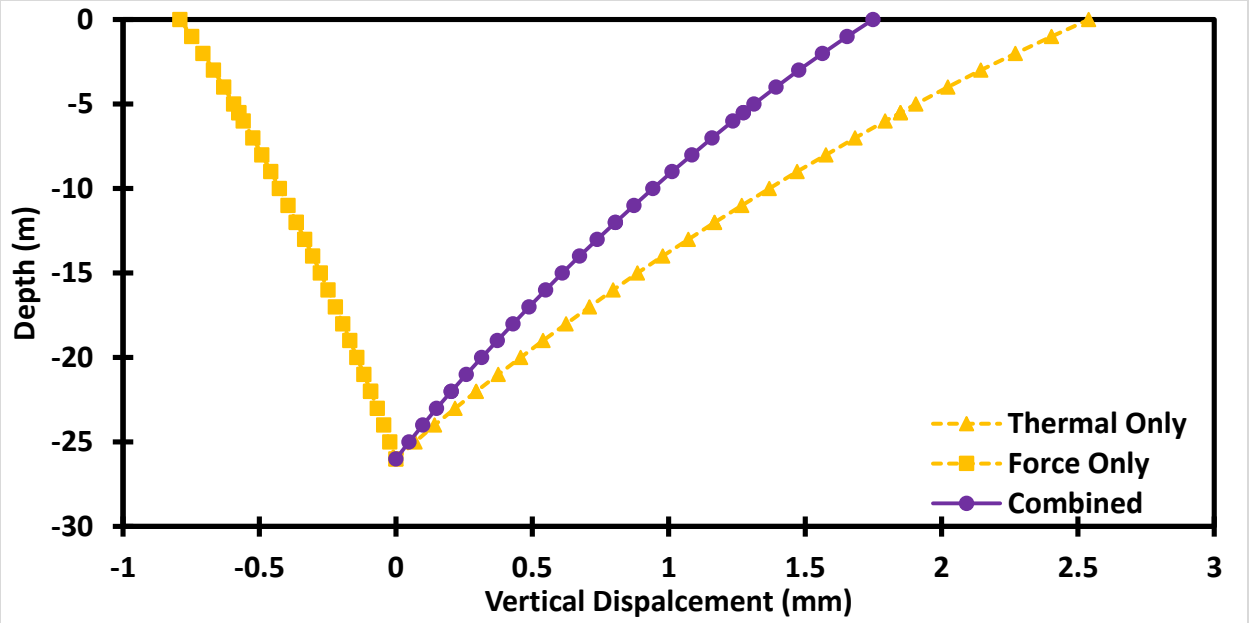

Figure 3.31 Displacement of End Bearing Pile Embedded in Layered Soil Profile (ΔT = 14°C, test T7, K_h=0)

Some disagreement between the experimental data and model predictions can be observed in figures 3.32 and 3.33. Nevertheless, it should be noted that the scale of strain is different in these two figures and thus, the disagreement observed in Fig. 3.32 is smaller than the one seen in Fig. 3.33. The disagreement is most likely due to not accounting for the stiffness of the building and over estimating the stiffness of the bedrock.

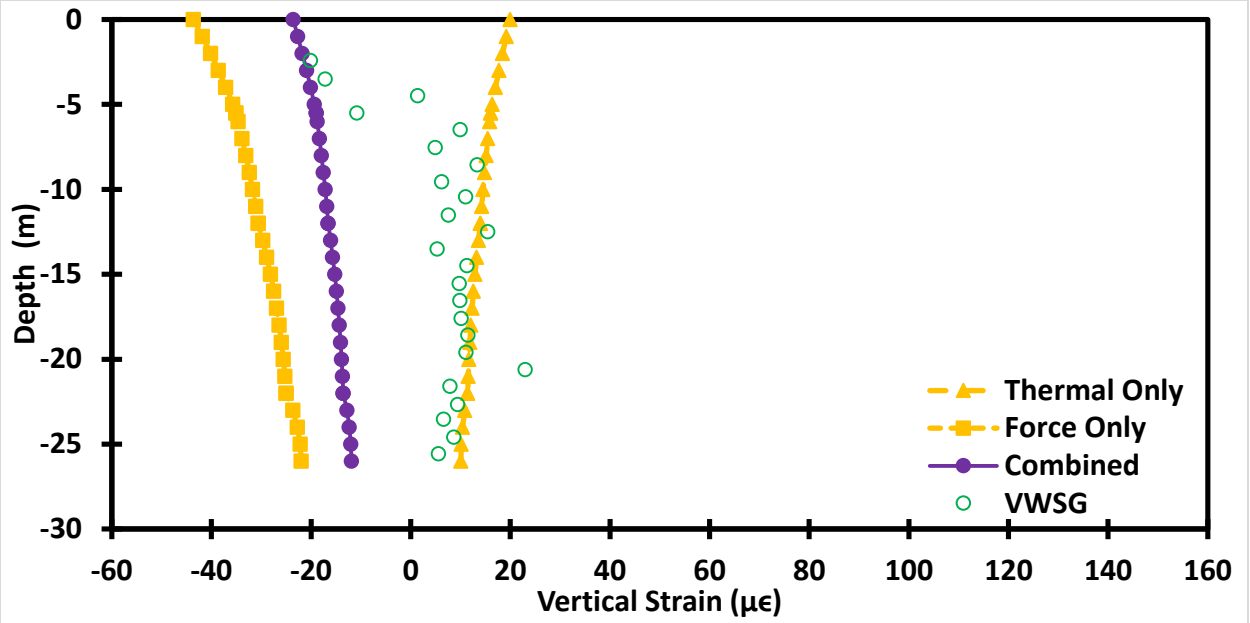

Figure 3.32 Strain in End Bearing Pile Embedded in Layered Soil Profile (ΔT =2°C, test T7, K_h=0)

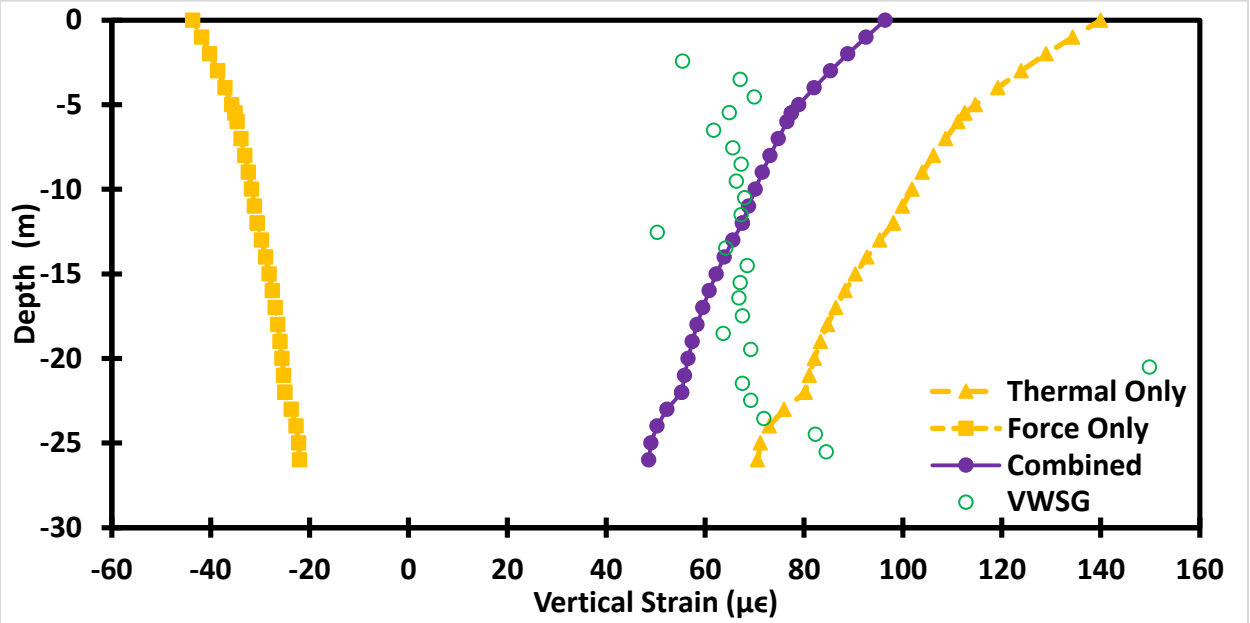

Figure 3.33 Strain in End Bearing Pile Embedded in Layered Soil Profile Fixed Strain (ΔT = 14°C, test T7, K_h=0)

Figure 3.34 again exhibits the trends similar to those observed in Fig. 3.33. This is expected since the stress in the full scale in situ test is obtained from the one dimensional thermos-elastic constitutive relationship based on the measured strain. Nevertheless, in this case the temperature change versus depth is accounted for.

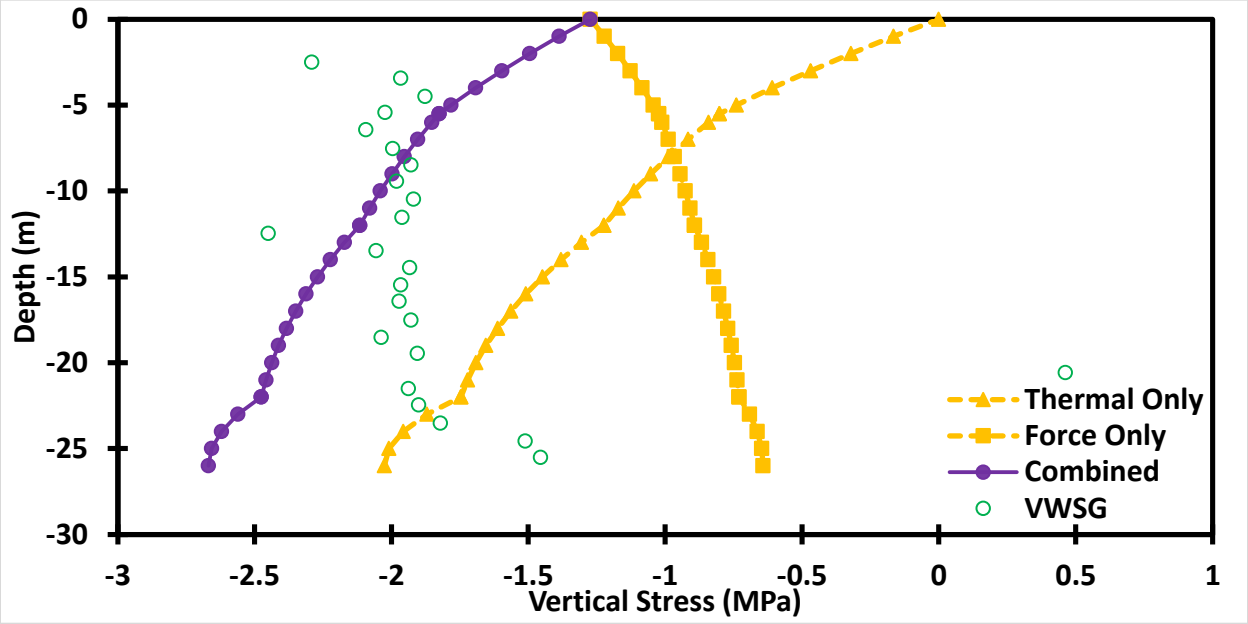

Figure 3.34 Layered Fixed Stress (14°C)

Figure 3.35 shows the predicted head displacement versus time for test T7. The downward displacement at time zero is due to the axial force imposed by the superstructure.

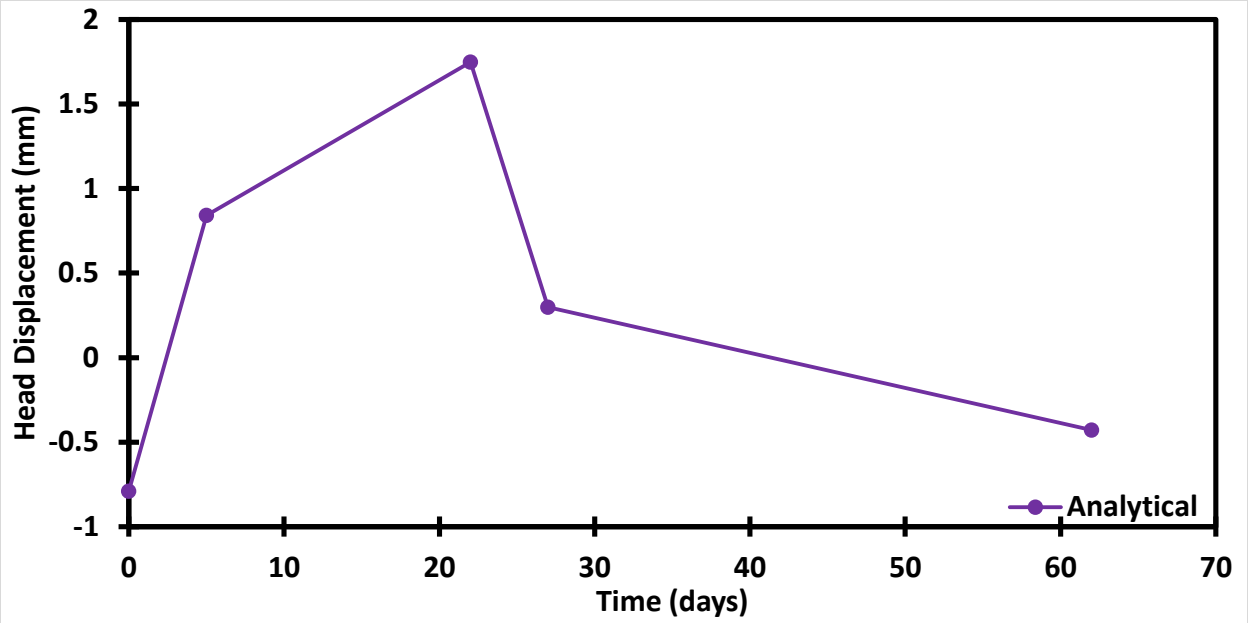

Figure 3.35 Head Displacement vs Time in End Bearing Pile Embedded in Layered Soil Profile (test T7, K_h =0)

Figures 3.36 and 3.37 show displacement versus depth at ΔT = 2°C and ΔT = 14°C respectively during test T7, and K_h = 125 MPa/m. As expected displacement in the presence of non-zero K_h is smaller as compared to the one corresponding to K_h = 0.

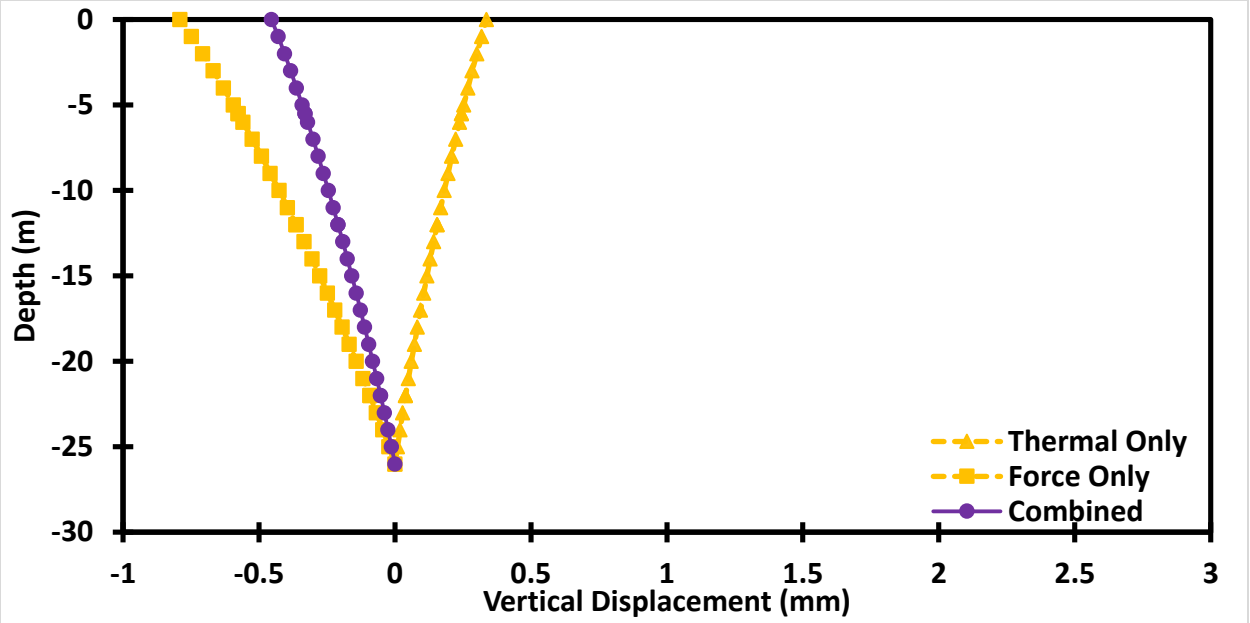

Figure 3.36 Displacement in End Bearing Pile Embedded in Layered Soil Profile (ΔT = 2°C, test T7, K_h = 125 MPa/m)

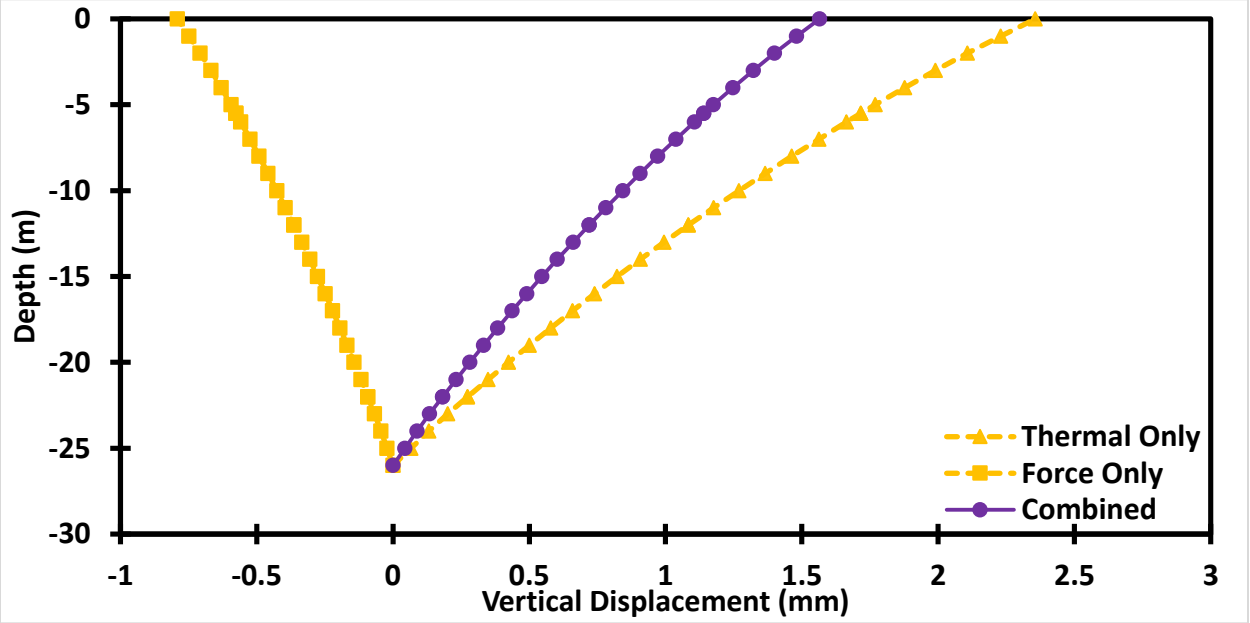

Figure 3.37 Displacement in End Bearing Pile Embedded in Layered Soil Profile (ΔT = 14°C, test T7, K_h = 125 MPa/m)

Figures 3.38 and 3.39 show that at 2°C and 14°C respectively the analytical model predictions and VWSG measurements are more closely correlated however the bedrock still seems to be causing problems in the bottom of the pile.

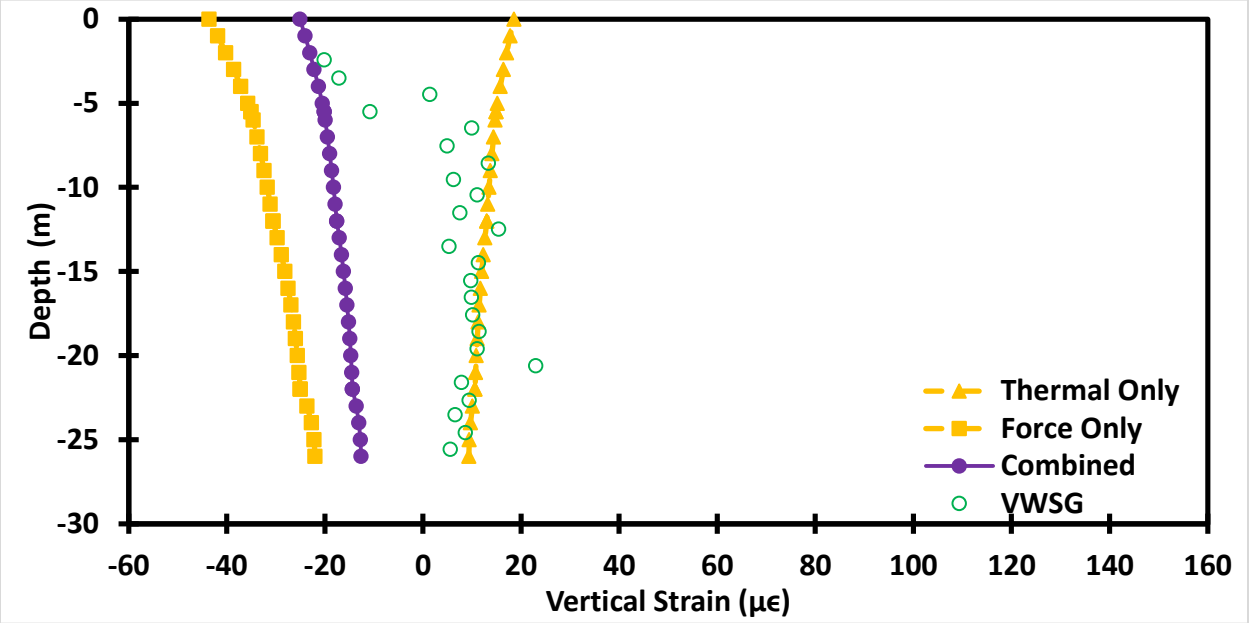

Figure 3.38 Strain in End Bearing Pile Embedded in Layered Soil Profile (ΔT = 2°C, test T7, K_h = 125 MPa/m)

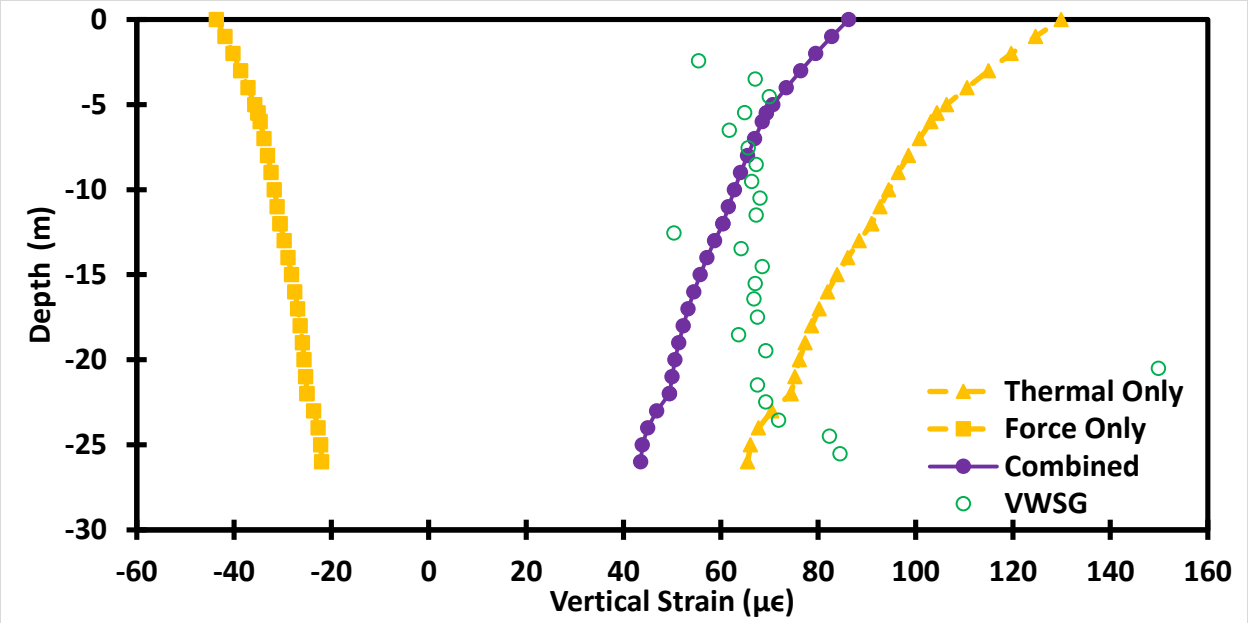

Figure 3.39 Strain in End Bearing Pile Embedded in Layered Soil Profile (ΔT = 14°C, test T7, K_h = 125 MPa/m)

Figure 3.40 shows that at 14°C the analytical and VWSG results are only close near the top of the HEP.

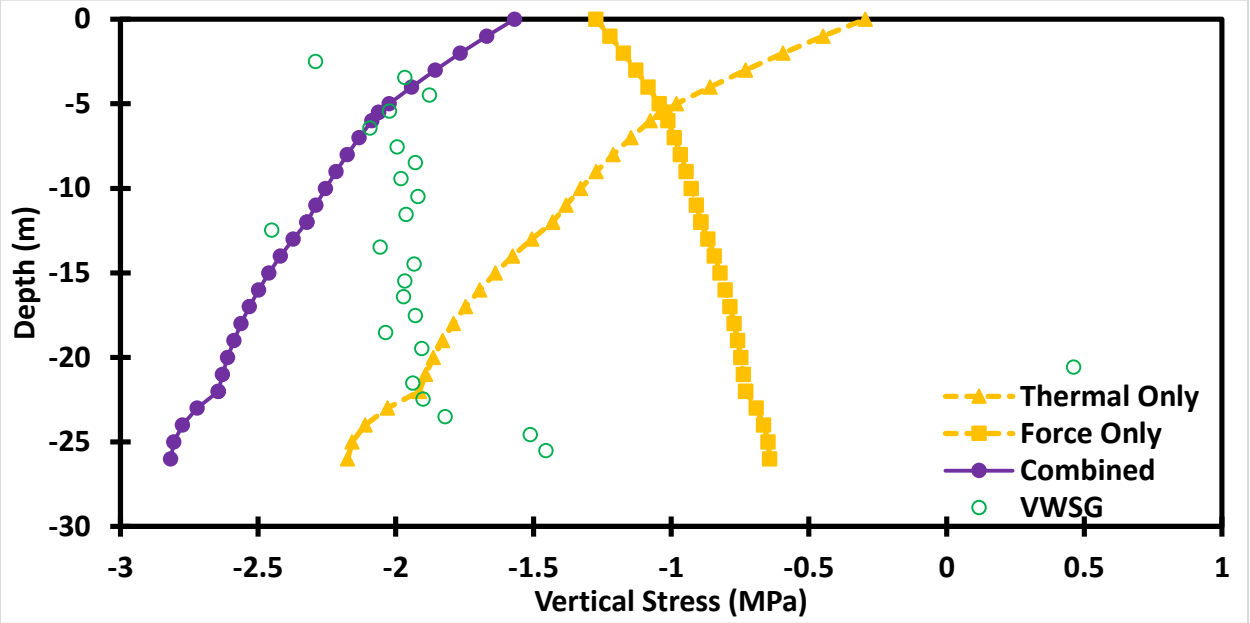

Figure 3.40 Stress in End Bearing Pile Embedded in Layered Soil Profile (ΔT = 14°C, test T7, K_h = 125 MPa/m)

Figure 3.41 depicts head displacement versus time for test T7 with non-zero K_h value. As expected the displacement is smaller for a non-zero K_h value as compared to zero K_h value.

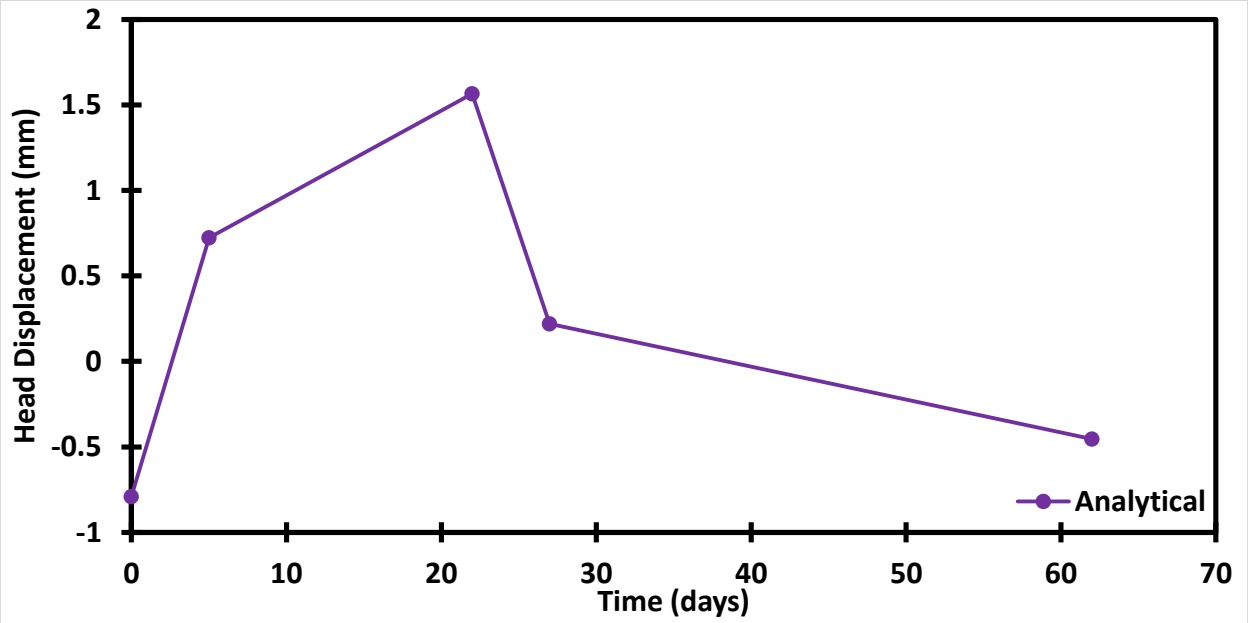

Figure 3.41 Head Displacement vs Time for End Bearing Pile Embedded in Layered Soil Profile (test T7, K_h = 125 MPa/m)

Semi Floating Pile

In this section the assumption of complete fixity at the pile tip is relaxed to account for the effects of softer bedrock on axial displacement, strain, and stress. This type of pile is referred to as semi floating pile.

Homogeneous Soil Profile

In this section, as in the case of end bearing energy pile, only a homogeneous soil consisting of a single soil layer underlain by the bedrock is considered. Effects of self-weight are neglected in this section.

Test T1

Figures 3.42 and 3.43 show vertical displacement versus depth for ΔT = 3°C and ΔT = 13.4°C during test T1. The main difference with respect to the end bearing pile is that the pile tip now moves downwards. With pile head moving upwards this indicates that the location of zero vertical displacement, also known as a null point, is located somewhere between the pile tip and pile head. Out of all parameters that affect the location of the null point according to Eq. (122) only the stiffness of shear spring (K_s) is different for different response curves depicted in Fig. 3.42. The softer the soil pile interface the deeper the null point is located. In addition, Eq. (122) indicates that the location of the null point does not depend on the amount of thermal loading. It is also noted that the head displacement in the case of semi floating pile is smaller than the head displacement in the case of end bearing pile.

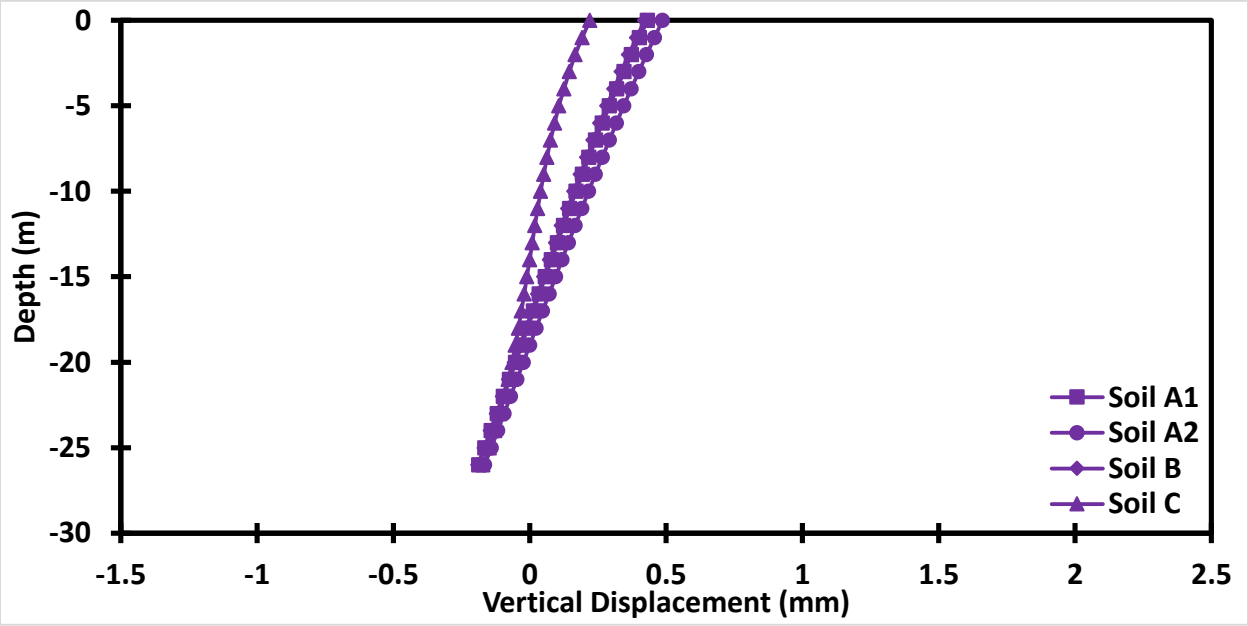

Figure 3.42 Displacement of Semi Floating Pile Embedded in Homogeneous Soil (*ΔT* = 3°C, test T1)

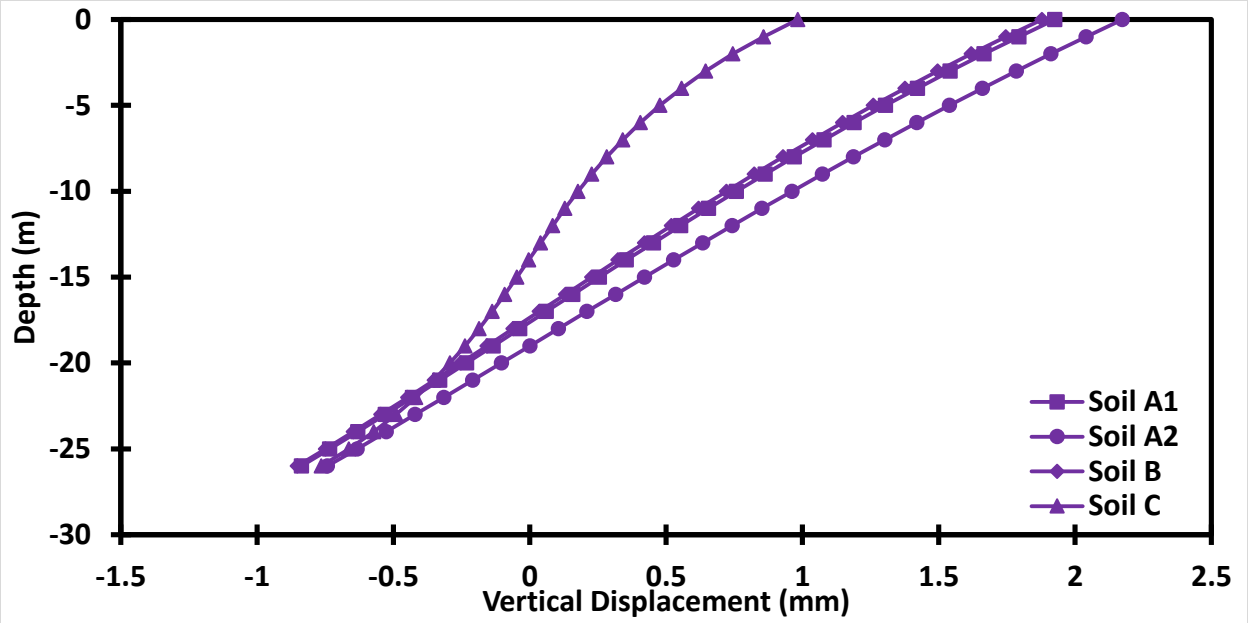

Figure 3.43 Displacement of Semi Floating Pile Embedded in Homogeneous Soil (ΔT = 13.4°C, test T1)

Another consequence of partial fixity of the pile tip in a semi floating pile is that strain exhibits absolute minimum (in the case of heating) at the null point. This can be observed figures 3.44 and 3.45 and verified by Eq. (120). The difference between magnitude of strains at the pile head and the null point and at the pile tip and null point affected by the soil stiffness and temperature difference.

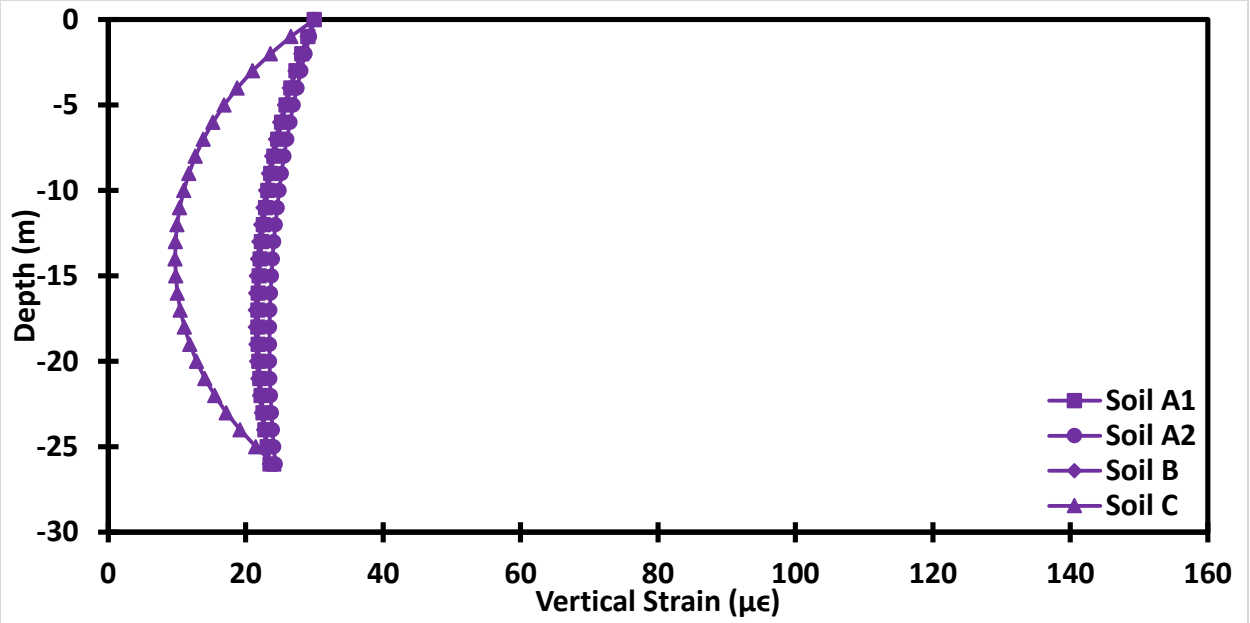

Figure 3.44 Strain in Semi Floating Pile Embedded in Homogeneous Soil (ΔT = 3°C, test T1)

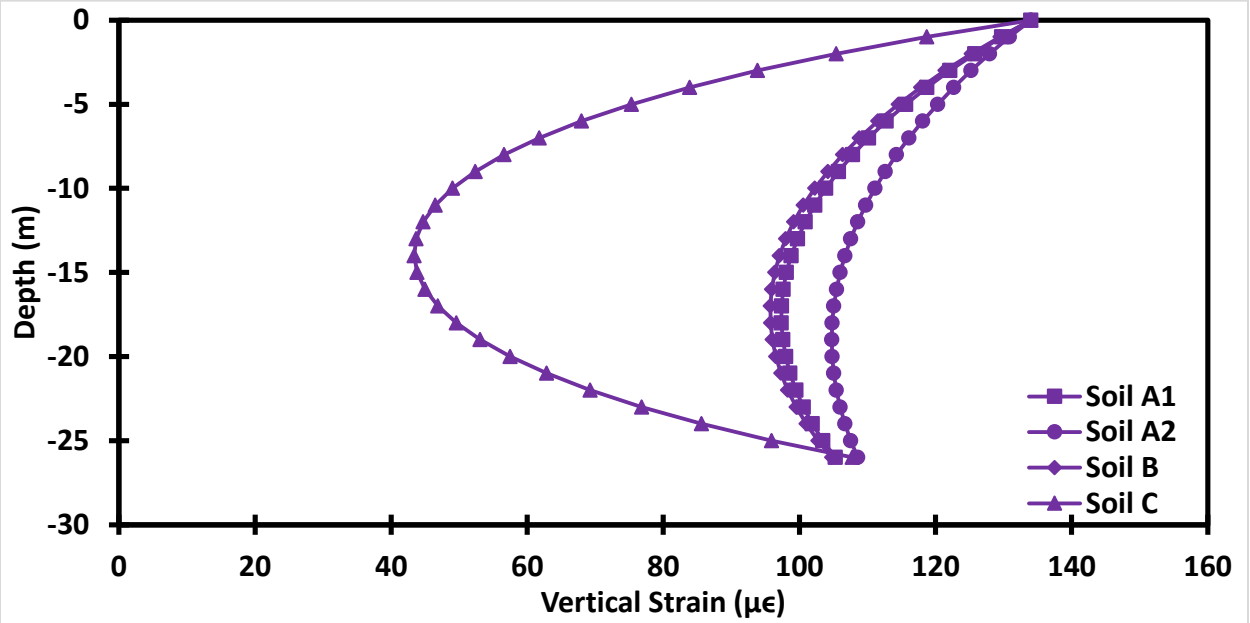

Figure 3.45 Strain in Semi Floating Pile Embedded in Homogeneous Soil (ΔT = 13.4°C, test T1)

Similarly to strain the stress magnitude exhibits the absolute maximum at the null point as shown in figures 3.46 and 3.47. The location of the maximum compressive stress in the case of heating is affected by the soil pile interface stiffness (K_s). This can also be verified by Eq. (121). Furthermore, for a given temperature different the maximum compressive stress in the semi-floating pile is smaller than the maximum compressive stress in the end bearing pile.

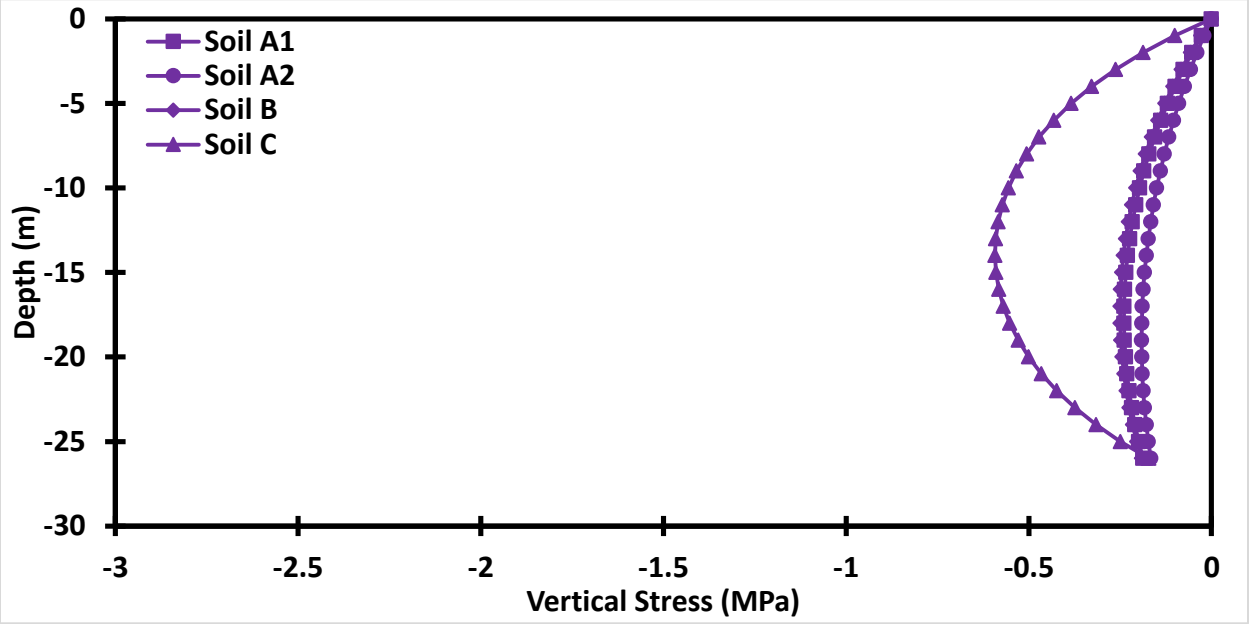

Figure 3.46 Stress in Semi Floating Pile Embedded in Homogeneous Soil (ΔT = 3°C, test T1)

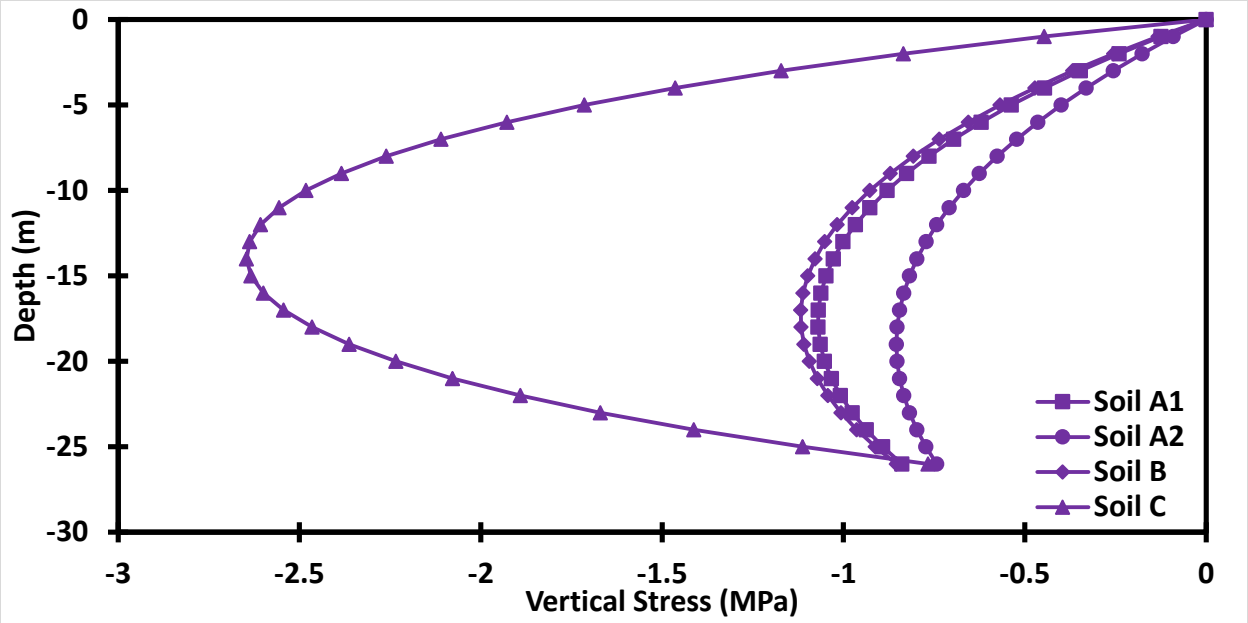

Figure 3.47 Stress in Semi Floating Pile Embedded in Homogeneous Soil (ΔT = 13.4°C, test T1)

Fig. 3.48 shows head displacement versus time for test T1 including four different soils. Head displacements in semi floating pile are smaller than head displacements in end bearing pile.

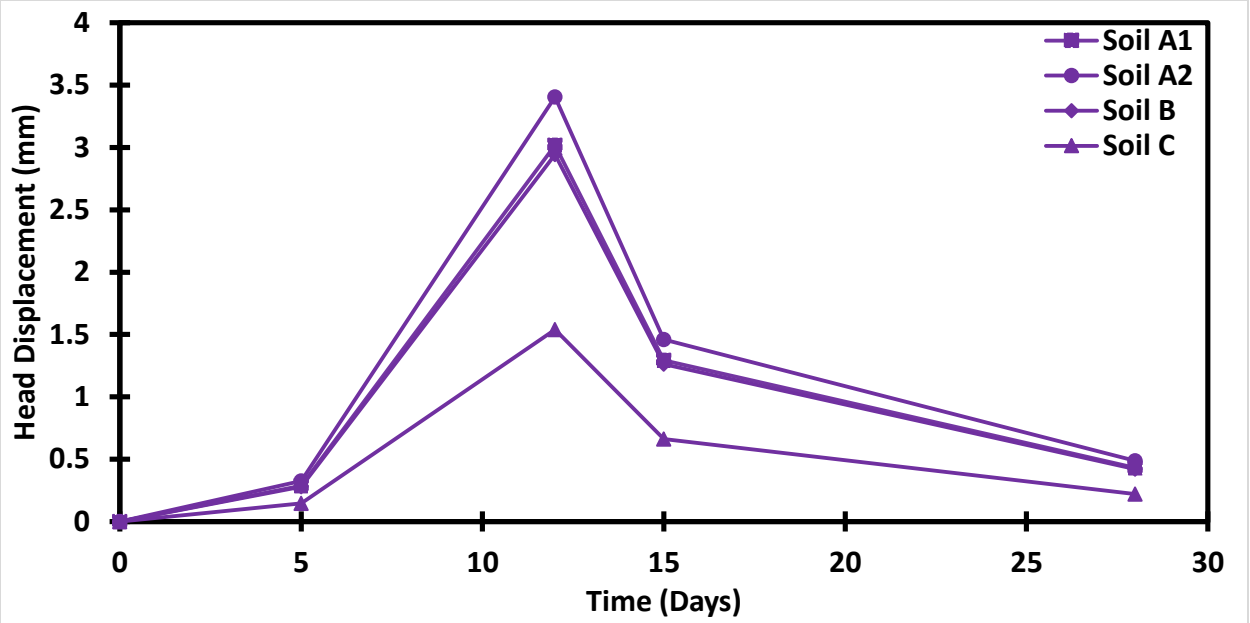

Figure 3.48 Head Displacement vs Time for Semi Floating Pile Embedded in Homogeneous Soil (test T1)

Test T7

Again both analytical models, with and without head restraint are considered in this section.

Figures 3.49 and 3.50 depict displacement at ΔT = 2°C and ΔT = 14°C during test T7. It is seen that mechanical loading has dominant effect on displacement at the former temperature difference while the thermal loading has dominant effect at the later temperature difference. Null point becomes evident only at ΔT = 14°C.

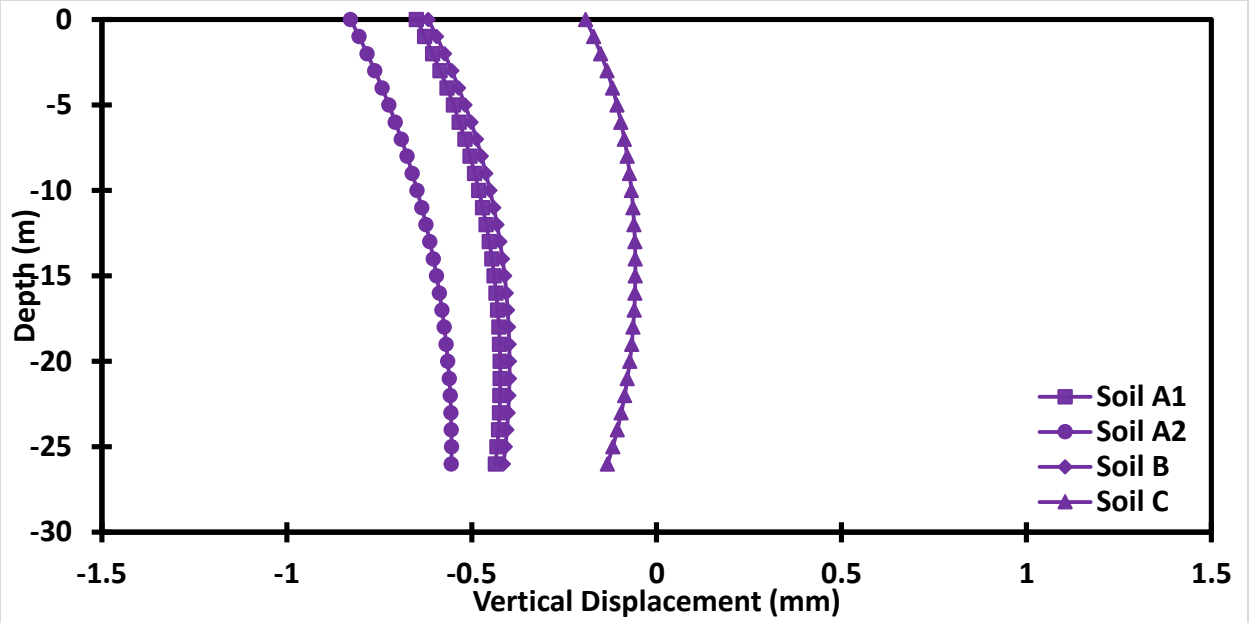

Figure 3.49 Displacement in Semi Floating Pile Embedded in Homogeneous Soil (ΔT = 2°C, test T7, K_h = 0)

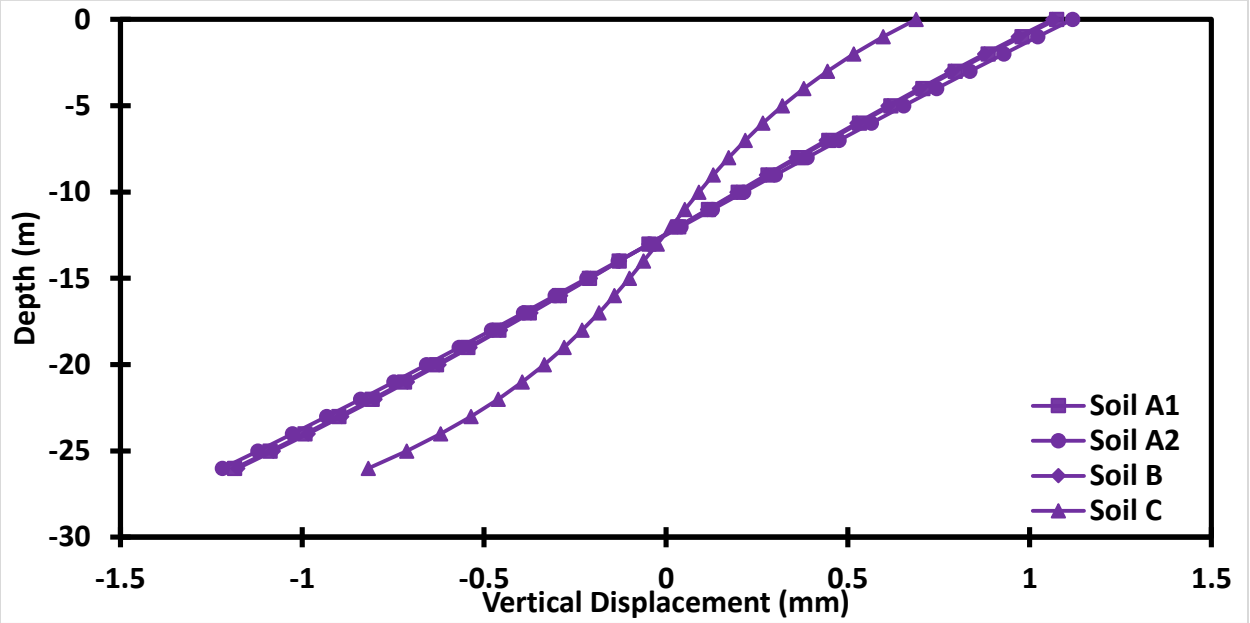

Figure 3.50 Displacement in Semi Floating Pile Embedded in Homogeneous Soil (ΔT = 14°C, test T7, K_h = 0)

Figures 3.51 and 3.52 show that with a combined axial and thermal loads the maximum strain can occur at the pile tip.

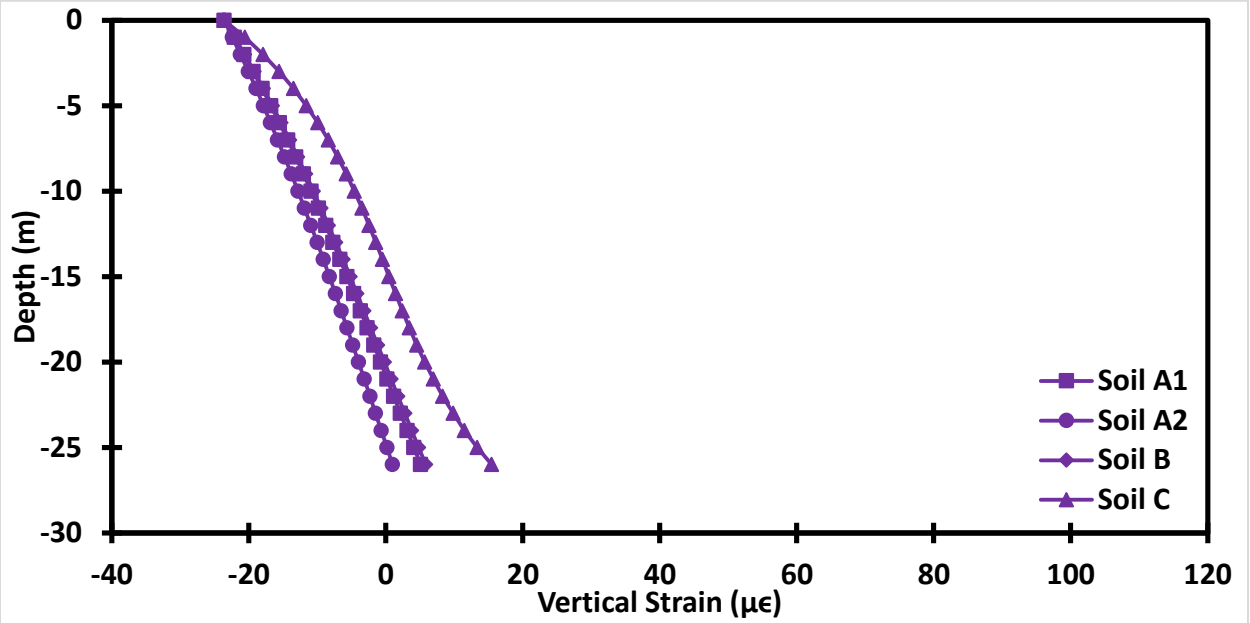

Figure 3.51 Strain in Semi Floating Pile Embedded in Homogeneous Soil (ΔT = 2°C, test T7, K_h = 0)

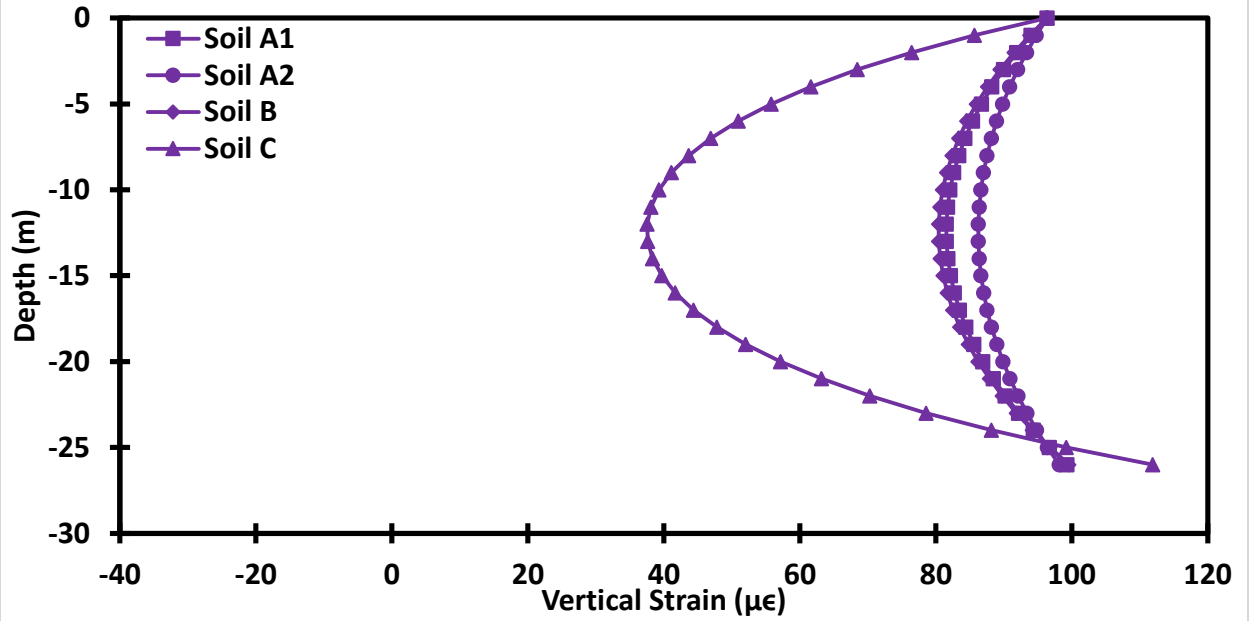

Figure 3.52 Strain in Semi Floating Pile Embedded in Homogeneous Soil (ΔT = 14°C, test T7, K_h = 0)

Figures 3.53 and 3.54 show that the location of the largest stress magnitude is dependent on the soil stiffness, temperature difference, and axial load.

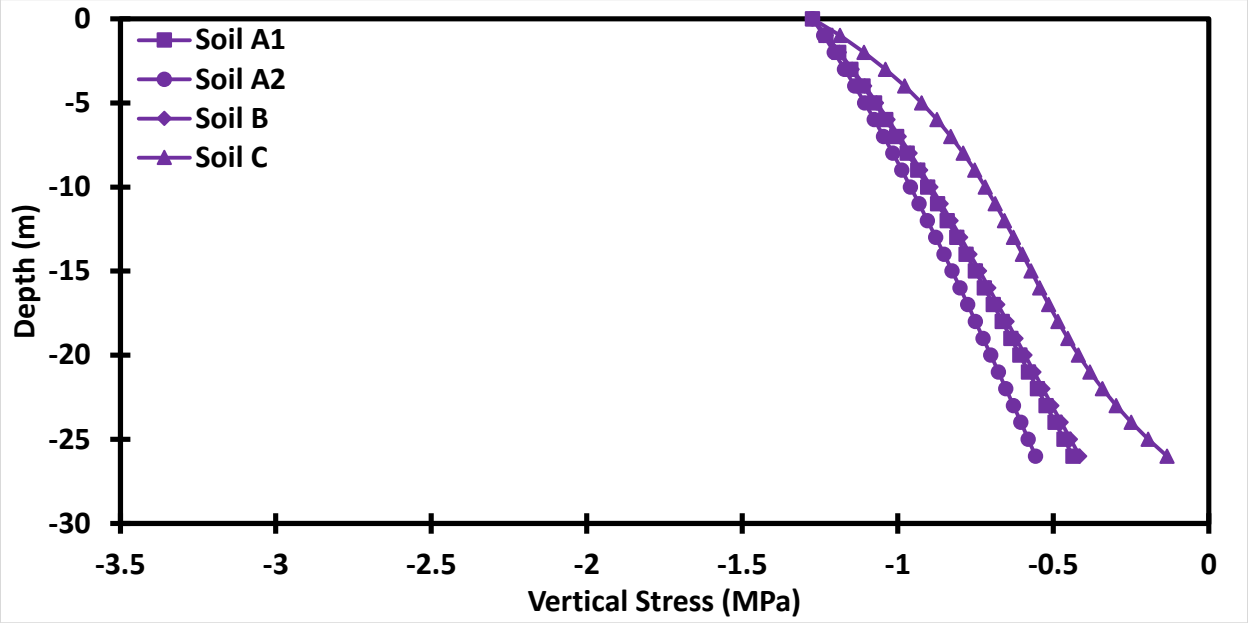

Figure 3.53 Stress in Semi Floating Pile Embedded in Homogeneous Soil (ΔT = 2°C, test T7, K_h = 0)

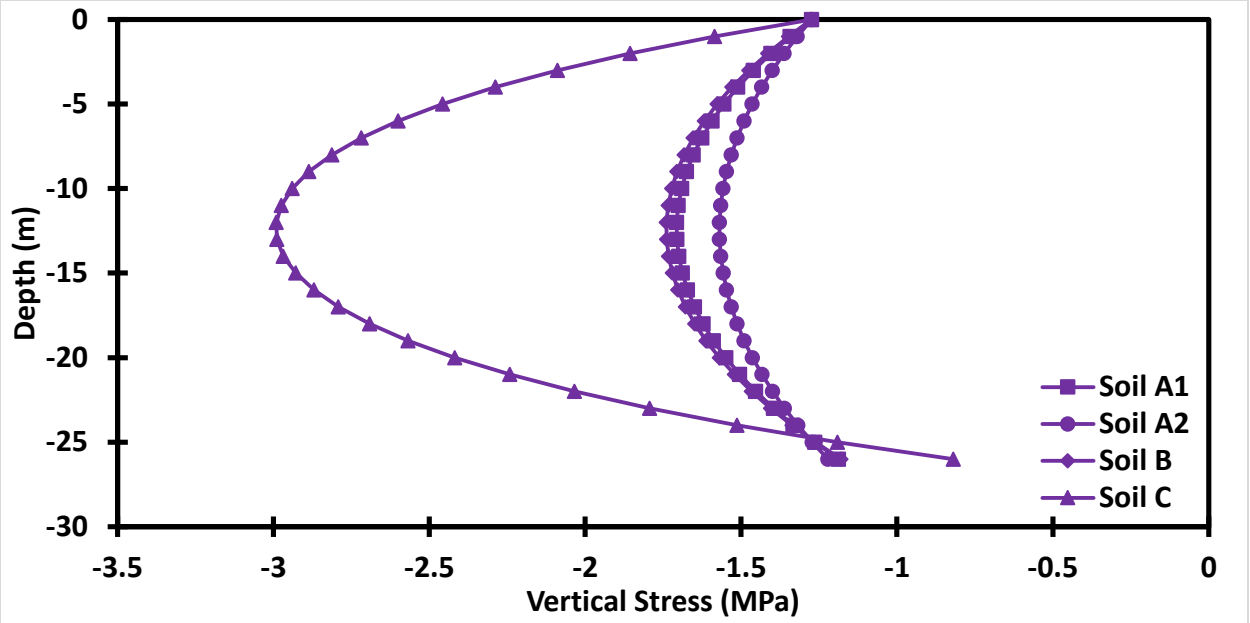

Figure 3.54 Stress in Semi Floating Pile Embedded in Homogeneous Soil (ΔT = 14°C, test T7, K_h = 0)

Figures 3.55 and 3.56 show displacement at ΔT = 2°C and ΔT = 14°C during test T7 with pile head restraint. As expected the magnitude head displacement at ΔT = 2°C in the presence of head restraint (Fig. 3.55) is larger than in the absence of head restraint (Fig. 3.49). The opposite situation occurs for ΔT = 14°C whereby the magnitude of head displacement is smaller in the presence of head restraint (Fig. 3.56) than in the absence of head restraint (Fig. 3.50).

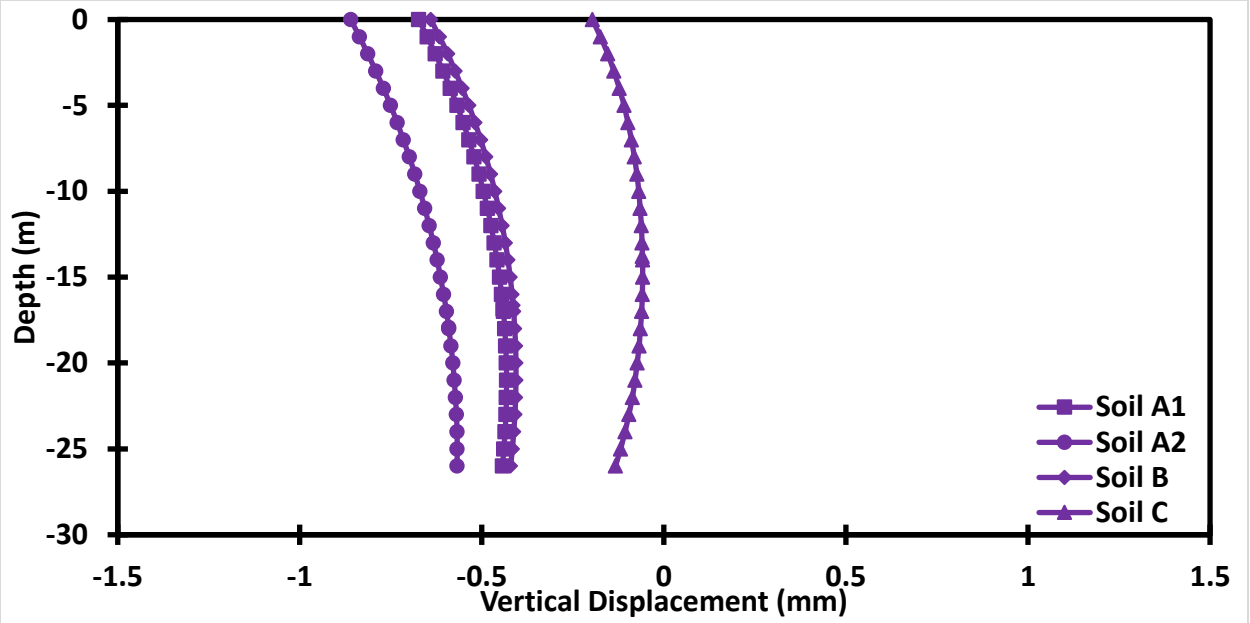

Figure 3.55 Displacement of Semi Floating Pile Embedded in Homogeneous Soil (ΔT = 2°C, test T7, K_h = 125 MPa/m)

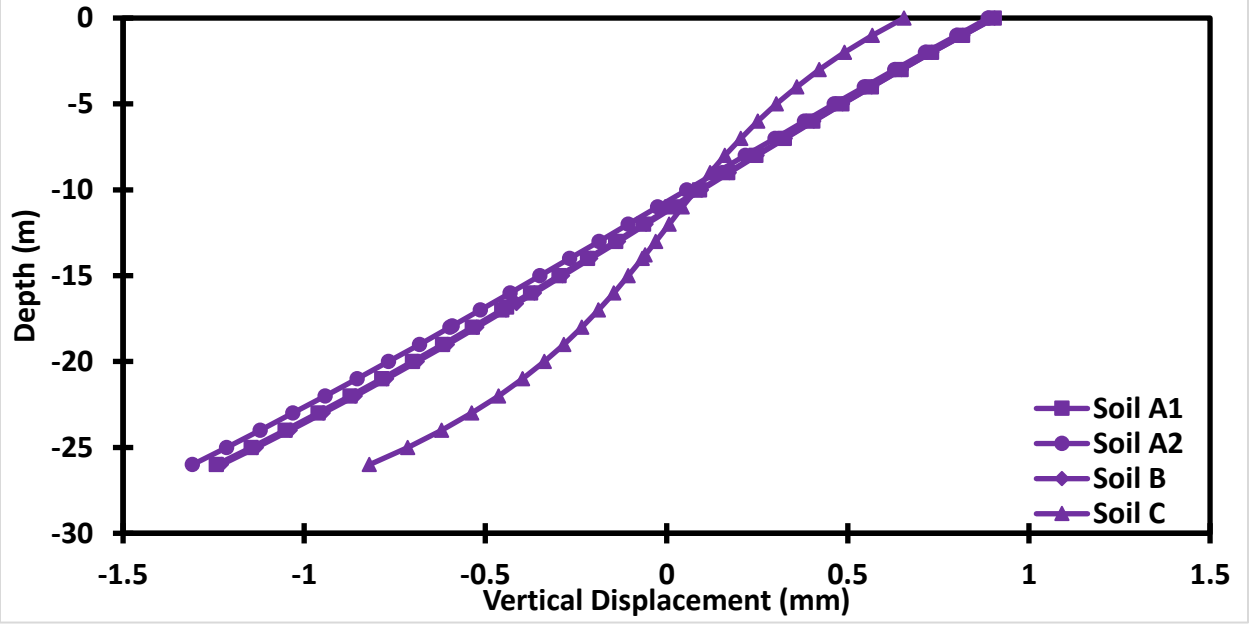

Figure 3.56 Displacement of Semi Floating Pile Embedded in Homogeneous Soil (ΔT = 14°C, test T7, K_h = 125 MPa/m)

Figures 3.57 and 3.58 depict strain versus depth at ΔT = 2°C and 14°C respectively during test T7 in the presence of head restraint

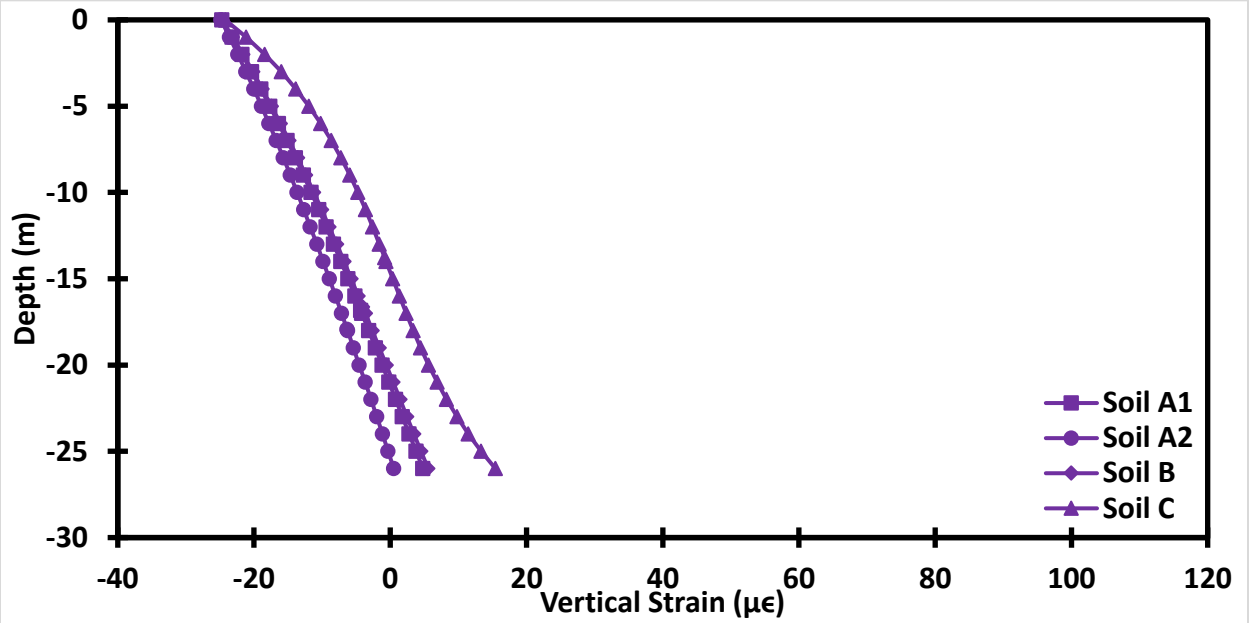

Figure 3.57 Strain in Semi Floating Pile Embedded in Homogeneous Soil Profile (ΔT = 2°C, test T7, K_h = 125 MPa/m)

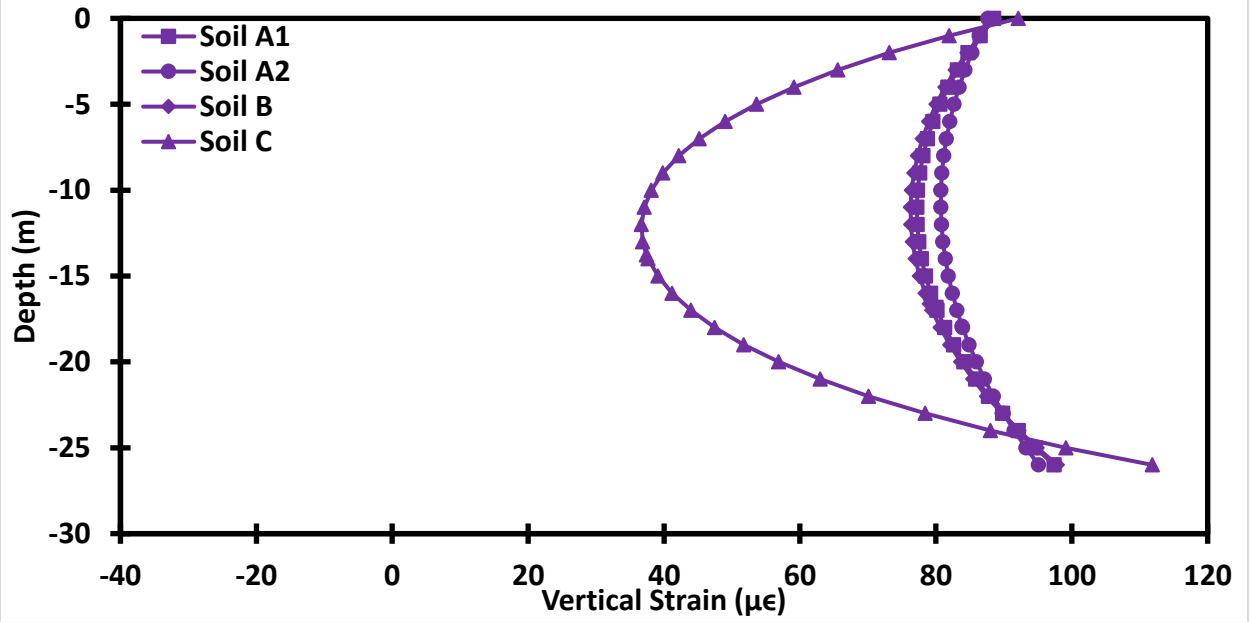

Figure 3.58 Strain in Semi Floating Pile Embedded in Homogeneous Soil Profile (ΔT = 14°C, test T7, K_h = 125 MPa/m)

The main difference in stress change versus depth in the presence (Fig. 3.59 and Fig. 3.60) and in the absence of head restraint (Fig. 3.53 and Fig. 3.54) is in the stress at the pile head. In the former case stress at the pile head is the same for all the soils while in the latter case it is not. This is the consequence of the corresponding different displacements at the pile head that directly affect the stress at the pile head.

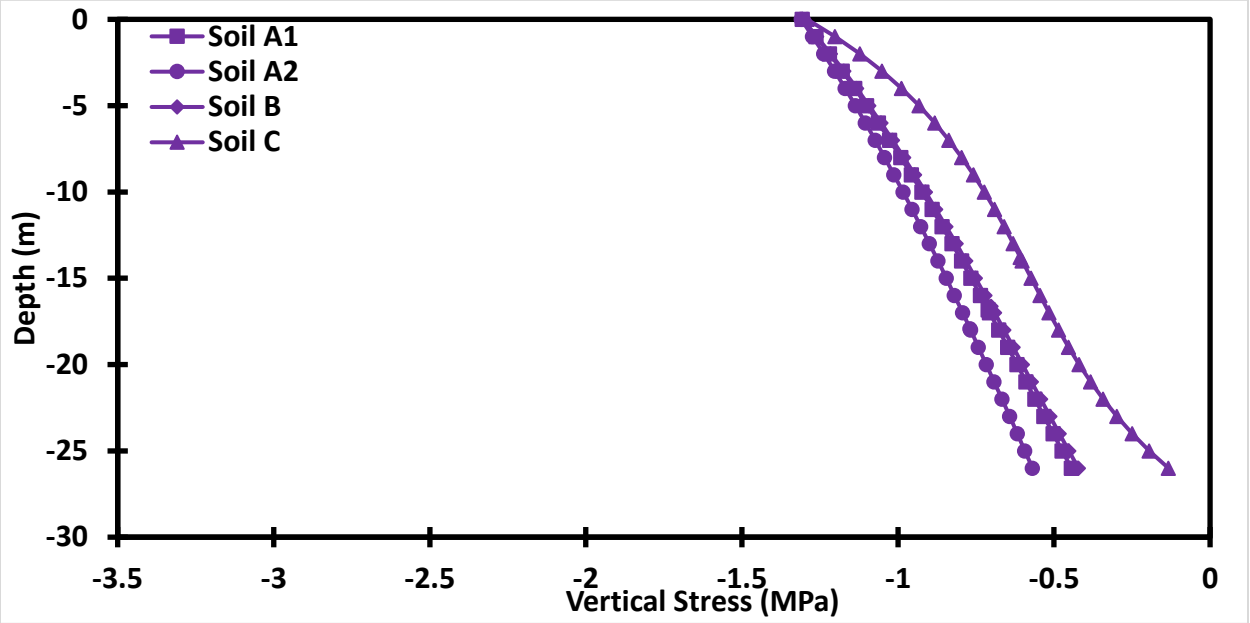

Figure 3.59 Stress in Semi Floating Pile Embedded in Homogeneous Soil (ΔT = 2°C, test T7, K_h = 125 MPa/m)

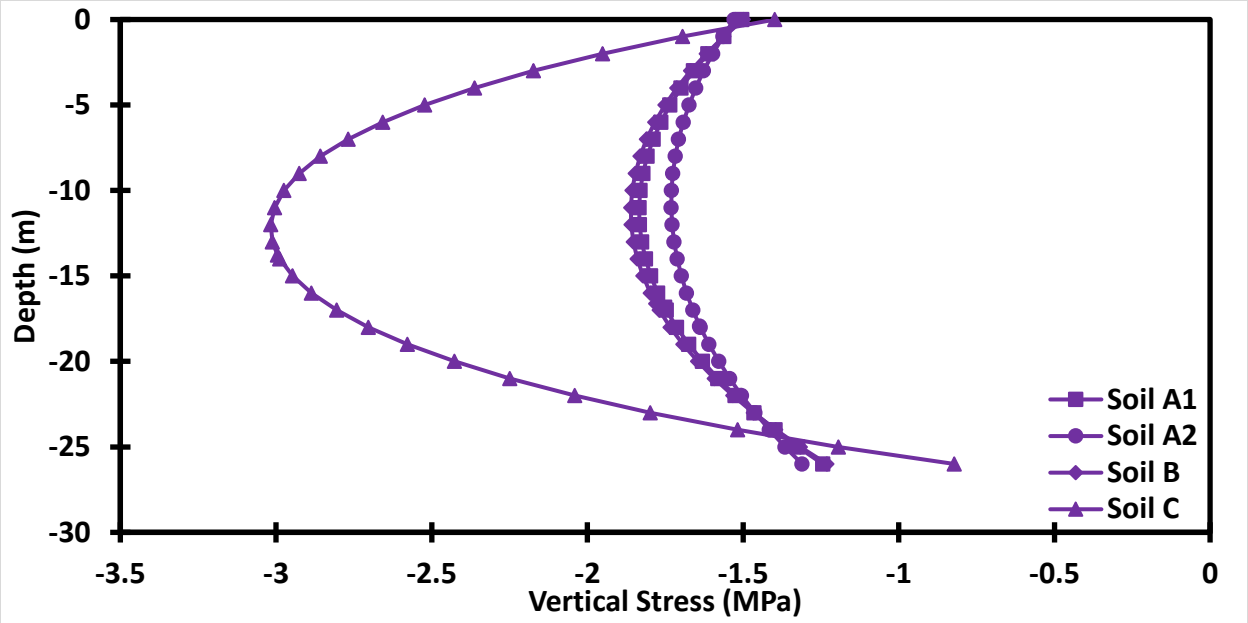

Figure 3.60 Stress in Semi Floating Pile Embedded in Homogeneous Soil (ΔT = 14°C, test T7, K_h = 125 MPa/m)

Layered Soil Profile

This section presents the results of validation of the analytical solutions for the semi floating pile embedded in the actual layered soil profile.

Test T1

It can be observed from Fig. 3.61 and Fig. 3.62 that the null point does not depend on the temperature difference. Furthermore, as expected the pile head displacement is now smaller than in the case of end bearing pile (Fig. 3.23 and Fig. 3.24). As mentioned previously the experimental data for change in displacement with depth are not available.

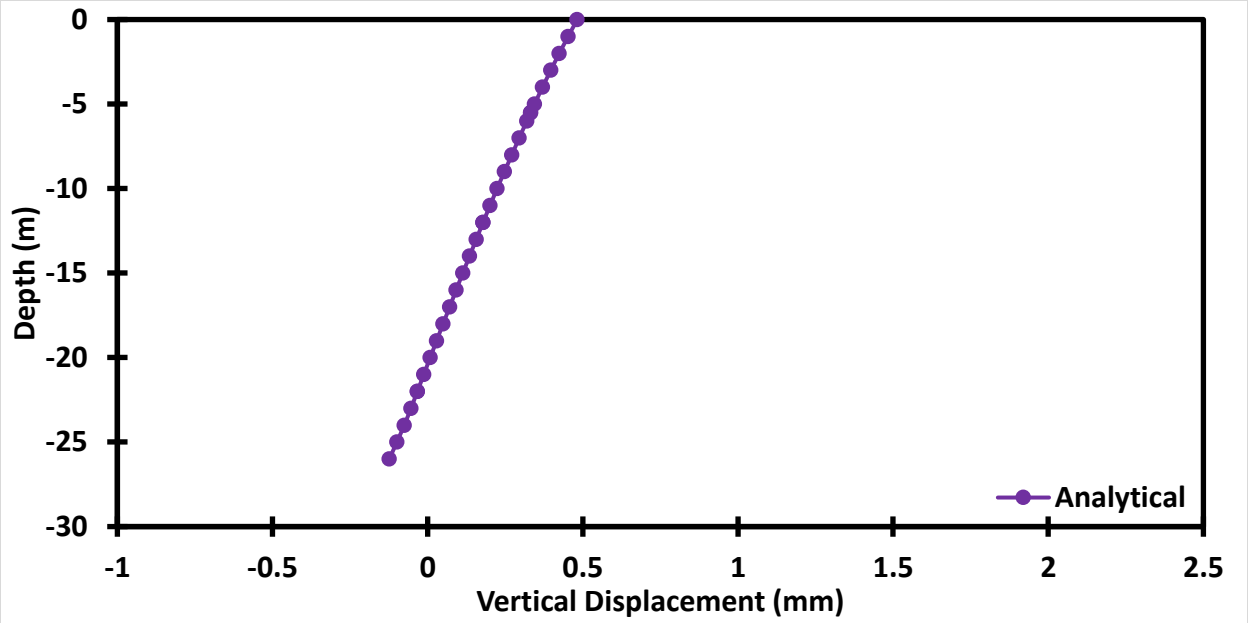

Figure 3.61 Displacement in Semi Floating Pile Embedded in Layered Soil Profile (*ΔT* = 3°C, test T1)

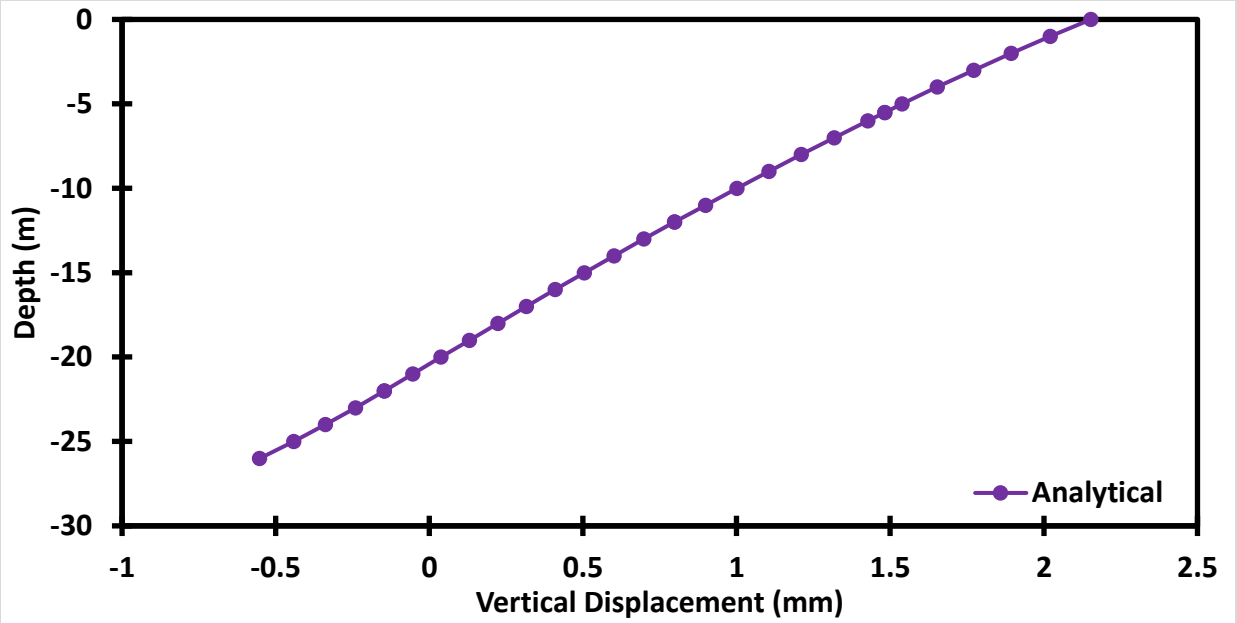

Figure 3.62 Displacement in Semi Floating Pile Embedded in Layered Soil Profile (*ΔT* = 13.4°C, test T1)

In the case of semi floating pile the predicted strain versus depth falls in the middle of the range of all experimental data including OF and VWSG (Fig. 3.63). However, it is noted that there is relatively small disagreement between the experimental data obtained from OF and VWSG. The former measurement resulted consistently in larger strain than the latter for ΔT = 2°C. The prediction of the model is very good.

For the temperature difference ΔT = 13.4°C measurements obtained from OF and VWSG seem to be closer to each other. The model prediction for the selected value of the stiffness of the normal spring at the pile tip produces slightly higher strain than measured. However, qualitative agreement between the measured and predicted strains is excellent.

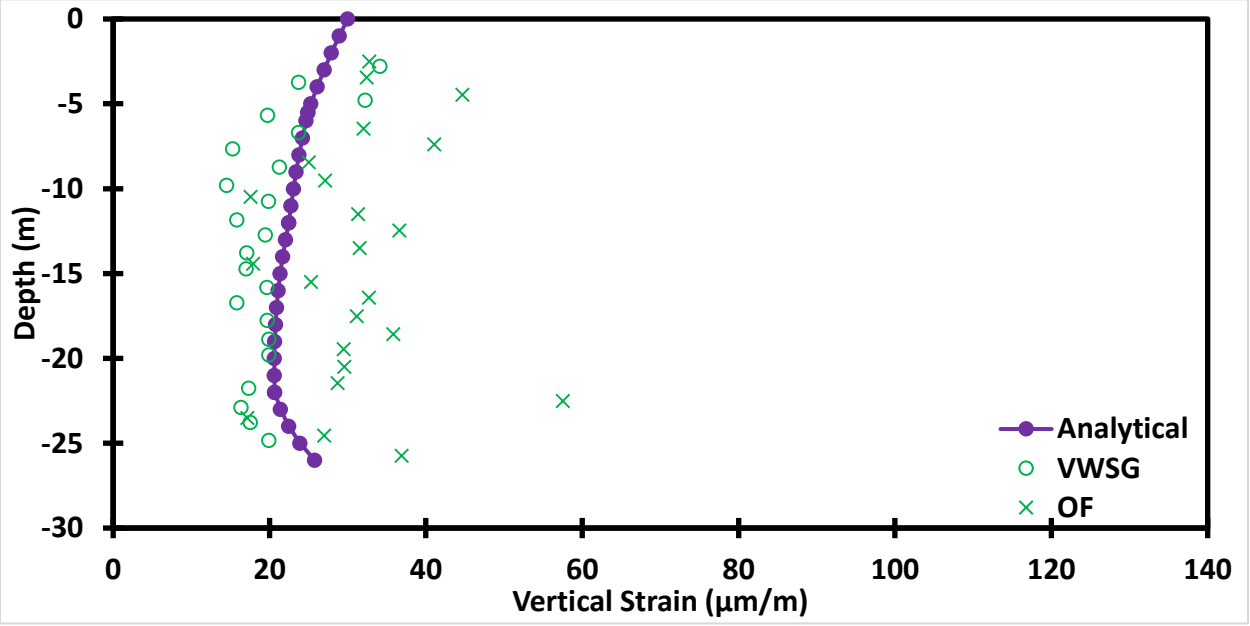

Figure 3.63 Strain in Semi Floating Pile Embedded in Layered Soil Profile (ΔT = 3°C, test T1)

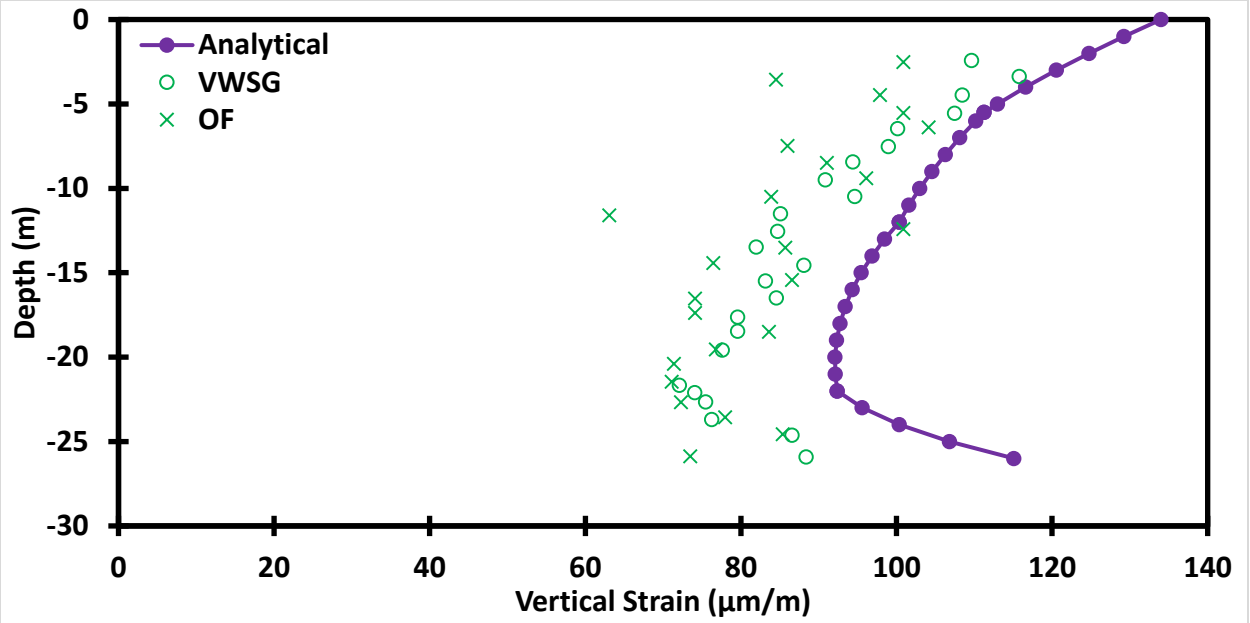

Figure 3.64 Strain in Semi Floating Pile Embedded in Layered Soil Profile (ΔT = 13.4°C, test T1)

Similarly to the predictions of strains, the analytical model provided a very good prediction of the stress change versus depth at ΔT = 3°C while at ΔT = 13.4 °C the predicted stress is somewhat smaller than measured. Nevertheless, it is important to note that the relaxed fixity of the pile tip in the analytical model for semi floating pile correctly captures decrease of the stress in the vicinity of the pile tip. Thus, in the present case where the bedrock is sandstone/claystone the semi floating pile is better model of the energy pile than the end bearing pile. Further improvements in the predictions for the former could be obtained by changing the stiffness of the normal spring located at the pile tip K_b. In the present case the midrange value of K_b from Knellwolf et al. (2011) is used.

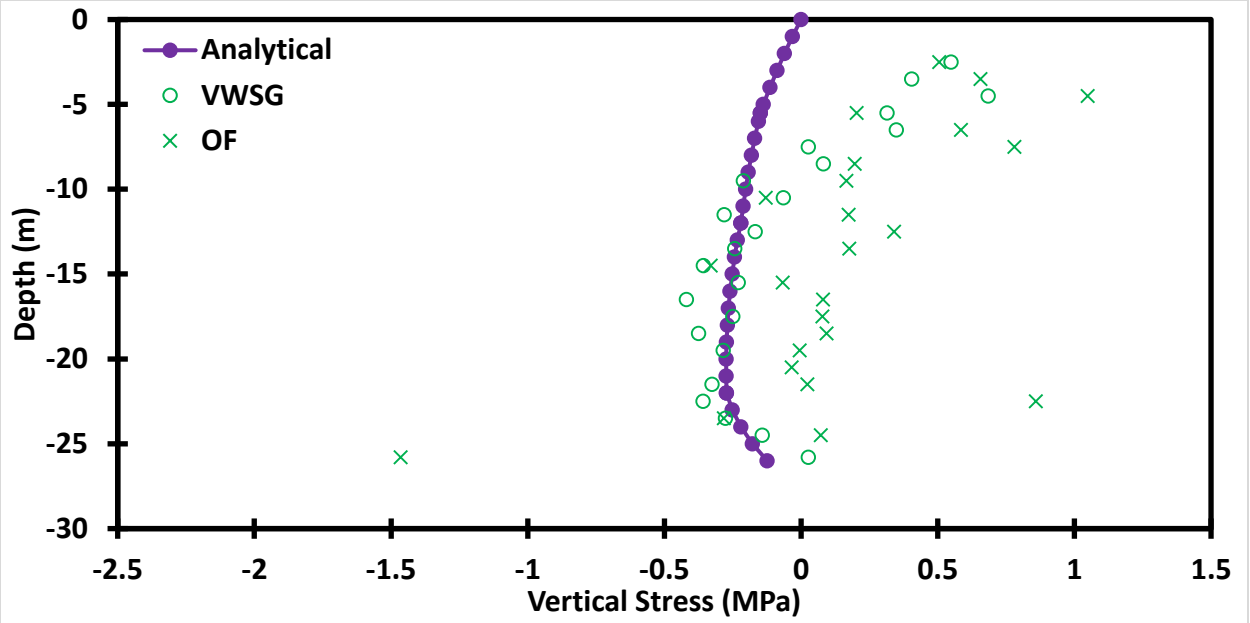

Figure 3.65 Stress in Semi Floating Pile Embedded in Layered Soil Profile (ΔT = 3°C, test T1)

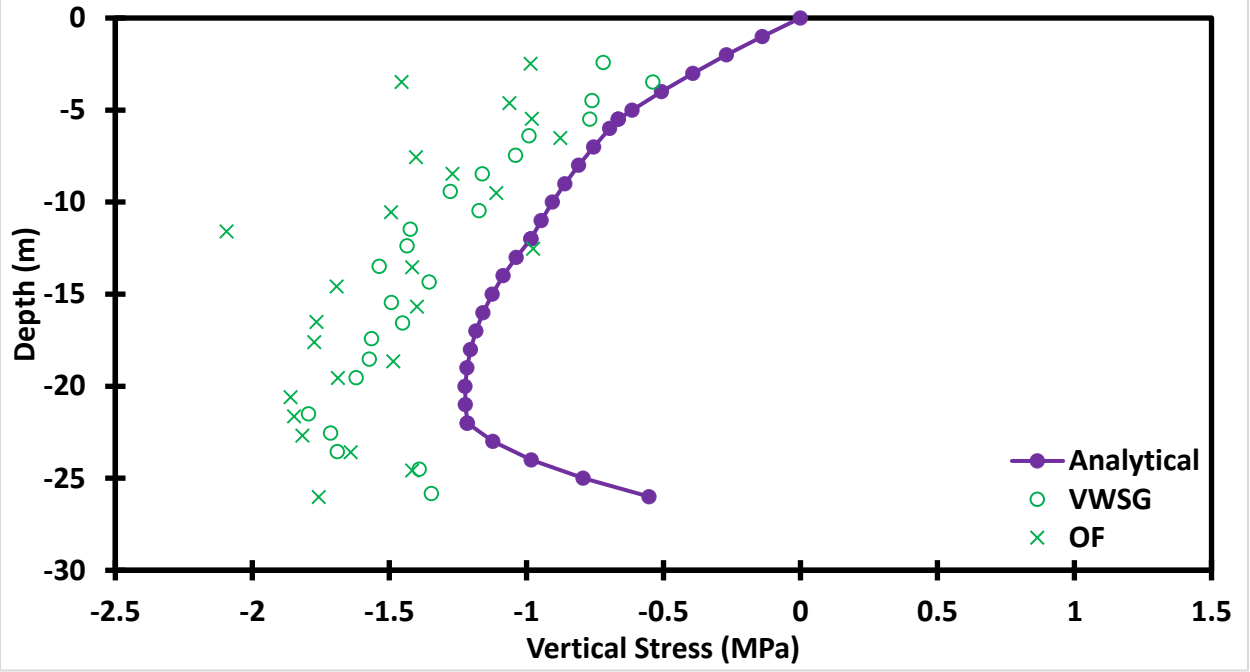

Figure 3.66 Stress in Semi Floating Pile Embedded in Layered Soil Profile (ΔT = 13.4°C, test T1)

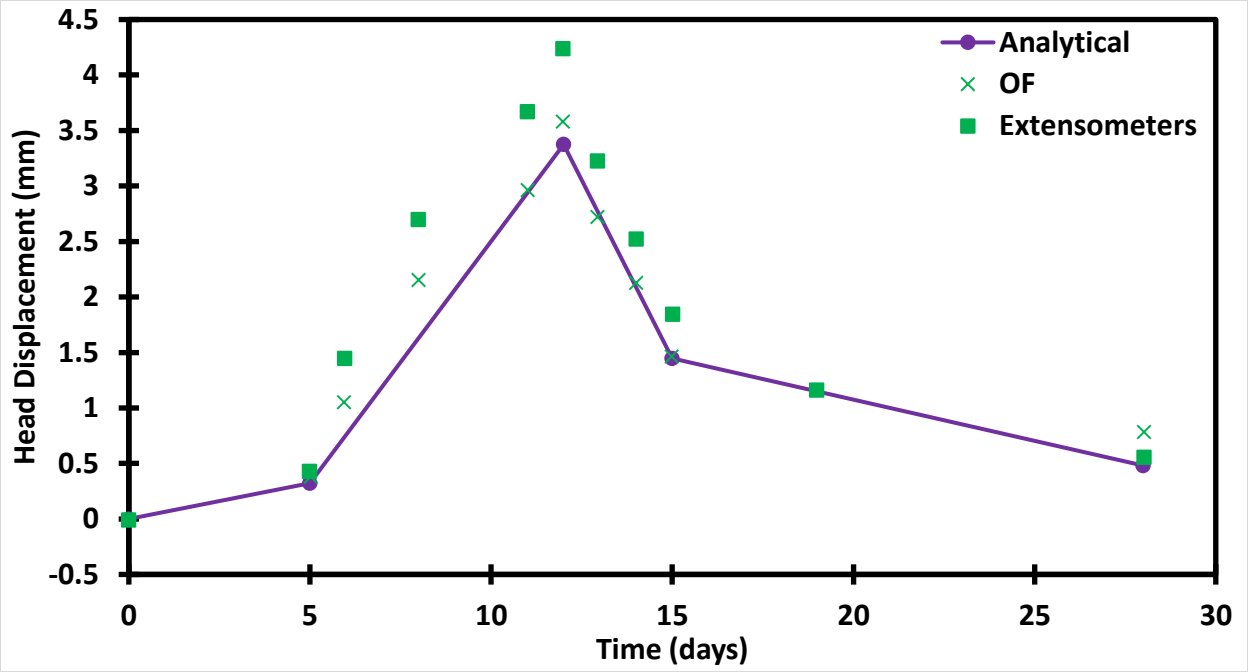

Figure 3.67 Layered Head Displacement vs Time

Test T7

Next, the predictions of the analytical model for semi floating energy pile subjected to the thermal and mechanical loads from test T7 are presented along with the relevant experimental data. The predictions for unrestrained pile head are presented first.

As expected magnitudes of pile head displacements depicted in figures 3.68 and 3.69 are smaller than those obtained for end bearing pile (Fig. 3.30 and Fig. 3.31), both with unrestrained pile head.

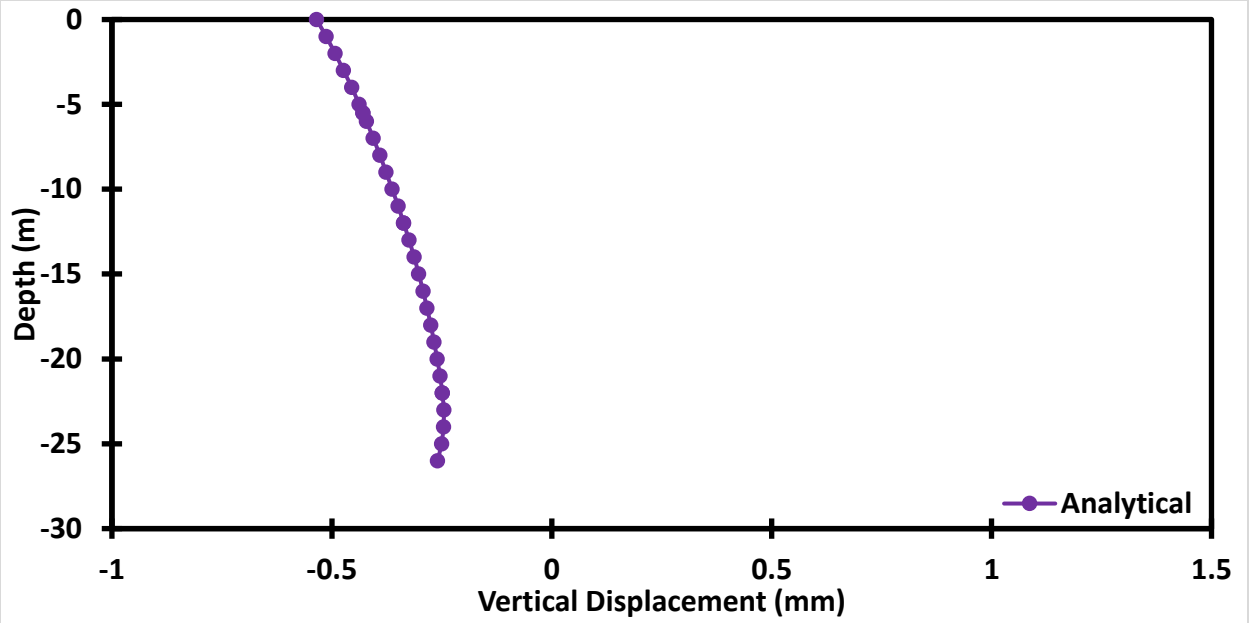

Figure 3.68 Displacement in Semi Floating Pile Embedded in Layered Soil Profile (ΔT = 2°C, test T7, K_h=0)

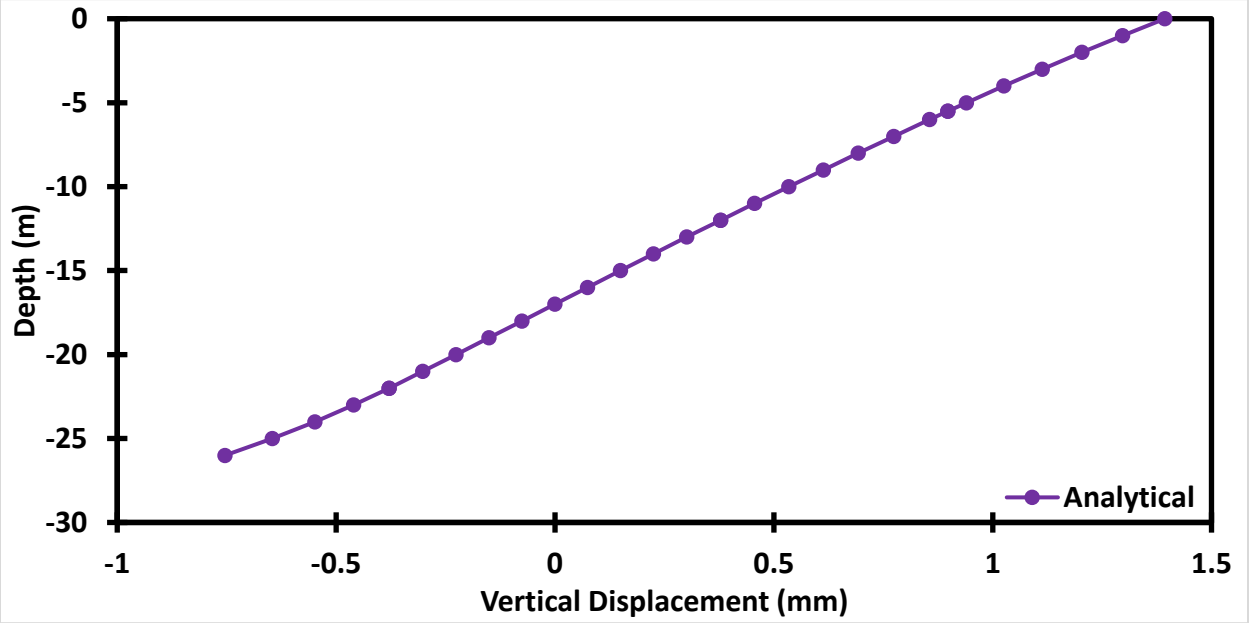

Figure 3.69 Displacement in Semi Floating Pile Embedded in Layered Soil Profile (ΔT = 14°C, test T7, K_h=0)

The predicted strain at ΔT = 14°C (Fig. 3.71) exhibits better quantitative and qualitative agreement with the experimental data than predicted strain at ΔT = 2°C (Fig. 3.70).

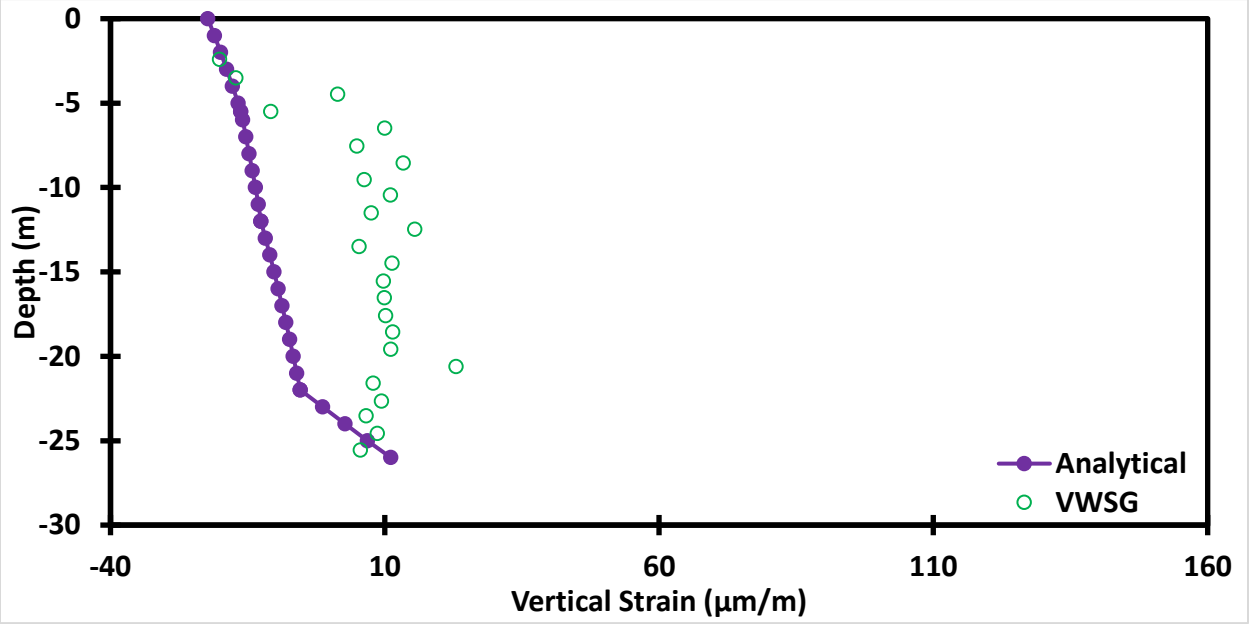

Figure 3.70 Strain in Semi Floating Pile Embedded in Layered Soil Profile (ΔT = 2°C, test T7, K_h = 0)

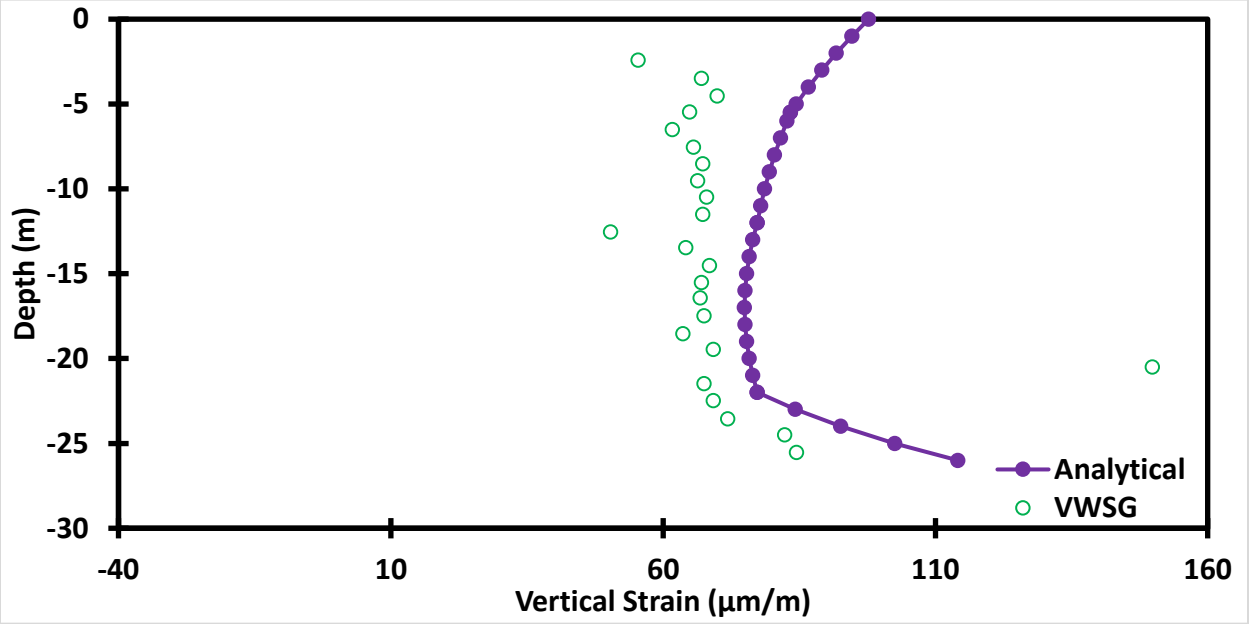

Figure 3.71 Strain in Semi Floating Pile Embedded in Layered Soil Profile (ΔT = 14°C, test T7, K_h = 0)

The predicted stress at ΔT = 14°C shows excellent agreement with the VWSG measurements in the bottom half length of the pile, except at the pile tip (Fig. 3.73).

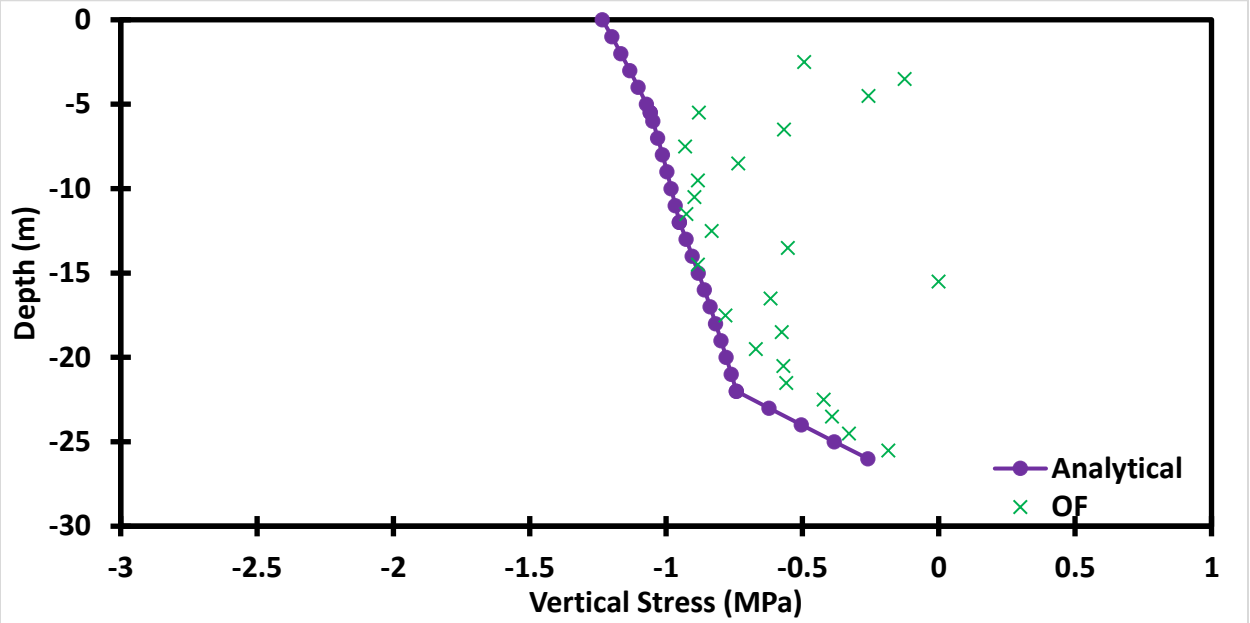

Figure 3.72 Stress in Semi Floating Pile Embedded in Layered Soil Profile (ΔT =2°C, test T7, K_h=0)

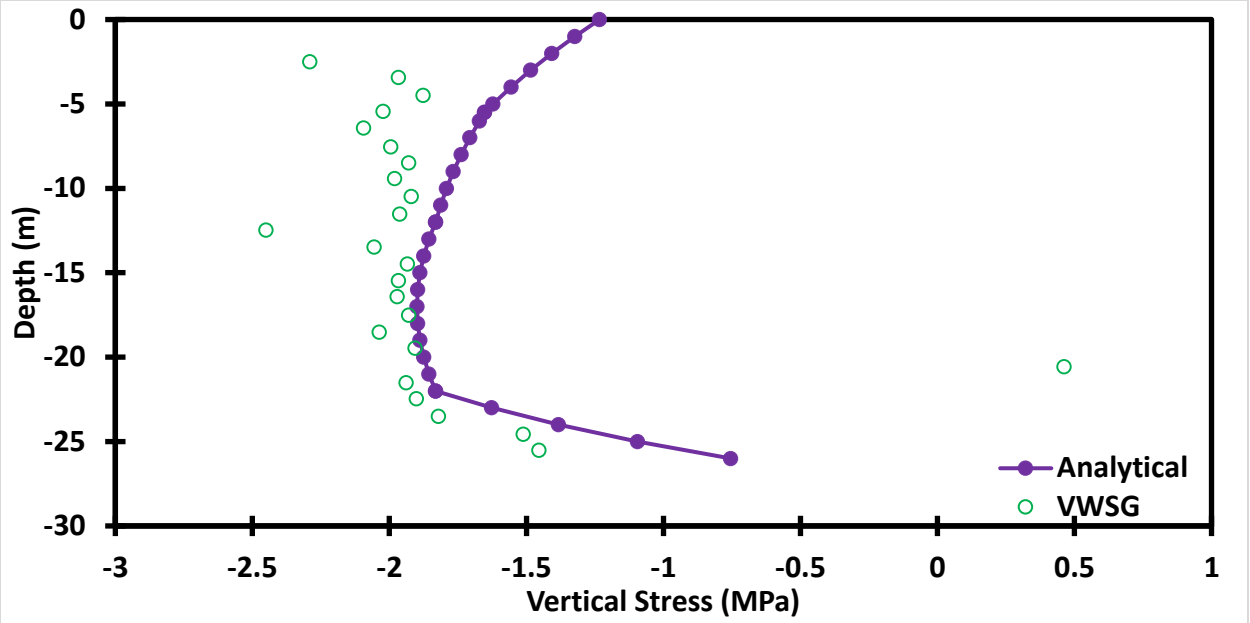

Figure 3.73 Stress in Semi Floating Pile Embedded in Layered Soil Profile (ΔT =14°C, test T7, K_h=0)

Fig. 3.74 depicts head displacement versus time during test T7 for semi floating pile without head restraint.

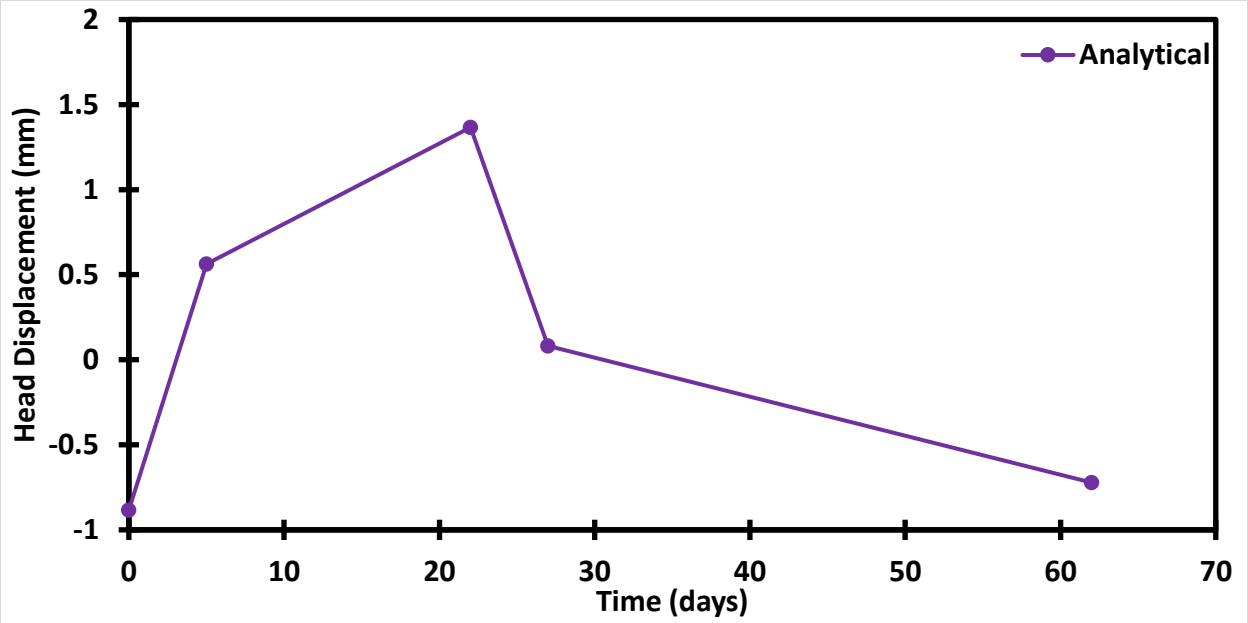

Figure 3.74 Head Displacement vs Time in Semi Floating Pile Embedded in Layered Soil Profile (test T7, K_h =0)

Head displacements without head restraint (Fig. 3.68 and Fig. 3.69) are larger than the displacement predicted in the presence of head restraint (Fig. 3.75 and 3.76).

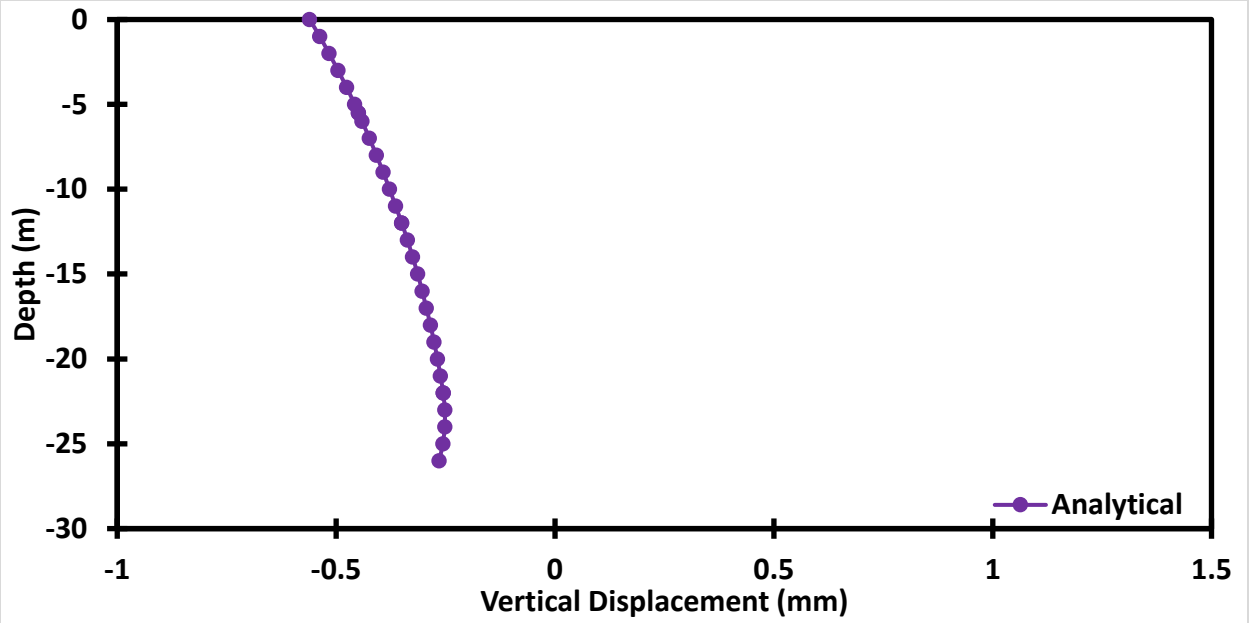

Figure 3.75 Displacement in Semi Floating Pile Embedded in Layered Soil Profile (ΔT = 2°C, test T7, K_h = 125 MPa/m)

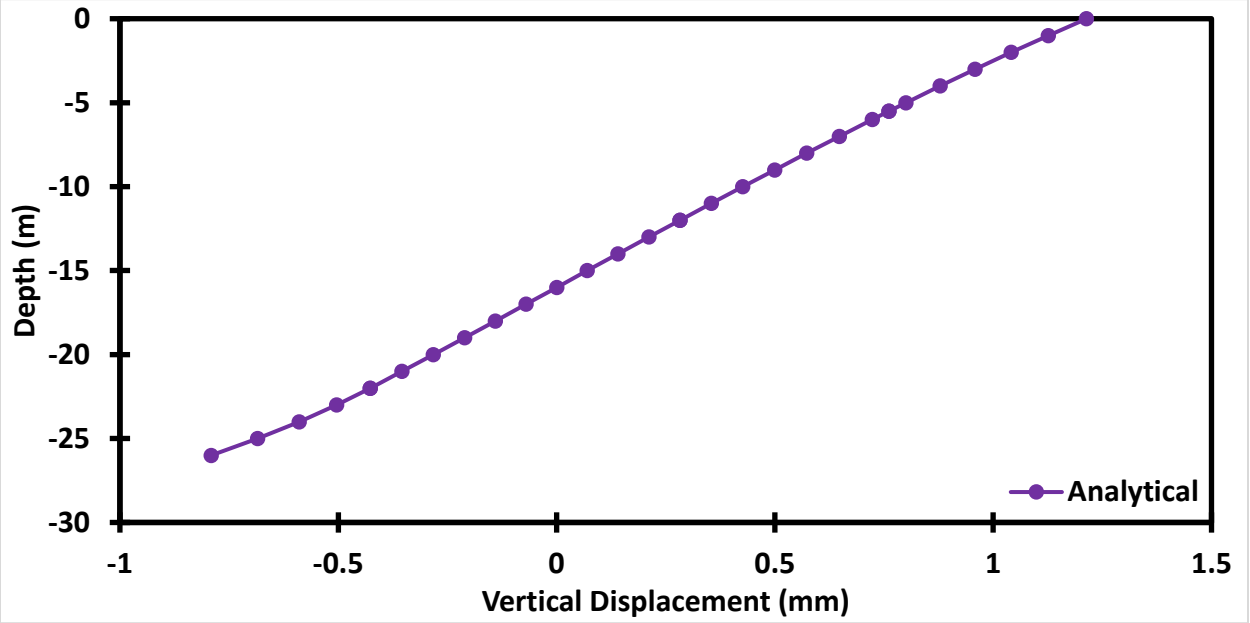

Figure 3.76 Displacement in Semi Floating Pile Embedded in Layered Soil Profile (ΔT = 14°C, test T7, K_h = 125 MPa/m)

Inclusion of head restraint does not significantly change the predicted strain at ΔT = 2°C (Fig. 3.77) as compared to the case without head restraint (Fig. 3.70). Nevertheless, the predicted strain at ΔT = 13.4°C (Fig. 3.78) shows improvement as compared to the case without head restraint (Fig. 3.71).

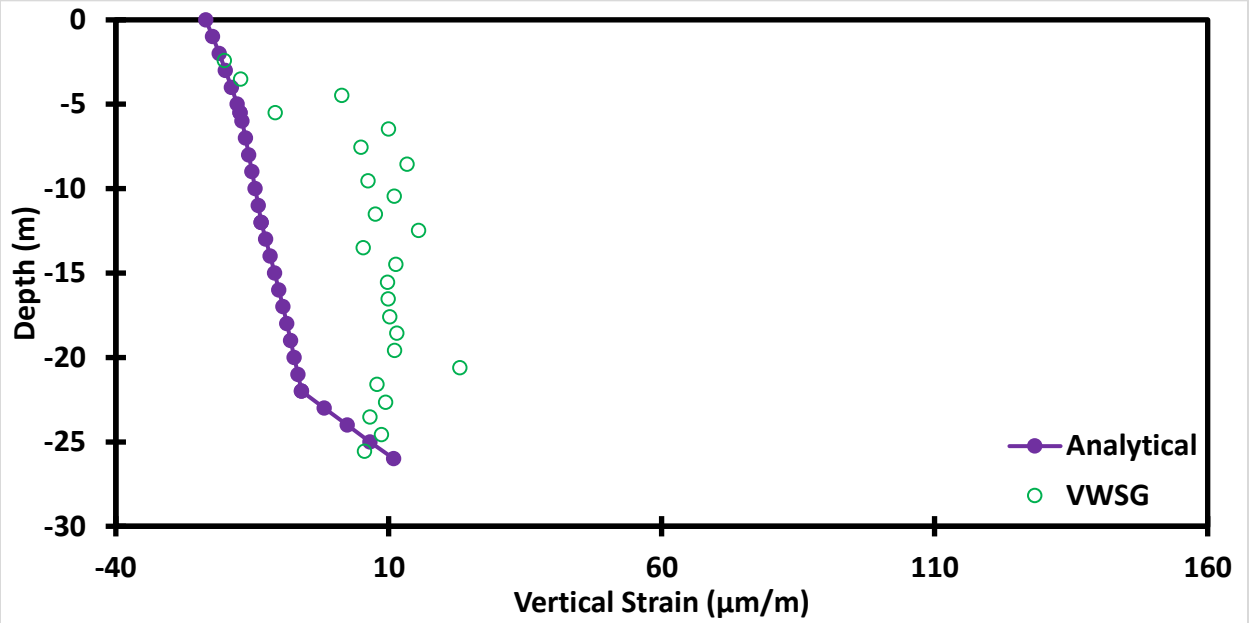

Figure 3.77 Strain in Semi Floating Pile Embedded in Layered Soil Profile (ΔT = 2°C. test T7, K_h = 125 MPa/m)

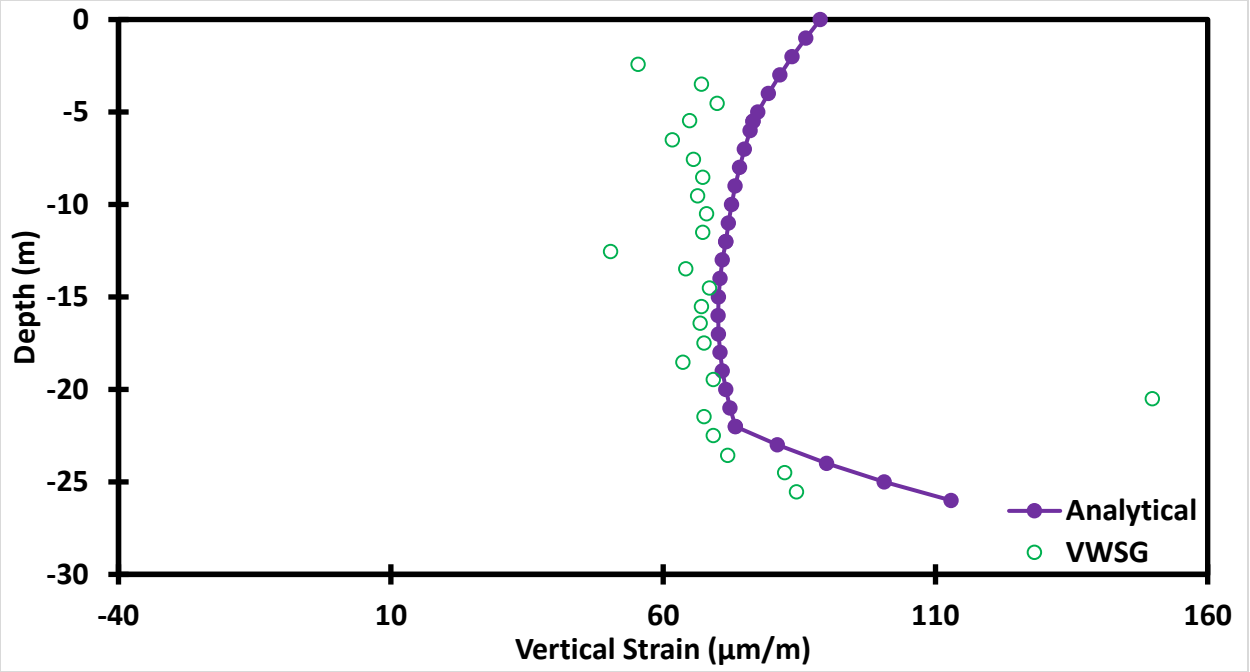

Figure 3.78 Strain in Semi Floating Pile Embedded in Layered Soil Profile (ΔT = 14°C. test T7, K_h = 125 MPa/m)

Similarly to predicted strain the predicted stress at ΔT = 14°C shows slightly better agreements with the experimental data in the presence of head restraint (Fig. 3.80) than in the absence of head restraint (Fig. 3.73).

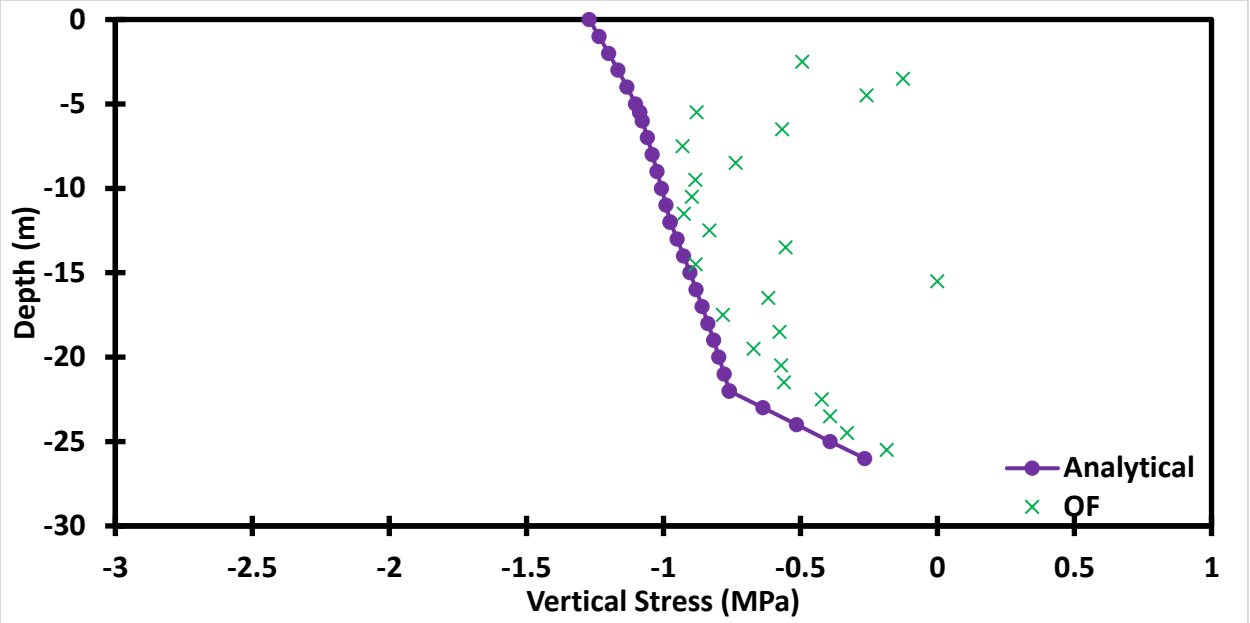

Figure 3.79 Stress in Semi Floating Pile Embedded in Layered Soil Profile (ΔT = 2°C, test T7, K_h = 125 MPa/m)

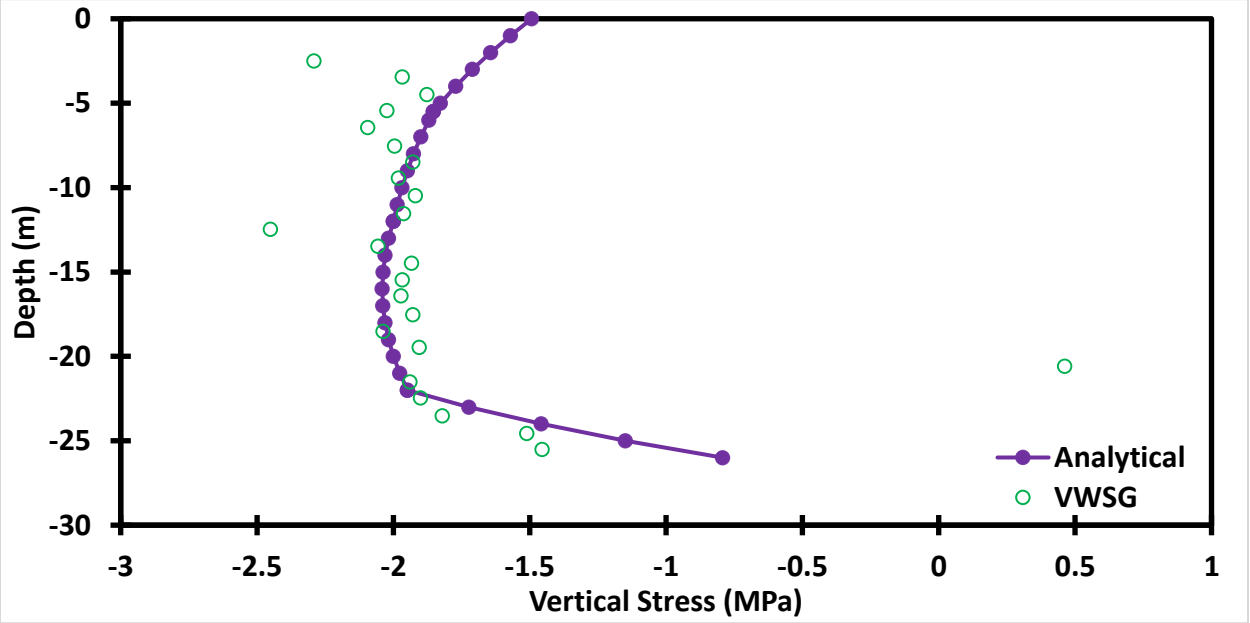

Figure 3.80 Stress in Semi Floating Pile Embedded in Layered Soil Profile (ΔT = 14°C, test T7, K_h = 125 MPa/m)

The maximum head displacement that occurred during test T7 is larger in the absence of the pile head restraint (Fig. 3.74) than in the presence of head restraint (Fig. 3.81).

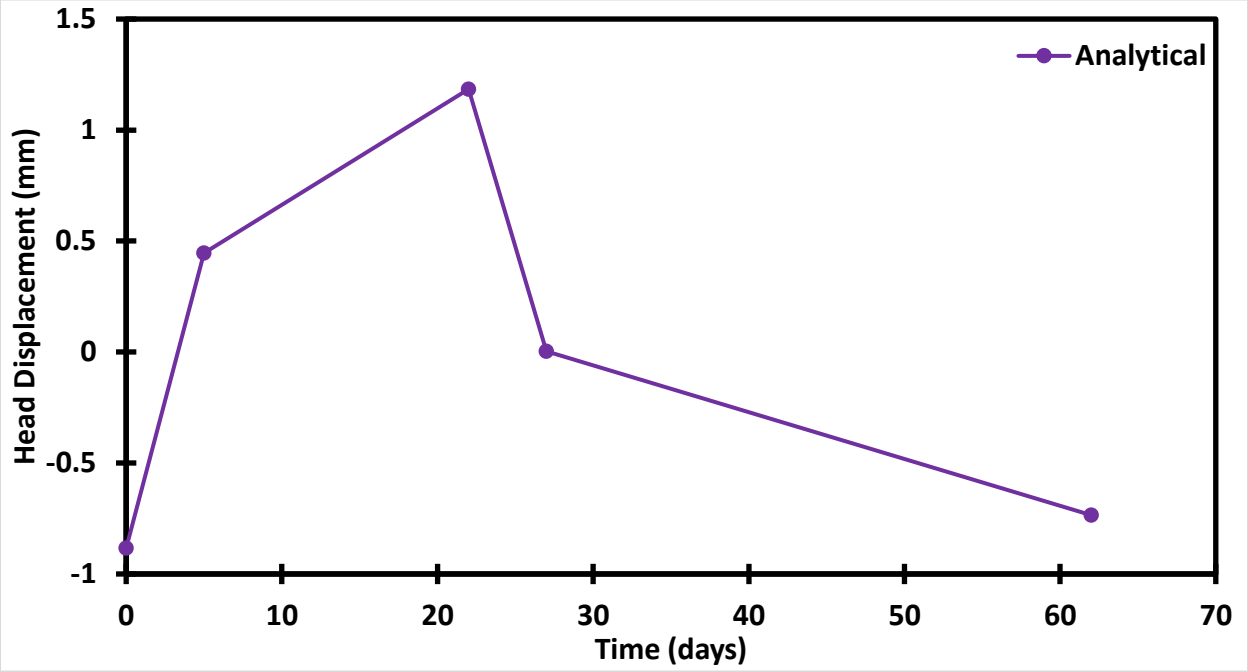

Figure 3.81 Head Displacement vs Time for Semi Floating Pile Embedded in Layered Soil Profile (test T7, K_h = 125 MPa/m)

Comparison Between End Bearing and Semi Floating Pile Tip

As seen above the Semi Floating Pile better accounts for what happens to a pile embedded in relatively soft bedrock. This is due to the semi floating model taking into account the deformation of the bedrock. A few drawback of the semi floating model however, there are additional parameters, K_b and x_0', to be calibrated. There are also significantly more equations generated to solve for x_0' is not known, needed, and theoretically could be in any layer. Due to the current nature of the semi floating solution the number of equation needed to be solved to find displacement, stress, and strain in every location and locate x_0' in the HEP is $3n^n + n$

where n is the number of layers. This can be reduced a bit due to the repetitive nature of the solutions as seen in the semi floating pile in a layered soil profile under thermal load with head restraint section in Chapter 2. However there are still significantly more equations that the end bearing solution of the same number of layers.

Chapter 4 - Conclusions and Recommendations

Geo-thermally active foundations decrease demand for traditional energy sources including fossil fuels by using naturally available renewable thermal energy stored in the ground. They are more environmentally friendly energy source as compared to current cooling and heating methods. To advance the knowledge of the soil-structure interaction in energy piles mechanics based mathematical models where formulated and solved analytically. The solutions where subsequently validated against field tests conducted in Lausanne, Switzerland on a four story 30m x 100m building (Laloui et al. 1999). The test was conducted on one of the 97 drilled piles used to support one of Swiss Federal Institute of Technology building.

Due to dominance of vertical displacement, strain and stress one dimensional analysis was possible. Stress, strain, and displacement where calculated every meter and at interfaces of different soil layers thus giving a total of 28 data points along the 26m long pile.

Conclusions

Based on the validation of the 1D model presented in Chapter 3, the following conclusions can be made

1. The 1D mathematical model based on the elastic load transfer functions and thermo-elastic behavior of the pile captured the observed response of the energy pile to thermal and mechanical loads very well.

2. The stresses induced by heating (at maximum temperature difference) where significantly larger than those generated by the mechanical load at this particular site in the case of a combined thermal and mechanical loading.

3. The semi floating pile model more accurately captured response of the energy pile in the case of a combined thermal and mechanical load.

4. The end bearing pile model more accurately captured response of the energy pile in the case of thermal loading only.

5. The analytical solutions found in this study provide quick, elegant and reliable predictions of axial displacement, stress and strain induced by working thermal and/or mechanical loads.

Recommendations

Recommendations for further research in the area of analytical modeling of energy piles include

1. A validation of the analytical solutions in the case of net cooling ($\Delta T < 0$) should be conducted to fully evaluate the magnitude of tensile stresses, which are more critical for energy piles constructed from reinforced concrete.

2. Find if there is a way to simplify the solution procedure for the semi floating pile embedded in the layered soil.

3. Implement the analytical solutions into a computer code that could address a realistic arbitrary number of soil layers for both thermal and mechanical loads.

References

Armaleh, S., and Desai, C. S. (1987). "Load-deformation response of axially loaded piles." J. *Geotech. Geoenviron*., 113(12), 1483–1500.

Bourne-Webb, P. J., Amatya, B., Soga, K., Amis, T., Davidson, C., and Payne, P. (2009). "Energy pile test at Lambeth College, London: geotechnical and thermodynamic aspects of pile response to heat cycles." *Géotechnique* 59, No. 3, 237-248.

Bourne-Webb, P. J., Amatya, B., & Soga, K. (2013). "A framework for understanding energy pile behaviour." *P. I. Civil Eng. Geotec*., 166(2), 170-177.

Brandl, H. (2006). "Energy foundations and other thermos-active ground structures." *Géotechnique* 56, No. 2, 81-122

Burger, A., Recordon, E., Bovet, D., Cotton, L. and Saugy, B. (1985). *Thermique des Nappes Souterraines*. Presses Polytechniques Romandes. Laussane, Switzerland.

Coyle, H. M., and Reese, L. C. (1966). "Load transfer for axially loaded piles in clay." J. Soil Mech. and Found. Div., 92(2), 1–26.

Frank, R., Kalteziotis, N.,Bustamante,M.,Christoulas, S., and Zervogiannis, H. (1991). "Evaluation of performance of two piles using pressuremeter method." J. Geotech. Eng., 117(5), 695–713.

Frank, R., and Zhao, S. R. (1982). "Estimation par les paramètres pressiométriques de l'enfoncement sous charge axiale de pieux forés dans des sols fins." Bull. Liaison Lab. Ponts Chaussees, 119, 17–24 (in French).

Knellwolf, C., Peron, H., and Laloui, L. (2011). "Geotechnical analysis of heat exchanger piles." Journal of Geotechnical and Geoenvironmental Engineering 2011; 137: 890-902.

Laloui, L., Moreni, M., Steinmann, G., Vulliet, L., Fromentin, A., and Pahud, D. (1999).Test en conditions réelles du comportement statique d'un pieu soumis à des solicitations thermos-mécaniques. Report of the Swiss Federal Office of Energy 1999.

Laloui, L., Moreni, M., and Vulliet, L. (2003). "Comportement d'un pieu bi-fonction, fondation et échangeur de chaleur." Can. Geotech. J., 40(2), 388–402 (in French).

Laloui, L., Nuth, M., and Vulliet, M. (2006). "Experimental and numerical investigations of the behavior of a heat exchanger pile." International Journal for Numerical and Analytical Methods in Geomechanics 2006; 30:763-781.

Ozudogru, T. Y., Olgun, C. G., & Arson, C. F. (2015). "Analysis of friction induced thermo-mechanical stresses on a heat exchanger pile in isothermal soil." Geotech. Geol. Eng., 33(2), 357-371.

Perić, D., Tran, T. V., and Miletić, M. (2017). “Effects of soil anisotropy on a soil structure interaction in a heat exchanger pile.” Comput. Geotech., 86, 193-202.

Plaseied, N. (2012). Load Transfer Analysis of Energy Foundations. MS Thesis. University of Colorado Boulder.

Randolph, M. F., and Wroth, C. P. (1978). “Analysis of deformation of vertically loaded piles.” J. Geotech. Eng., 104(GT12), 1465–1488.

Rotta Loria A.F., Laloui L. (2019). “Thermo-mechanical Schemes for Energy Piles.” In: Ferrari A., Laloui L. (eds) Energy Geotechnics. SEG 2018. Springer Series in Geomechanics and Geoengineering. Springer, Cham

Seed, H. B., and Reese, L. C. (1957). “The action of soft clay along friction piles.” Trans. Am. Soc. Civ. Eng., 122, 731–754.